Experimental and Numerical Investigation into the Adhesion of PVD Coatings on Minting Dies

by

Jason Tunis, B.Eng.

A thesis submitted to
the Faculty of Graduate Studies and Research
in partial fulfillment of the requirements for the
degree of Master of Applied Science

Ottawa-Carleton Institute for Mechanical and Aerospace Engineering
Department of Mechanical and Aerospace Engineering

Carleton University
Ottawa, Ontario
Canada

Library and Archives Canada

Published Heritage Branch

395 Wellington Street
Ottawa ON K1A 0N4
Canada

Bibliothèque et Archives Canada

Direction du Patrimoine de l'édition

395, rue Wellington
Ottawa ON K1A 0N4
Canada

Your file Votre référence
ISBN: 978-0-494-91506-6

Our file Notre référence
ISBN: 978-0-494-91506-6

Abstract

This thesis reports on the adhesion characterization of a PVD coating deposited onto mirror polished and laser frosted minting die surfaces. Experimental and numerical methods are both used to study the adhesion of the PVD coating. The Rockwell-C indentation, the stepped indentation, and the scratch adhesion testing methods are used to experimentally examine the coating adhesion. Finite element analyses of the stepped indentation and scratch adhesion tests are performed using critical loads determined from experimental testing. The analyses are performed to determine the stresses produced at the coating-substrate interface prior to coating adhesion failure and characterize the coating adhesion.

The coating applied to a mirror surface and to two of the four laser frosted surfaces passed the Rockwell-C indentation adhesion test. The stepped indentation adhesion testing determined the maximum survivable indentation load without coating adhesion failure for three of the five tested surfaces. The scratch test was found to be a suitable adhesion test method for all the coated surfaces except the roughest laser frosted surface.

The indentation and scratch simulations found that large compressive, shearing, and opening stresses were present at the coating-substrate interface in the regions where coating delamination was observed during experimental testing. The value of the compressive, opening, and shear critical stresses found during finite element simulation of the indentation and scratch tests are in reasonable agreement. These stress components provide good quantification of the coating adhesion strength.

Acknowledgements

I wish to express my sincere appreciation and gratitude to my thesis supervisor, Professor Xin Wang, for his constant support and encouragement. Without his guidance and patience this thesis would not have been possible.

I would like to thank Dr. Xianyao Li and the staff at the Royal Canadian Mint for providing direction and technical assistance during my work at the Mint.

I am grateful for the financial support from the Ontario Centre for Excellence and the Royal Canadian Mint.

Finally, I would like to thank my family and friends for their support and encouragement.

Table of Contents

List of Tables

List of Figures

List of Symbols

Symbol	Description
E	Elastic Modulus
F_N	Normal load
HF 1-6	Rockwell-C adhesion strength quality
n	Strain hardening exponent
R_i	Radius of Rockwell-C indenter tip
t_c	Coating thickness
α	Yield offset
	Angle between the x and x' axis for the scratch simulation
ε	Strain
θ	Angle between the x and x' axis for the indentation simulation
	Angle between the z and z' axis for the scratch simulation
σ	Normal stress
σ_{ij}	Cartesian components of the global normal stresses
$\sigma_{i'j'}$	Cartesian components of the local normal stresses
σ_1, σ_2	Principal normal stresses in the plane of the coating-substrate interface
τ	Shear stress
τ_{max}	Maximum principal shear stress in the plane of the coating-substrate interface
υ	Poisson's ratio
	Subscripts
c	Coating
s	Substrate
y	Yield
x, y, z	Global coordinate directions
x', y', z'	Local coordinate directions

Chapter 1: Introduction

Advances in the minting of coinage have led to the use of highly specialized die coatings. These coatings, in the form of thin hard films, are applied to die surfaces to improve their surface performance and increase their service life. The Royal Canadian Mint (RCM) uses a Cr-Ti-N based physical vapour deposition (PVD) coating applied to a hardened tool steel using magnetron sputter ion plating (Bodor, 2010).

Coin forming is achieved by the striking of a blank disc between two dies. A collar surrounding the blanks circumference limits radial expansion of the blank during striking. The forming process produces large stresses in the die coating and steel substrate. The coating is expected to survive thousands to multiple hundreds of thousands of these impacts. To achieve long die life, the coating must be well adhered to the tool steel substrate and for this reason it is very important to ensure that adequate adhesion is achieved.

In recent years, laser engraving and frosting has started to be used on minting dies prior to coating to produce highly detailed coins with new surface finishes. Limited research has been completed in examining the effect of these new surface finishes on coating adhesion.

Many test methods exist for examining the adhesion between the coating and substrate. Among them are the indentation and the scratch adhesion tests, both of which are commonly used for testing the adhesion of thin hard coatings. These adhesion tests can be used to characterize the coating adhesion semi-quantitatively and with added analyses quantitatively (Lacombe, 2006).

Recently, the combination of experimental testing and numerical simulation has been used by several researchers to quantify coating adhesion. Indentation adhesion tests have been

used together with finite element simulations to quantify the adhesion of thin hard coatings. Pachler et al. (2007) studied the failure of a TiN PVD coated tool steel using Rockwell-C indentation tests and ABAQUS 6.5 to simulate the indentation tests using an axisymmetric model. Nygards et al. (1998) examined the adhesion of a cermet coating by using several indentation tests to determine the highest survivable indentation load. This load was then used during ABAQUS simulations of the indentation test and the maximum normal stress at the coating-substrate interface was used to define the interface strength. Xu et al. (2006) studied the nano-indentation of a magnetron sputtered TiN PVD coating on substrates of varying hardness using ANSYS. Sun et al. (2008) used indentation test of increasing load to determine the critical load for delamination of a hard oxide scale. The critical load was used in ABAQUS simulations of the indentation test to determine the peak normal and shear stresses produced at the coating-substrate interface.

For the scratch test, the combination of experimental testing and numerical simulation has also been used to study coating adhesion. Li and Beres (2005) simulated the scratch test of a TiN coated titanium alloy using a three-dimensional finite element model in MSC.Patran and MSC.Marc to determine the stresses in the coating at the coating-substrate interface. Compressive stress in the coating and shear stress at the coating-substrate interface were determined to be the probable cause of coating failure observed during experimental testing. Similarly, Jiang et al. (2001) examined the adhesion of a TiN PVD coating using experimental and numerical analysis. The critical load for coating failure was determined using micro-scratch tests and it was used in two and three-dimensional finite elements simulations performed in ANSYS. The shear stress at the coating-substrate interface was found to be the primary cause of coating delamination.

In this thesis, the combination of experimental testing and finite element simulations of both the indentation and the scratch adhesion tests is used to quantify the adhesion of the PVD coating used by the RCM. The adhesion to a mirror polished surface and to four laser frosted surfaces are examined. The critical loads determined during experimental testing are used in the finite element simulations. The maximum opening stress, maximum shear stress and maximum compressive stress values at the coating-substrate interface determined from finite element simulations are used to characterize the adhesion strength.

1.1 Thesis Objectives

The objective of this thesis is to characterize the adhesion of the Cr-Ti-N coating used by the RCM on minting dies. The performance of the coating on polished and laser frosted surfaces is examined using experimental testing and corresponding finite element simulations. The suitability of indentation and scratch adhesion testing is analyzed for each surface finish. Finite element simulations of indentation and scratch tests at critical loads found during experimental testing are performed to determine the stresses at the coating-substrate interface prior to coating adhesion failure. The maximum opening, shear, and compressive stresses at the coating-substrate interface will be used to quantify the coating adhesion strength.

1.2 Thesis Outline

Chapter 2 provides background information on the PVD coating and laser frosting processes, followed by a review of adhesion experimental testing and numerical simulation focusing on indentation and scratch adhesion testing. Chapter 3 details the Rockwell-C

indentation, the stepped indentation, and the scratch adhesion tests performed on five different coated die surface finishes. The test procedures are presented and the results are reported. Chapter 4 documents the finite element simulation of indentation tests using a two-dimensional axisymmetric model and the critical loads found during stepped indentation adhesion testing. The maximum stresses at the coating-substrate interface are obtained. In Chapter 5, the three-dimensional finite element simulation of the scratch adhesion test is presented. The critical loads determined during experimental scratch testing are used as the scratch load and the maximum stresses at the coating-substrate are presented. The important maximum stress components found during the indentation and scratch simulations are then compared. Chapter 6 presents the major conclusions determined in this thesis and provides recommendations for future research.

Chapter 2: Background and Literature Review

In this chapter, the PVD coating and laser frosting processes are examined and their importance in the minting industry is outlined. This is followed by an examination of the adhesion of thin-film systems and the testing of their adhesion. A detailed review of the use of experimental adhesion testing combined with numerical simulations to quantify the stresses produced during testing is presented for the indentation and scratch adhesion tests.

2.1 PVD Coating Process

PVD coatings are used in industrial applications to increase surface hardness, wear resistance, and reduce the need for lubricant when machining. By depositing a hard and wear resistant material onto a softer substrate, part life and cutting speeds can be increased (Martin, 2010).

The PVD coating process occurs in a vacuum chamber where coating material is vaporized from what is called a target and this vaporized material later condenses on the material being coating, called the substrate. Low pressure is achieved within the chamber using a multistage pump system and inert gas is pumped into the chamber to ensure the removal of unwanted gases. The material to be deposited is vaporized using evaporation or sputtering techniques. The vaporized material, being either ionized or neutrally charged, makes its way to the part being coated and is deposited. The deposited material can also include some of the gas being pumped into the chamber (Martin, 2010).

The most common PVD coating processes are cathodic arc deposition, electron beam deposition, evaporative deposition, pulsed laser deposition, and sputter deposition. The

process used by the RCM is a variation of the sputter deposition method called closed field unbalanced magnetron sputter ion plating. This process is explained in Appendix A of this thesis. The PVD coating parameters are controlled to ensure adequate adhesion is achieved.

2.2 Laser Frosting Process

Although traditionally, PVD coatings are applied to polished machined surfaces, laser processed surfaces can also be used. Laser texturing and engraving is used in die manufacturing to form small features. The use of laser machining can reduce manufacturing time, eliminate tool wear, and is highly accurate and repeatable. The RCM has incorporated laser machining processes into die manufacturing. Detailed features can be created using laser engraving and surface textures can be formed using laser frosting techniques.

The laser machining process is an automated process where a high energy laser is applied to the part and a small amount of material is vaporized. The laser assembly focuses photons onto a small area using a lens and gas pressure is applied to create the gas flow needed to remove the vaporized material. The source of photons is traditionally a lamp or diode. The laser is often pulsed to minimize or eliminate the heat effect zone on the part surface (György et al, 2002). Surface defects and inclusions are preferentially vaporized during laser machining potentially leading to a higher then desired surface roughness (Li et al., 2006). Surface roughness increases with laser intensity and can be reduced by increasing the number of laser pulses and reducing laser intensity (Li et al., 2006).

In addition to testing the adhesion of the PVD coating on a polished mirror surface, the coating adhesion to four types of laser frostings will also be studied in this thesis. Figure 2.1 shows four dies used for testing in this thesis. Each die has one of the four laser frostings on

three quarters of the die surface, while the other one quarter remained an unfrosted polished mirror surface. The four laser frostings are named Bullion (BUL), Glass Bead (GB), Aluminum Oxide (AlOx) and Four-to-One (4:1) and are applied before the coating to produce surface finishes desired by the RCM. The laser frosted surfaces are shown at 1000X magnification using an optical microscope in Figure 2.2. The Bullion and Glass Bead laser frostings appear significantly smoother than the Aluminum Oxide and Four-to-One laser frostings. The laser frostings have been found to reduce the life of minting dies due to coating failure. The reduction in die life is believed to be caused by a reduction in coating adhesion strength (Bodor, 2010).

2.3 Adhesion of Thin-Film Systems

Depositing a thin hard film onto a softer substrate is only beneficial if the film has good adhesion and does not fail during normal operation. For this reason, coating adhesion must be closely examined and well understood.

Adhesion is defined as an attractive process between dissimilar materials which brings two compounds into direct contact. The strength of adhesion is difficult to quantify, but can be determined qualitatively, semi quantitatively, and under certain scenarios quantitatively using various adhesion tests. The adhesion measurement between two materials estimated during experimental testing is generally dependent on the test method employed to determine it. For this reason, adhesion test results must be stated with the method used to determine them. Common adhesion test methods are the indentation test, scratch test, peel test, tape test, blister test, self loading test, beam bending test, pull test, and laser spallation test (Lacombe, 2006). The indentation and scratch adhesion tests are reviewed below, while

the other tests are briefly explained in Appendix B of this thesis. Indentation and scratch adhesion tests will be used in this thesis to quantify the adhesion strength of the PVD coating.

2.4 Indentation Adhesion Test

Indentation testing was first developed to quantify the hardness of materials. By applying a specific load using a standardized indenter, the hardness of a material can be determined by measuring the size of the resultant indentation crater and/or the vertical displacement of the indenter. Several varieties exist and the following is a list of the most common indentation tests:

- Brinell hardness test (ASTM E10-10, 2010)
- Rockwell hardness test (ASTM E18-08b, 2008)
- Vickers hardness test (ASTM E384-11, 2011)
- Knoop hardness test (ASTM E384-11, 2011)

Indentation tests can also be used to test the adhesion of coatings. The procedure is very similar to indentation tests completed to determine hardness except instead of measuring the indentation size, the damage caused to the coating is examined. A schematic of an indentation adhesion test is shown in Figure 2.3 and the apparatus used for testing in this thesis is shown in Figure 2.4. The advantages of this test method are:

- sample preparation is minimal
- the test equipment is readily available (cost effective)
- test standards are well established
- semi-quantitative or quantitative results can be achieved

2.4.1 Experimental Indentation Adhesion Testing

Indentation adhesion tests have been used by various researchers to investigate the adhesion of PVD coatings. The following is a review of one such research work.

Heinke et al. (1995) performed Rockwell-C adhesion tests on three types of sputtered PVD coatings (TiN, CrN and Cr_2N) to investigate their adhesion. All coatings were deposited onto a SAE 52100 steel polished and hardened surface. The effect of coating thickness was examined by using three deposition times (60 min, 120 min, 240 min) for each coating type. The produced coating thicknesses varied from approximately 1.5-25 μm. Rockwell-C indentation adhesion tests were completed following the VDI Guideline 3198 (1991). The indentation craters were examined using an optical microscope and compared to the reference craters shown in Figure 2.5. The damage is graded between HF 1 and HF 6, HF 1 being very good adhesion and HF 6 being very poor adhesion. Adhesion values from HF 1 to HF 4 represent adequate adhesion and a pass of the test, while HF 5 and HF 6 are deemed to have poor adhesion and fail the test due to significant delamination. Figure 2.6 shows one indentation crater for each coating type along with their respective adhesion quality measurement. Coating cracking is visible around the TiN crater while significant delamination is found around the CrN and Cr_2N craters. The Rockwell-C indentation adhesion testing found that the TiN coating had the best adhesion with results ranging from HF 2 to HF 3. All the CrN and Cr_2N coatings tests were graded HF 6 and failed the adhesion test. The coating thickness was found to not significantly affect the Rockwell-C results.

2.4.2 Finite Element Analysis of indentation adhesion testing

In order to further understand the causes of coating failures during indentation adhesion testing the stress state in the coating can be determined using finite element analysis. Radial and circular cracking the coatings has been studied by examining the tangential and radial stresses induced during indentation. This provides insight into through thickness coating failure. Delamination along the coating-substrate interface (adhesion failure) has been studied by examining the shear and opening stresses at the interface. Compressive stress in the coating are also be studied if buckling failure of the coating is present in experimental testing. The following provides a review of finite element analysis of indentation adhesion tests conducted by several researchers.

Pachler et al. (2007) studied the maximum stresses developed during Rockwell-C indentations of a TiN PVD coated high-strength tool steel. Experimental testing showed that the radial and tangential stresses caused circular and radial cracking. Figure 2.7 shows an example indentation with radial and circular crack, while Figure 2.8 defines the crack types and important stress components. The radial cracks are not continuous across the circular cracking, which indicates that circular cracking occurs prior to radial cracking. In Pachler et al. (2007), ABAQUS 6.5 was used to model the Rockwell-C test using an axisymmetric model discretized using three and four node elements. The model is highly refined near the indentation site as can be seen in Figure 2.9. The coating section is defined as being perfectly adhered to the substrate section. The substrate and coating material were modeled as elastoplastic materials using a plastic modulus of 1 GPa until 20% plastic deformation is reached. TiN coatings are sometimes defined as a purely elastic material, but if this simplification is made when simulating the indentation test, a large overestimation of the

coating stresses occurs (Piana et al., 2005). Examining stress components during loading and unloading, radial stress was found to reach a peak during maximum loading, while the tangential stress reaches a peak after unloading. This timeline agrees with the experimental results which show that circular cracks occur prior to radial cracking.

Nygards et al. (1998) focused on quantifying the coating-substrate interfaces adhesion strength by estimating the opening stress at the coating-substrate interface. A 250 μm thick cermet coating (80% Cr_3C_2, 20% Ni-Cr) underwent a series of indentations with the load being increased in steps of 5 N until a delamination was indentified. The maximum survivable indentation load without delamination was found to be 150 N. The indentation test was simulated using ABAQUS with the 150 N threshold load being used as the indentation load. The indentation test geometry was modeled using a two-dimensional axisymmetric model. Four node bilinear axisymmetric elements were used to discretize the geometry with greater mesh refinement in the vicinity of the indentation zone. The coating-substrate interface was modeled as perfect adhesion since delamination did not occur during experimental testing using a 150 N indentation load. The interaction between the indenter and the coating surface was modeled using the standard contact algorithm in ABAQUS. The indenter was defined as the master surface and the substrate as the slave surface. Friction between the two surfaces was neglected. The coating and substrate materials were defined as elastoplastic. The tensile opening stress at the coating-substrate interface after removal of the indentation load was defined as the critical stress for delamination failure. Using the opening stress, the interfacial strength was estimated to be between 78 and 102 MPa.

Xu et al. (2006) modeled the nano-indentation of a magnetron sputtered TiN coating on substrates of different hardness values. Finite element analysis was completed using an

axisymmetric model defined in ANSYS with perfect adhesion between the coating and substrate. A friction coefficient of 0.03 is defined between the coating and the indenter surfaces. The materials are defined as elastoplastic. The model was discretized using four node elements. The tensile radial stress and shear stress at the coating-substrate interface was found to be significantly reduced for coatings deposited on harder substrates.

Sun et al. (2007) used a stepped indentation process where indentation tests are performed under several loads to determine the critical load for the delamination of an oxide scale. First, ABAQUS was used to simulate indentation testing with the coating and substrate being defined as elastic materials. A small crack was defined at the coating-substrate interface and the stress intensity factors K_I, K_{II}, and K_{III} were determined. As shown in Figure 2.10, Mode I is the opening mode driven by tensile opening stresses normal to the coating-substrate interface, Mode II is the shear mode driven by shear stress acting in the plane of the coating-substrate interface, and Mode III is the tearing mode driven by out of plane shear stress. Mode III was found to be insignificant due to the indentation being axisymmetric. K_{II} was found to be at least double K_I for all loading conditions and therefore the shear mode (Mode II) was found to be the dominant mode of the extension of interface cracks. Then Sun et al. (2007) used a second model with more realistic elastoplastic material properties and no interface cracking to determine the critical shear stress at the interface. It is important to note that the shear stress provided by ABAQUS is in the global coordinate system and a coordinate transformation is required to calculate the shear stress along the interface.

In this thesis, indentation adhesion tests will be performed to obtain the critical load at which adhesion failure occurs for the PVD coating on each die surface. These loads will

then be used in finite element analysis. The corresponding maximum opening, shear, and compressive stresses at the coating-substrate interface will be used to quantify the coating adhesion.

2.5 Scratch Adhesion Test

The scratch test is another adhesion test method which performs well on thin hard coatings. A schematic of the scratch adhesion test is shown in Figure 2.11 and the apparatus used for testing in this thesis is shown in Figure 2.12. During the test, a loaded stylus is drawn across the coating surface and the load is increased linearly along the path or is increased on subsequent passes. The scratch path is then examined to determine if a coating failure has occurred, and if yes, at what loading condition. Depending on the apparatus, failure can be monitored using acoustic emission, frictional force measurement, or examined under microscope after the scratch test. Multiple failures types can occur during scratch testing (see Figure 2.13) and appropriate failure criteria must be chosen. The adhesion strength of the coating-substrate interface is defined semi-quantitatively by load at which adhesion failure occurs. Significant variability is common in scratch adhesion testing with measurement uncertainties of 20% with a 95% confidence interval being typical (ISO 20502:2005(E), 2005). The following two sections provide a review of experimental and finite element analysis methods for characterizing coating adhesion using the scratch adhesion test.

2.5.1 Experimental Scratch Adhesion Testing

In addition to the indentation adhesion testing discussed in section 2.4.1, Heinke et al. (1995) performed scratch adhesion tests on the same PVD coated samples. Five scratch tests

were performed on each sample. A Rockwell-C indenter was used as the stylus and normal load, acoustic emissions, and frictional force were all measured during the stylus translation. The scratch paths were evaluated using an optical microscope and the failure loads for the following three failure criteria were determined: first cracking of the coating, first delamination at the edge of the scratch path, and first point where the substrate was revealed in the scratch path. An example of the failure of each coating type (TiN, CrN, and Cr_2N) tested is shown in Figure 2.14. The TiN coating was found to have the highest failure loads and much smaller delamination failures than the CrN, and Cr_2N coatings. These results were attributed to superior adhesion and ductility of the TiN coating. Coating cracking was attributed to tensile stress behind the indenter, while coating delamination was attributed to compressive stress in front of the indenter. Comparing the critical load values determined using an optical microscope to results determined using friction and acoustic data it was found that the results were only comparable when the coating thickness was greater than 5 μm.

2.5.2 Finite Element Analysis of scratch adhesion testing

In order to further analyze the failure of coating systems due to scratch adhesion tests, finite element analysis of the tests can be performed. Opening stress, shear stress, and compressive stress at the coating-substrate interface must also be examined to evaluate coating adhesion.

Li and Beres (2005) performed a three-dimensional finite element analysis of the scratch adhesion test of a 5 μm TiN coated titanium alloy to determine the stress state at the top of the coating, in the center of the coating, and at the coating-substrate interface. MSC.Patran and MSC.Marc program were used for the finite element analysis and ABAQUS /Standard Ver. 6.4 was used for comparison. Figure 2.15 shows the three-dimensional model used and

mesh refinement can be seen near the path. Only half of the scratch path need be modeled due to the symmetry of the test. The coating and substrate were modeled as elastoplastic materials following a bilinear law with isotropic hardening. The indenter was modeled in the shape of the Rockwell-C indenter and was defined as perfectly rigid. The coating and substrate were defined as perfectly bonded and roughness and residual stresses were neglected. Coulomb friction was defined between the indenter and coating surfaces with a friction coefficient of 0.26. A convergence study was performed and found that an element size of approximately half the coating thickness was acceptable. The indenter motion and loading rate was defined to match the European standard EN 1071-3 (2005) with a loading rate of 10 N/min and a transverse speed of 10 mm/min. Large compressive stresses were found to occur in front of the indenter which can cause buckling and delamination of the coating. Opening stress normal to the coating-substrate interface was found to be quite small, but the shear stress along the coating substrate interface was found to be the probable cause of coating adhesion failure.

Jiang et al. (2001) analyzed the effect of varying the coefficient of friction between the indenter and coating surface on the coating stress state and found that higher coefficients of friction lead to slightly higher stress values. Scratch simulations were completed in ANSYS using two and three-dimensional models. The coating was defined as an elastic material while the substrate was defined as elastoplastic. The indenter was translated with the load held constant at the critical loading condition found during experimental testing to simulate the critical stresses. Compressive stresses were found in front of the indenter scratch path, while tensile stresses occurred behind the indenter. High interfacial shear stress was found at

the coating-substrate interface and this stress component was deemed the probable cause of the coating-substrate interface failure.

In the present research, scratch adhesion tests will be used to establish the maximum load that can be applied before coating adhesion failure. Three-dimensional finite element simulations of scratch tests will then performed using the critical loads determined from experimental testing. The maximum opening, shear, and compressive stresses at the coating-substrate interface will be determined for the critical load conditions.

2.6 Summary

In this chapter, background and literature review of PVD coatings and methods of testing their adhesion were presented. In particular, the combination of experimental testing and numerical simulation of indentation and scratch adhesion tests was reviewed. In the following chapters, these techniques are used to quantify the adhesion of the PVD coating used by the RCM on a mirror polished die surface and on four laser frosted die surfaces.

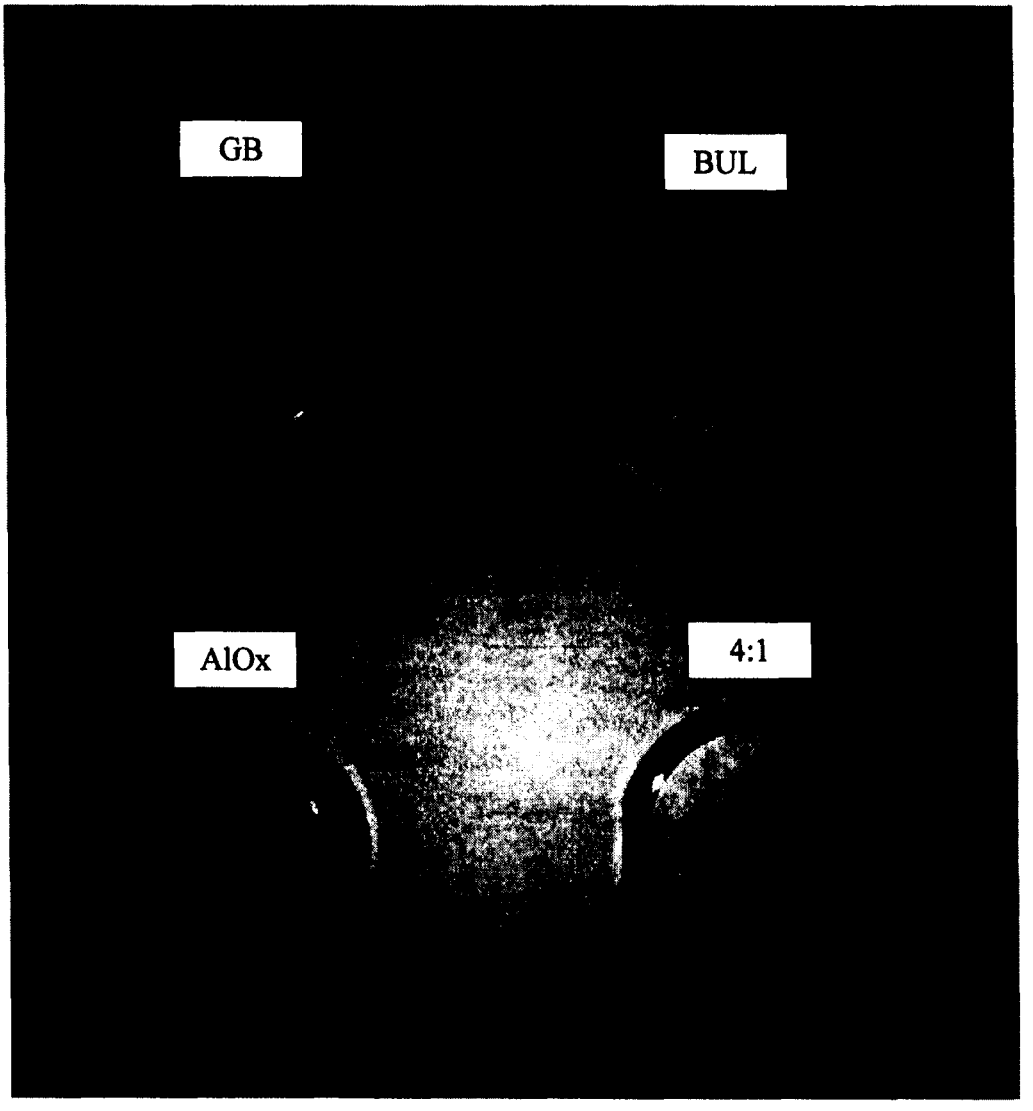

Figure 2.1: Test dies with three-quarter laser frosted surfaces

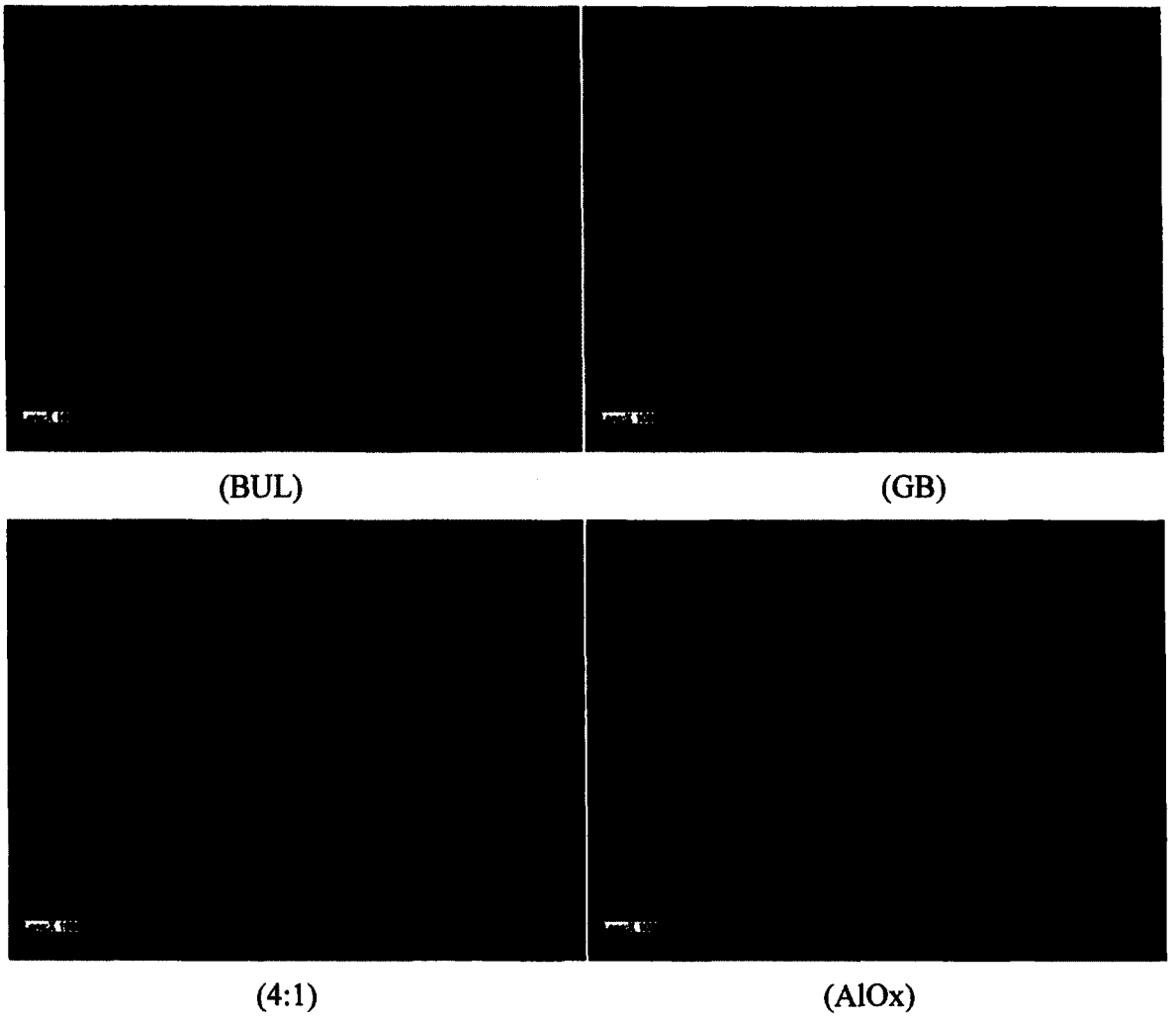

Figure 2.2: Laser frostings at 1000X magnification

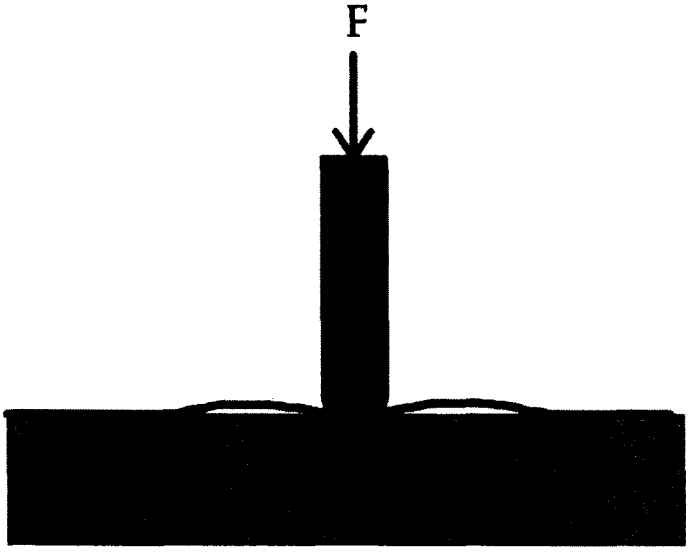

Figure 2.3: Schematic of indentation test causing coating adhesion failure (Lacombe, 2006)

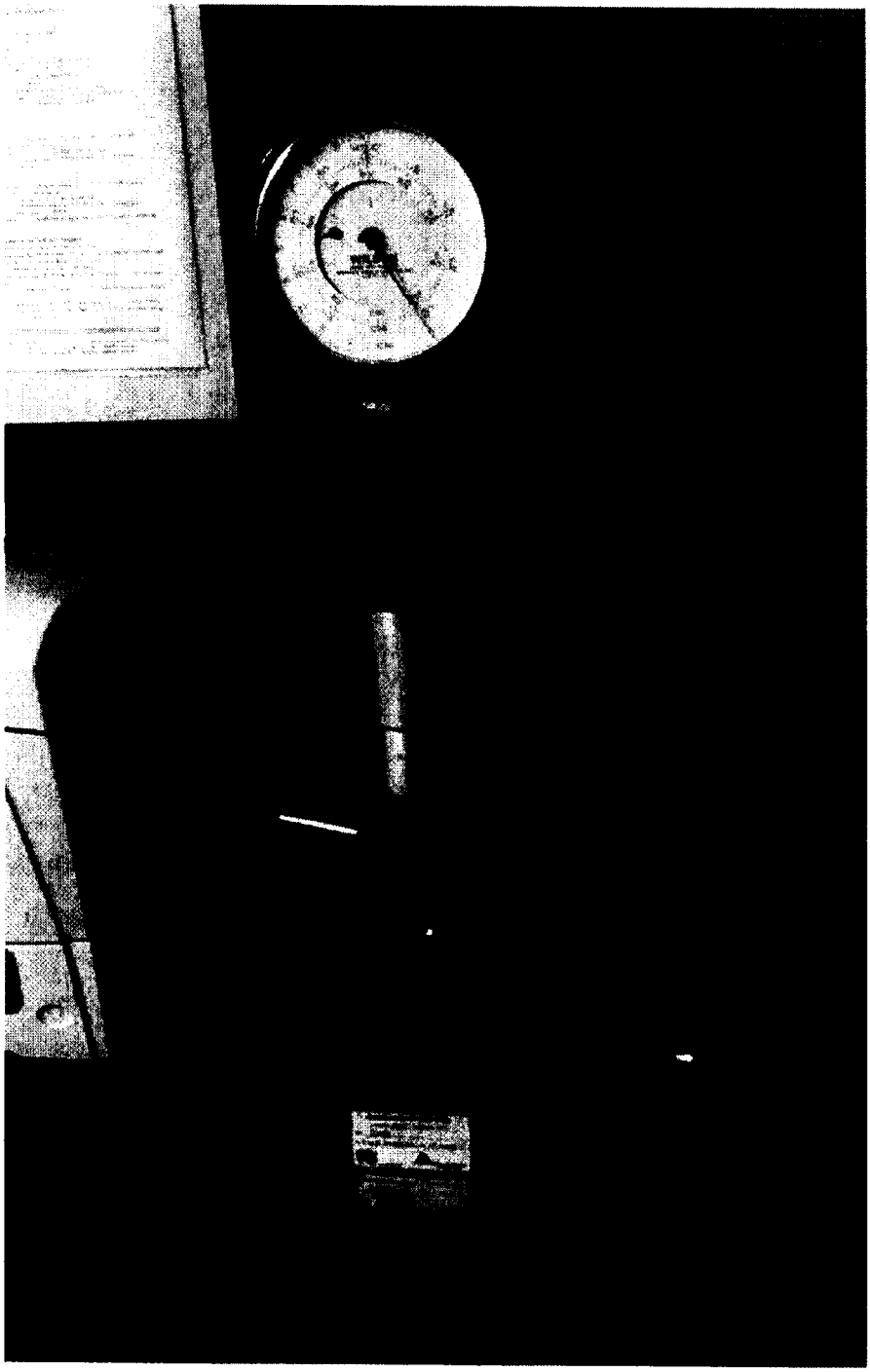

Figure 2.4: Wilson Rockwell 3TT Twin Hardness Tester

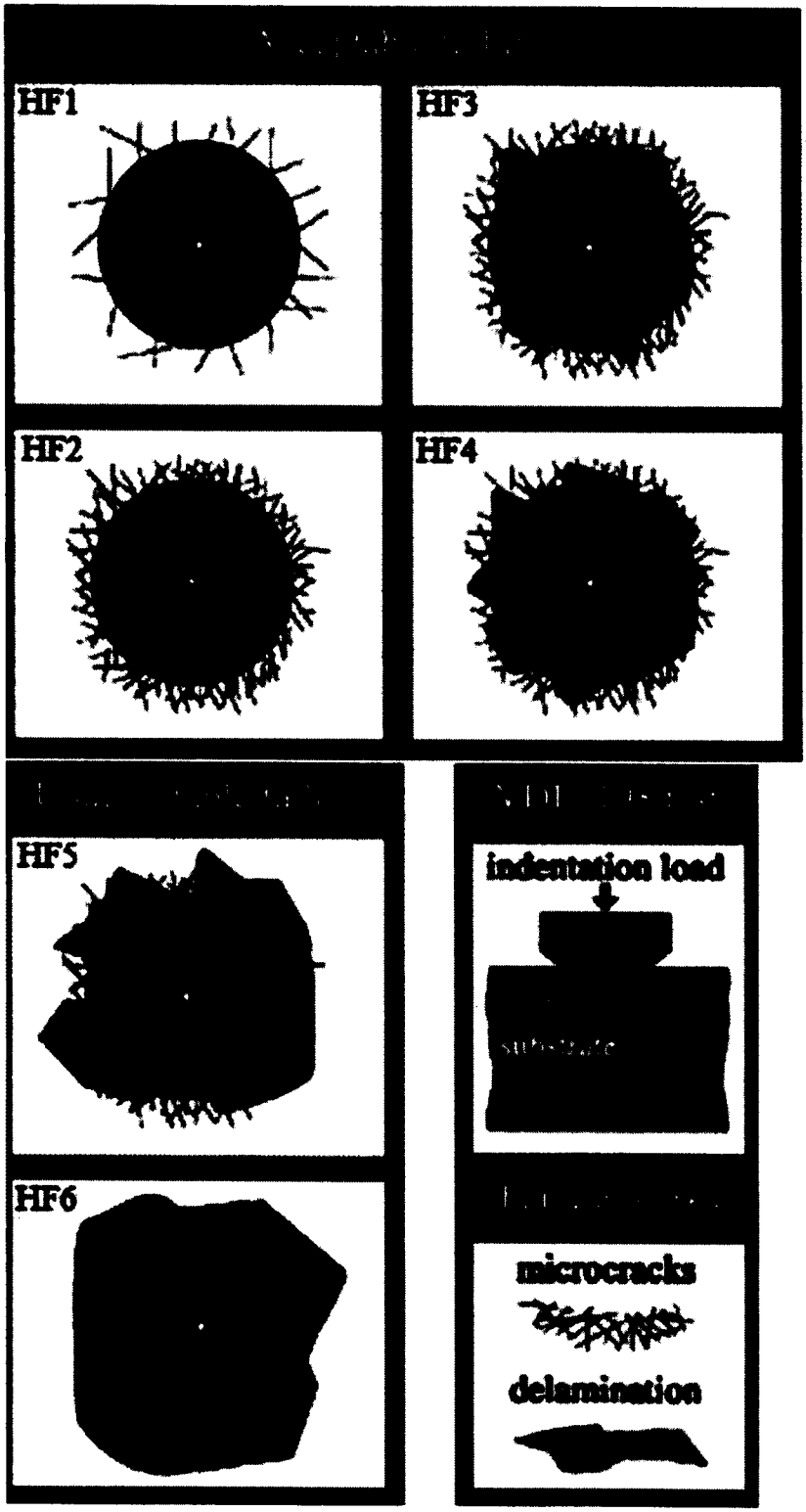

Figure 2.5: Rockwell-C adhesion test grading as defined by VDI Guideline 3198 (1991)

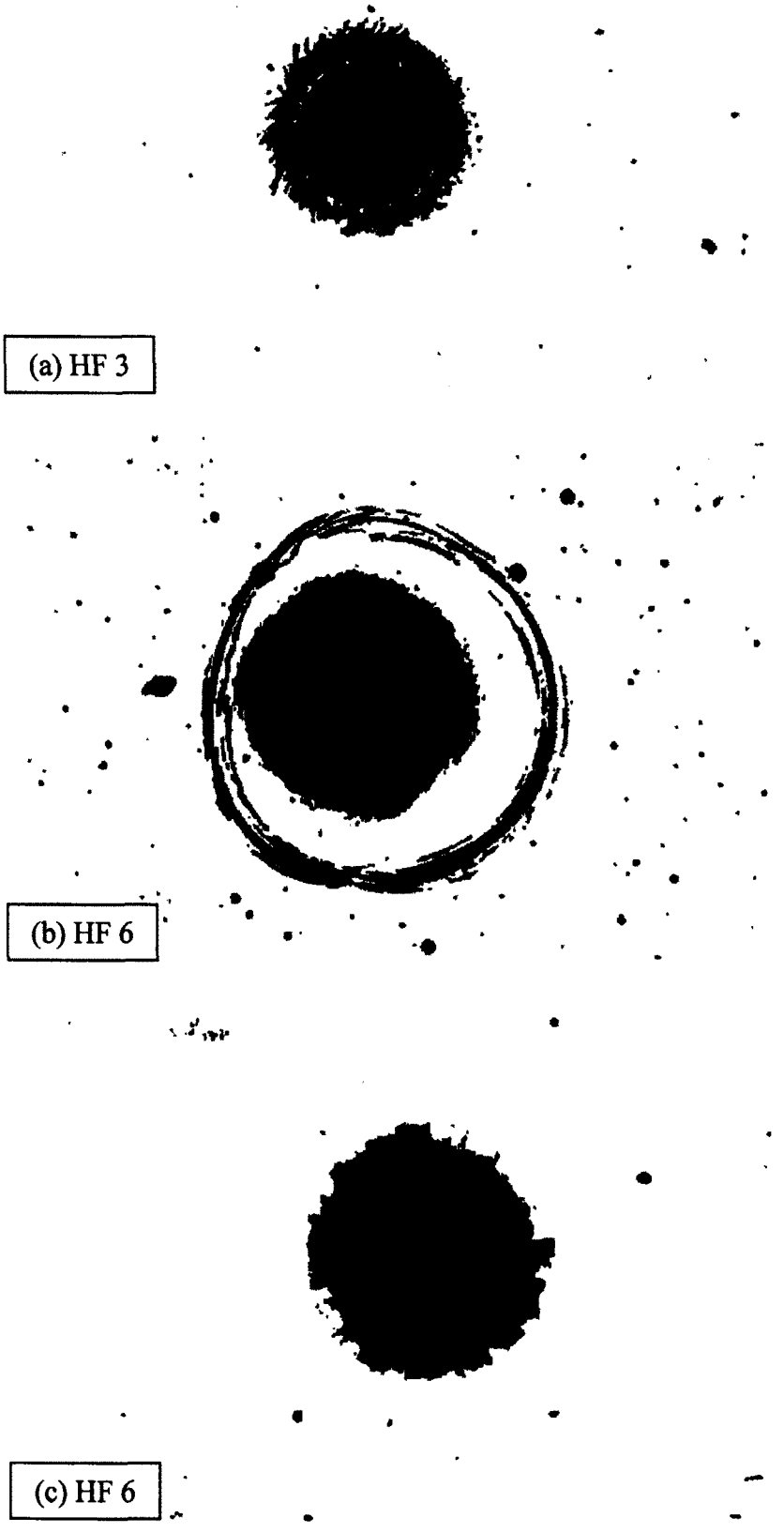

Figure 2.6: (a) TiN 240 min deposition and 3.88 μm coating thickness, (b) Cr_2N 240 min deposition and 22.45 μm coating thickness, (c) CrN 60 min deposition and 5.08 μm coating thickness (Heinke et al., 1995)

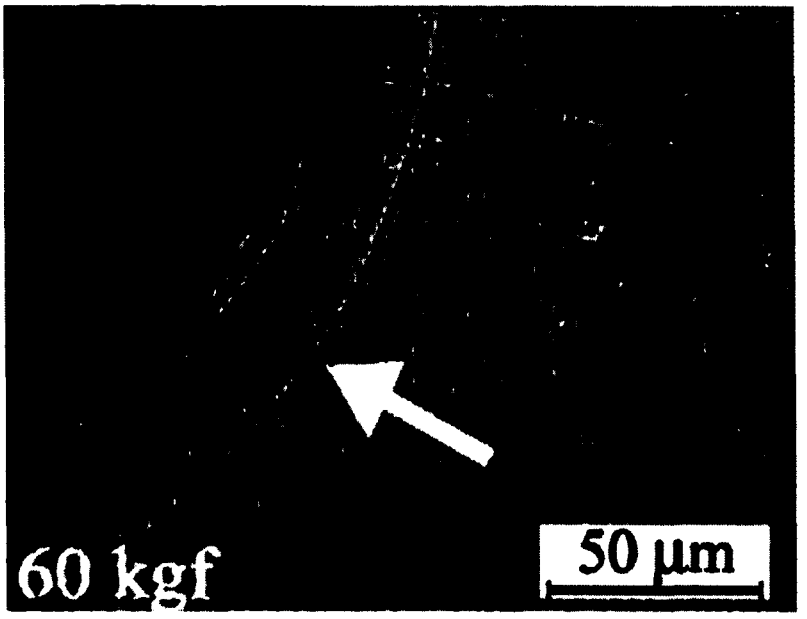

Figure 2.7: Radial and circular cracks at the indentation edge, of a H13 steel nitride for 3 hours and coated with TiN. The black arrow indicates a radial crack, while the white arrow indicates a circular crack (Ribeiro, 2003)

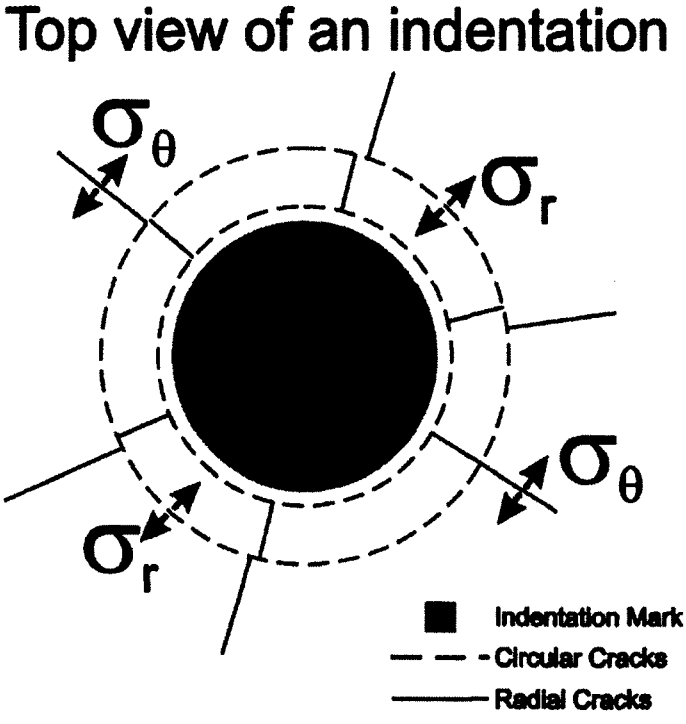

Figure 2.8: Top view of an indentation mark, σ_r is the radial stress and σ_θ is the tangential stress (Pachler et al., 2007)

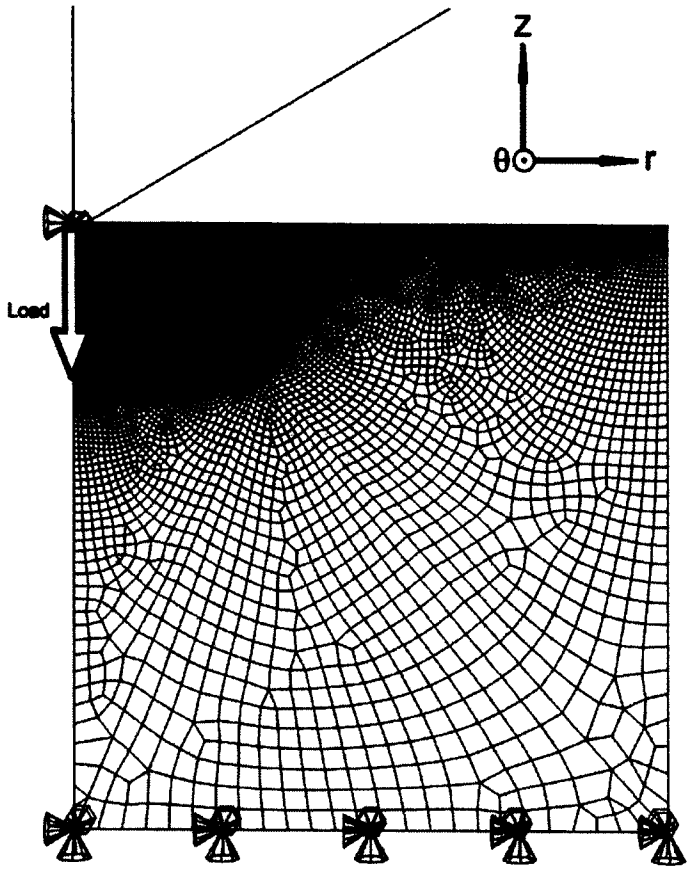

Figure 2.9: Axisymmetric finite element model of indentation adhesion test (Pachler, 2007)

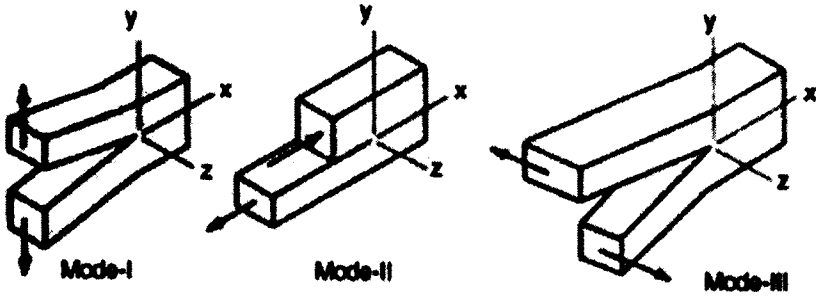

Figure 2.10: Delamination failure modes (Benham et al., 1996)

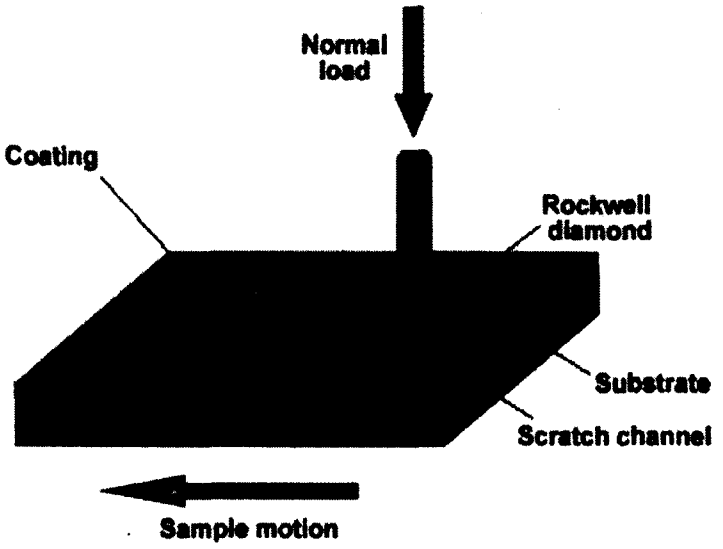

Figure 2.11: Scratch adhesion test schematic (Lee, 1991)

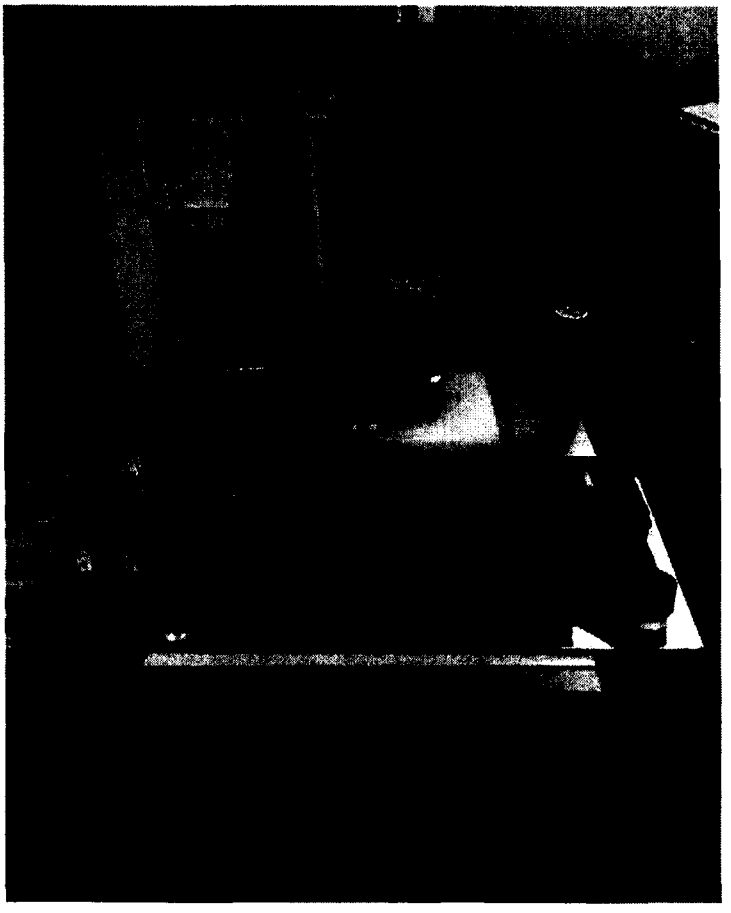

Figure 2.12: Teer Scratch Tester

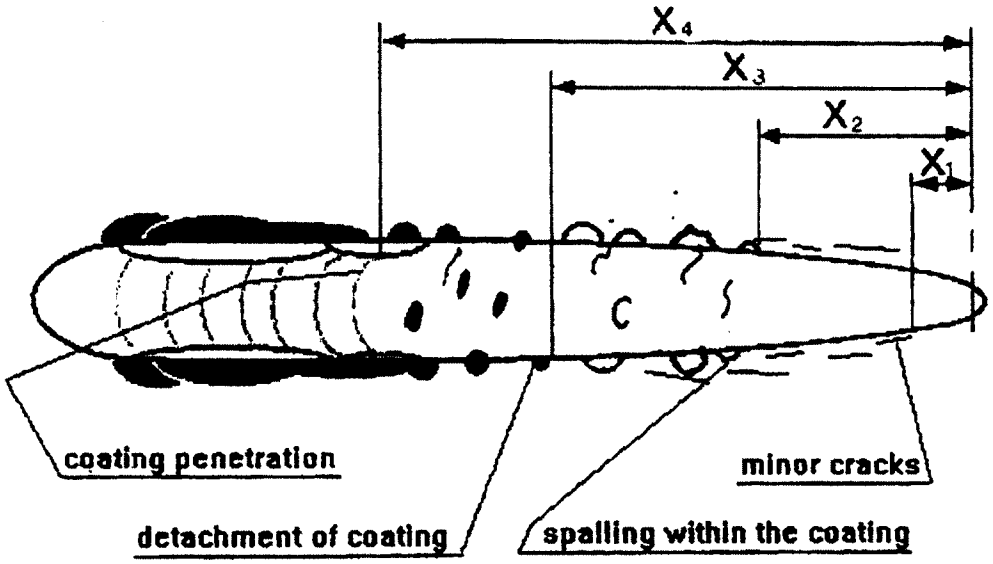

Figure 2.13: Schematic of the possible failures during scratch adhesion testing (Meneve et al., 2001)

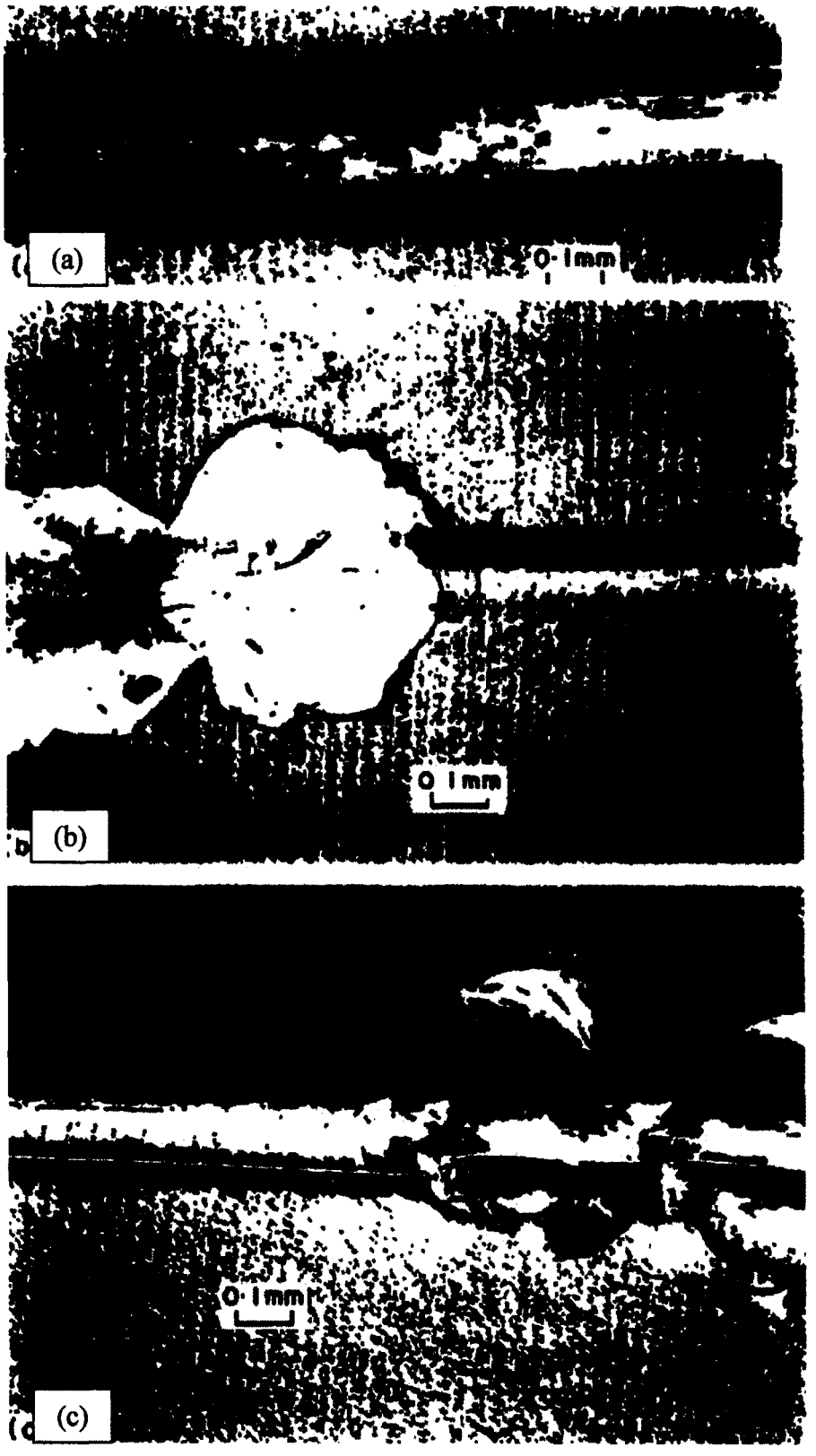

Figure 2.14: (a) TiN 1.54 μm coating thickness, 30-40 N load, (b) Cr_2N 5.08 μm coating thickness, 15-22 N load, (c) CrN 6.54 μm coating thickness, 20-30 N load (Heinke et al., 1995)

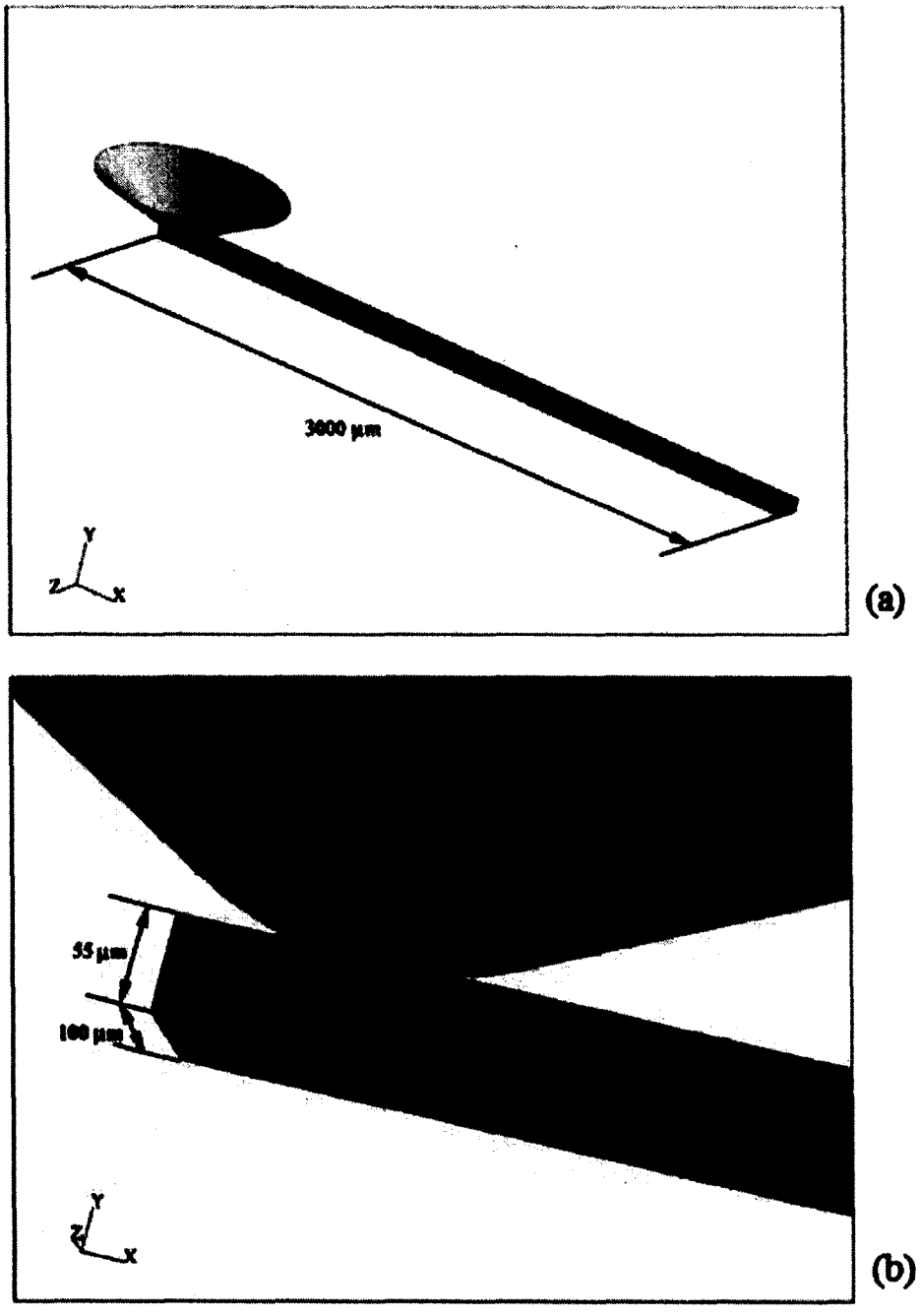

Figure 2.15: Three-dimensional model for simulating the scratch adhesion test, (a) overall model, (b) detail near the indenter tip (Li et al., 2006)

Chapter 3: Experimental Testing of Coating Adhesion

This chapter presents the experimental setup, procedure, and results of the adhesion testing completed on the hard PVD coating used by the RCM. Eight dies were prepared and the adhesion of the coating to a mirror surface and to four laser frosted surfaces was investigated using three different adhesion tests. These tests are the Rockwell-C indentation adhesion test, a stepped variation of the Rockwell-C indentation adhesion test, and the scratch adhesion test.

3.1 Sample Preparation

The dies used for testing were machined from a soft annealed bar stock of a tool steel. The bar stock was first cut to length and the top and bottom surface were machined flat using a lathe. The machined substrates were then heat treated using a vacuum heat treatment furnace. The top surface of the substrates was then polished to a mirror surface. In total eight test dies were manufactured. Four of the eight dies were laser frosted on three quarters of their surface, each with a different surface frosting (Bullion, Glass Bead, Four-to-One, and Aluminum Oxide) as shown in Figure 2.1. The remaining four were not laser frosted. After preparing the die surface, the hard PVD coating was applied using a Teer UDP650/4 magnetron sputter ion plating system. The thickness of the Cr-Ti-N PVD coating is controlled to between 2 and 3 μm.

3.2 Rockwell-C Indentation Adhesion Test

This section outlines the procedures and results for the Rockwell-C indentation adhesion test. The Rockwell-C indentation adhesion test is a commonly used test to verify the

resistance to detachment of a coating. The test is simple and requires less time than other techniques which makes it ideal for quality control purposes. Multiple Rockwell-C indentation adhesion tests were completed on each of the eight dies in order to semi-quantitatively analyze the adhesion of the coating on the five different die surface finishes.

3.2.1 Experimental Setup

The Rockwell-C adhesion test begins by following the Rockwell C hardness test procedure as described by ASTM standard E18-8b (2008) and finish with an examination of the indentation using guidelines prescribed by VDI Guideline 3198 (1991). A Wilson Rockwell 3TT Twin hardness tester (shown in Figure 2.4) equipped with a Rockwell-C indenter was used to perform the indentations. The indentations were then examined using a Carl Zeiss Axiovert 200 Max inverted microscope fitted with Sony ExwaveHAD video camera (see Figure 3.1).

3.2.2 Procedure

First the die surface was cleaned using isopropyl alcohol and then placed on the test platform. Weights equivalent to 150 kg_f were mounted on the back of the apparatus and a Rockwell indenter was mounted in the indenter holder. The test platform was raised until a preload defined by the apparatus is reached. The indentation load (150 kg_f) is then applied to the die surface. Once a steady indentation depth is reached, the applied load is removed. It is important to note that prior to using the Rockwell-C hardness tester, a reference block was used to ensure the apparatus was properly calibrated.

The indentation crater was then examined under an optical microscope and damage to the coating-substrate system was graded from HF1 to HF6 using the VDI Guideline 3198 (1991)

shown in Figure 2.5. HF being the German short form of adhesion strength. The grading provides a semi-quantitative assessment of the coating adhesion strength. The six levels of adhesion, HF1 being the best adhesion and HF6 being the worst, are defined as:

HF1 - Minor microcracking and no delamination

HF2 - Significant microcracking and no delamination

HF3 - Significant microcracking and minor delamination

HF4 - Significant microcracking and delamination within the microcracked area

HF5 - Significant microcracking and delamination extending past the microcrack region

HF6 - Delamination around entire circumference

In most applications adhesion results from HF1 to HF4 are deemed sufficient adhesion and a pass, while adhesion value of HF5 and HF6 are deemed insufficient adhesion and a failure.

3.2.3 Results

Multiple indentation tests were performed on each die to verify the consistency of the results. Indentations were performed near the centre of the die, halfway between the centre and the die edge (1/2 radius) and near the edge of the die. The four coated mirror surface dies were named Mirror_1 to Mirror_4 and the laser frosted dies were named after their laser frosting type (¾_Bul, ¾_GB, ¾_4:1, ¾_AlOx). A complete list of the Rockwell-C indentation adhesion tests completed can be seen in Table 3.1 and a summary is presented in Table 3.2. Observations from the five different die surfaces are summarized in the following subsections.

PVD coating deposited on a mirror surface

The results for the PVD coating deposited onto a mirror surface show that good adhesion is achieved. All test results were a pass with 80% of the indentations falling within the HF3 category and the remaining 20% in the HF4 category. Figure 3.2 and Figure 3.3 show representative examples of indentation graded HF3 and HF4 respectively. Microcracking was significant in all cases and delamination was contained within the microcracked region.

PVD coating deposited on a Bullion type laser frosted surface

All indentation adhesion tests of the PVD coating deposited on the Bullion type laser frosted surface were graded HF3. Minor microcracking and small delaminations are visible at high magnification (see Figure 3.4).

PVD coating deposited on a Glass Bead type laser frosted surface

The results for the Glass Bead tests were very similar to the Bullion tests with both getting adhesion values of HF3. The delaminations are slightly larger for the Glass Bead tests than the Bullion tests (see Figure 3.5).

PVD coating deposited on a Four-to-One type laser frosted surface

The PVD coating deposited on the Four-to-One type laser frosting did not pass the Rockwell-C indentation adhesion test and received a grade of HF6 for all tests. Figure 3.6 shows the delamination at the edge of the indent that goes around the entire indentation circumference. The rough surface of the Four-to-One sample helps disguise the delamination, but it is clearly visible at higher magnification.

PVD coating deposited on a Aluminum Oxide type laser frosted surface

The Aluminum Oxide frosted sample gave inconclusive results. As can be seen in Figure 3.7 the severe roughness of the surface does not lend itself to the Rockwell-C indentation adhesion test.

3.3 Stepped Indentation Adhesion Test

The stepped indentation adhesion test is a variation on the Rockwell-C indentation adhesion test. The indentation load is increased in steps and the produced indentation craters are examined for signs of coating failure. Coating delamination was defined as the failure criteria and the highest loading case which causes no coating delamination was examined for each coated die surface. The maximum survivable load provides a semi-quantitative measurement of the PVD coating adhesion and will also be used in Chapter 4 during finite element simulations. The maximum survivable load will be the indentation load used in simulations of indentation tests examining the stress state at the coating-substrate interface prior to coating adhesion failure.

3.3.1 Experimental Apparatus and Procedure

The experimental apparatus is the same as that used for the Rockwell-C indentation adhesion tests, but for this test multiple loading conditions were used. The available weight options were 15, 30, 45, 60, 100, 150 kg_f and all were used. Coating failure was defined as any visible delamination of the coating.

3.3.2 Results

Multiple indentation tests were performed on each different die surface to determine the maximum load at which the respective coating-substrate systems could withstand. More tests were performed at loadings where the coating changed from a pass to a fail. The stepped indentation results for the PVD coating on the mirror surface and laser frosted surfaces are shown in Table 3.3 and Table 3.4 respectively. The following subsections provide observations for each die surface.

PVD coating deposited on a mirror surface

A summary of the results for the stepped indentation test of the PVD coating deposited on a mirror surface is shown in Figure 3.8. The indentation tests using a 45 kg_f load caused a delamination for half of the 14 tests and the tests performed using a 30 kg_f load only caused one delamination out of 14 tests. The typical results for indentations of 15, 30, and 45 kg_f can be seen in Figure 3.9. Cracking is visible around the circumference of the indent crater and small radial cracks are also visible. Figure 3.10 shows the typical results of indents using 60, 100, and 150 kg_f. Small delaminations are visible around the edge of the craters and the cracking is no longer radial. The 30 kg_f load was found to be the maximum load the coating could reliably survive without coating delamination.

PVD coating deposited on a Bullion type laser frosted surface

The Bullion test results show in see Table 3.4, and the coating failed all three 45 kg_f and passed all three 30 kg_f. Figure 3.11 shows typical results for 30 and 45 kg_f loading conditions. The 30 kg_f loading condition only causes cracking, while the 45 kg_f loading

condition causes cracking and delamination. Therefore, the 30 kg_f loading was found to be the maximum survivable indentation load for the Bullion laser frosted surface.

PVD coating deposited on a Glass Bead type laser frosted surface

The Glass Bead test results show that the maximum safe load is 15 kg_f (see Table 3.4). Typical results are shown in Figure 3.12 for 15 and 30 kg_f loading conditions. The 15 kg_f loading condition only causes cracking, while the 30 kg_f loading condition causes cracking and delamination. The 15 kg_f loading case was found to be the maximum survivable load for the Glass Bead laser frosted surface.

PVD coating deposited on a Four-to-One type laser frosted surface

The Four-to-One test results show that the coating fails even at the lowest loading condition available (15 kg_f) and for this reason a maximum survivable load could not be determined (see Table 3.4). The delaminations are not noticeable at low magnification due to high surface roughness, but are clearly visible at higher magnification (see Figure 3.13).

PVD coating deposited on a Aluminum Oxide type laser frosted surface

The PVD coating on the Aluminum Oxide type frosting failed at the lowest loading condition available (15 kg_f) and therefore a maximum survivable load could not be determined (see Table 3.4). As can be seen in Figure 3.14, the surface roughness makes finding coating failure difficult. To locate delaminations the microscope focus was moved in and out to find sharp discontinuities in the surface. Also surface coloration was examined for regions lighter coloration indicative of the substrate.

3.4 Scratch Adhesion Test

The scratch adhesion test was also used to evaluate the adhesion of the PVD coating to each die surface. Scratch adhesion tests were performed on each of the five coated surface types to determine their respective failure loads. All presented results are from the four dies with three quarters of the area laser frosted since the four mirror surface dies were used for determining a suitable testing procedure. The determined critical loads found during scratch adhesion testing provide a semi-quantitative characterization of the coating adhesion. The determined critical load found for the mirror surface is used in Chapter 5 during finite element analysis examining the critical coating interface stresses.

3.4.1 Experimental Apparatus

A Teer scratch tester (shown in Figure 2.12) equipped with a Rockwell-C indenter was used to perform all the scratch adhesion tests. A Mitutoyo Profile Projector model PJ-H3000F (see Figure 3.15) shadowgraph capable of 50X magnification was then used to examine the scratch path. The scratch adhesion test procedure is defined by ASTM standard C1624-05 (2010).

3.4.2 Procedure

First the die surface was cleaned using isopropyl alcohol and then placed on the test platform against the fixture. The table was then moved to a position suitable for starting the scratch. Table angle was set using a micrometer on the right of the table; 9.5 mm was used since it provided a suitable scratch length (6 to 9 mm) to allow for multiple scratch tests per die. The Rockwell-C indenter was then lowered until a preload between 5 and 10 N was reached. This range of preload was chosen since a 5 N or more indentation load provided a

visible start to the scratch when using the shadowgraph and the 5 N range between 5 and 10 N was achievable for a cautious operator. A maximum load of 60 N was used since during preliminary testing, coating failure almost always occurred below 60 N. During the test, the table moves to the right powered by a small electric motor and stops once the maximum load is reached. The indenter is then raised and the sample is removed.

The scratch path was then examined using the shadowgraph. First the scratch length was measured and then the distance from the scratch start point to observed failures are measured. For this analysis, four failure criteria are proposed and used in this thesis:

1. First delamination at the edge of the scratch path
2. Sustained edge delamination at the edge of the scratch path
3. First failure at bottom of the scratch path
4. Sustained failure at the bottom of the scratch path

These four failure criteria were chosen after examining several scratch tests and observing the common coating failure types. The loading at the four failure points was then linearly interpolated between the preload and max load by comparing the distance to failure to the overall scratch length.

3.4.3 Results

Twenty scratch tests were performed on the mirror coated surface and five scratch tests were performed on each of the laser frosted surface types except for the PVD coating on the Aluminum Oxide laser frosted surface due to its high roughness. The complete results for the scratch tests on the mirror surface and frosted surface are shown in Table 3.5 and Table

3.6 respectively. A summary of the scratch adhesion tests is shown in Table 3.7. The results for each tested surface are discussed in the following sections.

PVD coating deposited on a mirror surface

A typical scratch path formed from a scratch adhesion test on a mirror surface is shown in Figure 3.16. Chipping can be seen at the path edge, as well as at the bottom of the scratch path. The failure at the bottom of the scratch path is indicative of buckling spallation occurring in front of the indenter during translation (ASTM C1624-05, 2010). The calculated failure loads have a large degree of variation, as can be seen by the relatively large standard deviations in Table 3.7. The first bottom and sustained bottom average failure loads are 22.0 N and 32.3 N respectively and their respective standard deviations are over half of that value. The first and sustained edge failure loads calculated are more consistent with average values being 30.8 N and 43.1 N respectively, with smaller relative standard deviations. From the test data, a critical load of 30 N was selected to approximate the critical adhesion failure load of the PVD coating on the mirror surface. This load is used in the scratch test simulations in Chapter 5.

PVD coating deposited on laser frosted surfaces

The point of failure for the scratch tests on laser frosted surfaces is difficult to determine using the shadowgraphs due to the surface roughness. The Bullion and Glass Bead type laser frostings are the least rough frosting and provided some consistent results. The sustained edge failure load of 46.8 N (7.9 stdv) for Bullion and the first edge failure load of 13.3 N (1.6 stdv) for Glass Bead were consistent during the scratch tests. The Four-to-One laser frosted surface results have less variation, but the failure points were difficult to determine at

50 X magnification. The scratch test was found unsuitable for the Aluminum Oxide laser frosted surface due to its higher surface roughness. Due the large variability and uncertainty in the laser frosted results, as well as the computational costs of running three-dimensional simulations for the laser frosted surfaces, it was decided that only the 30 N critical load for the mirror surface would be used in simulations of the scratch adhesion test.

3.5 Summary

The adhesion tests performed were able to provide consistent evaluation of the PVD coating adhesion with a few exceptions. The Rockwell-C indentation adhesion test graded all but the roughest surface. The stepped adhesion test estimated the maximum loading the PVD coating could survive without delamination for three of the five surfaces. Finally, the scratch adhesion test yielded some consistent failure load results for 4 of the 5 surfaces. The first edge and sustained edge failure load results were found to be more consistent than the failure at the bottom of the scratch path. The examination of the scratch paths was found to be difficult using a 50 X magnification shadowgraph for the rougher laser frosted surfaces. The critical load of 30 kg_f (294 N) for the indentation of the coated mirror surface is nearly an order of magnitude larger than the corresponding scratch critical load of 30 N.

In Chapter 4, the maximum survivable loads of 15 kg_f (147 N) for the Glass Bead surface and 30 kg_f (294) for the mirror and Bullion surfaces found during stepped adhesion testing will be used in finite element simulations of the indentation tests. The critical scratch load of 30 N, found for the mirror surface, will be used in Chapter 5 during finite element simulation of the scratch test. The indentation and scratch simulations in Chapter 4 and 5 will provide an estimate of the stress state at the coating-substrate interface, and the coating

adhesion strength will be quantified using the maximum opening, shear, and compressive stresses at the coating-substrate interface.

Die Name	Indentation Location	Surface Type	Adhesion Strength Quality (HF1-HF6)
Mirror_1	Center	Mirror	HF4
	1/2 Radius	Mirror	HF4
	Edge	Mirror	HF4
Mirror_2	Center	Mirror	HF3
	1/2 Radius	Mirror	HF3
	Edge	Mirror	HF3
Mirror_3	Center	Mirror	HF3
	1/2 Radius	Mirror	HF3
	Edge	Mirror	HF3
Mirror_4	Center	Mirror	HF3
	1/2 Radius	Mirror	HF4
	Edge	Mirror	HF3
3/4_Bul	Center	Bullion	HF3
	Edge	Bullion	HF3
	Center	Mirror	HF3
	Edge	Mirror	HF3
3/4_GB	Center	Glass Bead	HF3
	Edge	Glass Bead	HF3
	Center	Mirror	HF3
	Edge	Mirror	HF3
3/4_4:1	Center	4 to 1	HF6
	Edge	4 to 1	HF6
	Center	Mirror	HF3
	Edge	Mirror	HF3
3/4_AlOx	Center	AlOx	Inconclusive
	Edge	AlOx	Inconclusive
	Center	Mirror	HF3
	Edge	Mirror	HF3

Table 3.1: Rockwel-C adhesion test results

Surface Type	Adhesion Strength Rating			
	HF3	HF4	HF5	HF6
Mirror	80%	20%	0	0
Bullion	100%	0	0	0
Glass Bead	100%	0	0	0
4 to 1	0	0	0	100%
AlOx	Inconclusive results			

Table 3.2: Summary of Rockwell-C adhesion test

Die Name	Load (kg_f)	Delamination (Yes/No)		
		Trial 1	Trial 2	Trial 3
Mirror_1	15	No	No	
	30	No	No	No
	45	Yes	Yes	Yes
	60	Yes	Yes	
	100	Yes	Yes	
	150	Yes	Yes	Yes
Mirror_2	15	No	No	
	30	No	No	No
	45	No	Yes	No
	60	Yes	Yes	
	100	Yes	Yes	
	150	Yes	Yes	Yes
Mirror_3	15	No	No	
	30	No	No	No
	45	No	No	No
	60	No	Yes	
	100	Yes	Yes	
	150	Yes	Yes	Yes
Mirror_4	15	No	No	
	30	No	Yes	No
	45	Yes	Yes	No
	60	Yes	Yes	
	100	Yes	Yes	
	150	Yes	Yes	Yes

Table 3.3: Stepped indentation delamination results for mirror surface dies

Die Name	Laser Frosting	Load (kgf)	Delamination (Yes/No)		
			Trial 1	Trial 2	Trial 3
3/4_Bul	Bullion	15	No	No	
		30	No	No	No
		45	Yes	Yes	Yes
		150	Yes	Yes	
3/4_Gb	Glass Bead	15	No	No	No
		30	Yes	Yes	Yes
		150	Yes	Yes	
3/4_4:1	4 to 1	15	Yes	Yes	
		30	Yes	Yes	
		45	Yes	Yes	
		150	Yes	Yes	
3/4_AlOx	AlOx	15	Yes	Yes	Yes
		30	Yes	Yes	Yes
		150	Yes	Yes	

Table 3.4: Stepped indentation delamination results for laser frosted surfaces

			Failure Position (mm)				Failure Load (N)			
Die Name	**Preload (N)**	**Length (mm)**	**First Edge**	**Sustained Edge**	**First Bottom**	**Sustained Bottom**	**First Edge**	**Sustained Edge**	**First Bottom**	**Sustained Bottom**
3/4_Bul	6.4	7.345	3.474	3.474	0.611	0.972	31.8	31.8	10.9	13.5
	8.1	7.598	2.842	5.292	5.387	6.221	27.5	44.2	44.9	50.6
	8	7.463	5.204	6.532	0.619	1.978	44.3	53.5	12.3	21.8
	6.9	7.68	1.652	6.178	0.969	6.33	18.3	49.6	13.6	50.7
	8.8	6.899	2.968	5.036	0.453	5.144	30.8	46.2	12.2	47.0
3/4_GB	7.8	6.744	3.493	3.789	2.554	3.571	34.8	37.1	27.6	35.4
	8.2	7.785	3.844	4.065	0	1.671	33.8	35.2	8.2	19.3
	7.8	7.674	4.549	5.095	1.382	4.697	38.7	42.5	17.2	39.7
	9.2	6.588	4.455	4.901	0.443	0.077	43.6	47.0	12.6	9.8
	6.7	7.219	4.16	4.902	0.49	0.889	37.4	42.9	10.3	13.3
3/4_4:1	7	7.043	2.148	3.338	2.487	3.496	23.2	32.1	25.7	33.3
	6.6	5.958	2.344	4.436	3.995	5.047	27.6	46.4	42.4	51.8
	5.5	6.061	2.357	4.844	4.901	5.228	26.7	49.1	49.6	52.5
	6.9	7.826	0.82	5.343	0.646	6.448	12.5	43.2	11.3	50.7
3/4_AlOx	7.6	7.315	5.112	5.112	5.906	5.9	44.2	44.2	49.9	49.9
	6.2	8.19	1.151	4.414	3.162	3.411	13.8	35.2	27.0	28.6
	5.7	6.737	5.256	5.74	0.939	0.0939	48.1	52.0	13.3	6.5
	5.9	7.494	1.466	4.564	1.721	3.025	16.5	38.8	18.3	27.7
	6.9	6.67	3.065	5.083	0.606	0.606	31.3	47.4	11.7	11.7

Table 3.5: Scratch test data for the coating deposited on a mirror surface

Die Name	Preload (N)	Length (mm)	Failure Position (mm)				Failure Load (N)			
			First Edge	Sust. Edge	First Bottom	Sust. Bottom	First Edge	Sust. Edge	First Bottom	Sust. Bottom
3/4_Bul	6.8	7.783	2.005	4.297	1.611	5.831	20.5	36.2	17.8	46.7
	8.8	7.279	0.267	6.416	0.596	4.845	10.7	53.9	13.0	42.9
	6.7	7.358	5.373	5.6	0	0	45.6	47.3	6.7	6.7
	7.2	7.164	2.754	4.7	0	0	27.5	41.8	7.2	7.2
	6.3	7.306	2.192	6.593	0.765	5.372	22.4	54.8	11.9	45.8
3/4_GB	5.9	7.991	0.884	2.013	1.599	4.285	11.9	19.5	16.7	34.9
	9.3	7.06	0.936		0.172	0.172	16.0		10.5	10.5
	6.5	7.035	0.826		0.269	0.269	12.8		8.5	8.5
	7.4	7.681	0.722		0	0	12.3		7.4	7.4
	6.5	6.974	0.887		0	0	13.3		6.5	6.5
3/4_4:1	6.5	6.33	1.05		1.05	1.869	15.4		15.4	22.3
	6	7.382	0.536		0.536	1.969	9.9		9.9	20.4
	5.8	7.682	1.139		1.04	2.18	13.8		13.1	21.2
	6.7	5.387	0.419		0.844	1.734	10.8		15.1	23.9
	6.9	5.865	0.124		0.64	1.054	8.0		12.7	16.4
3/4_AlOx	6.4	7.074	0	0	0	0				

Table 3.6: Scratch test data for the coating deposited on laser frosted surfaces

Surface	Value	Failure Load (N)			
		First Edge	Sustained Edge	First Bottom	Sustained Bottom
Mirror	Average	30.8	43.1	22.0	32.3
	Standard Deviation	10.6	6.4	14.3	16.7
Bullion	Average	25.3	46.8	11.3	29.8
	Standard Deviation	12.9	7.9	4.6	20.9
Glass Bead	Average	13.3		9.9	13.6
	Standard Deviation	1.6		4.1	12.0
4:1	Average	11.6		13.2	20.8
	Standard Deviation	3.0		2.2	2.8

Table 3.7: Summary of scratch adhesion test results

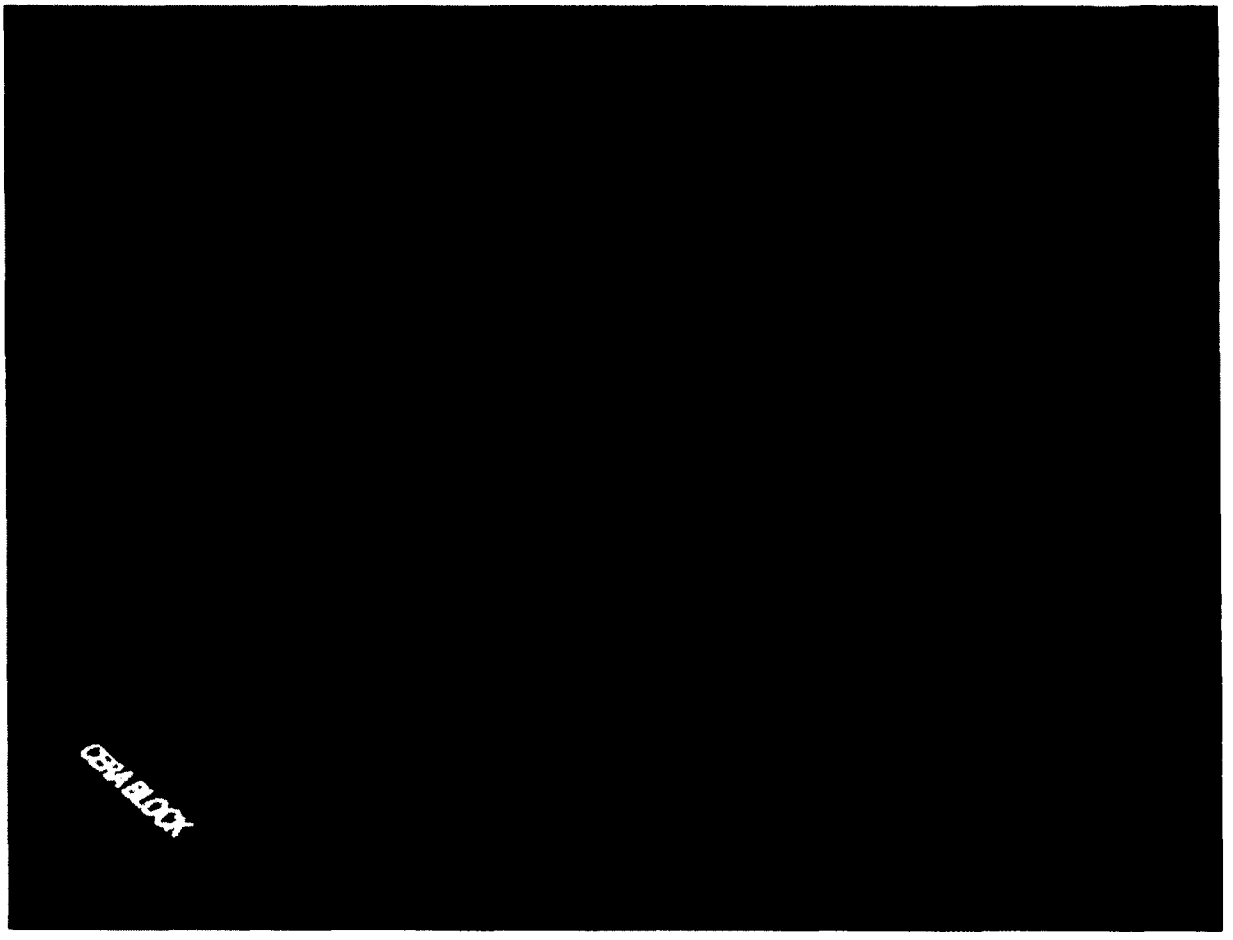

Figure 3.1: Carl Zeiss Axiovert 200 Max inverted microscope fitted with Sony ExwaveHAD video camera

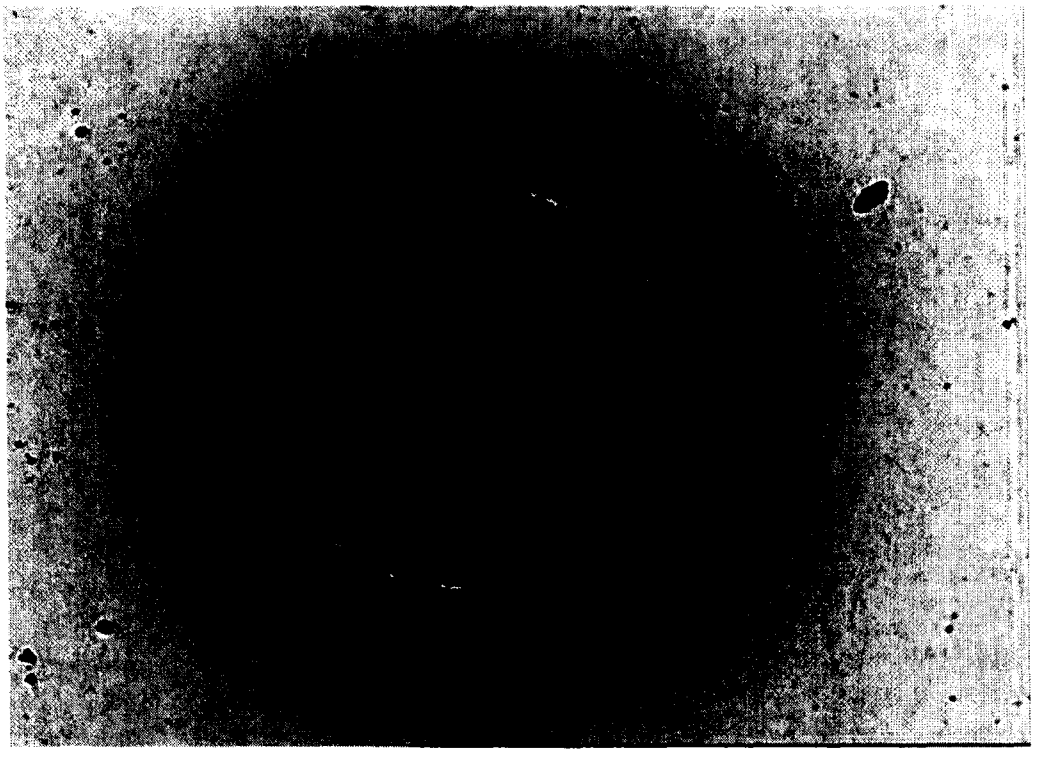

(a)

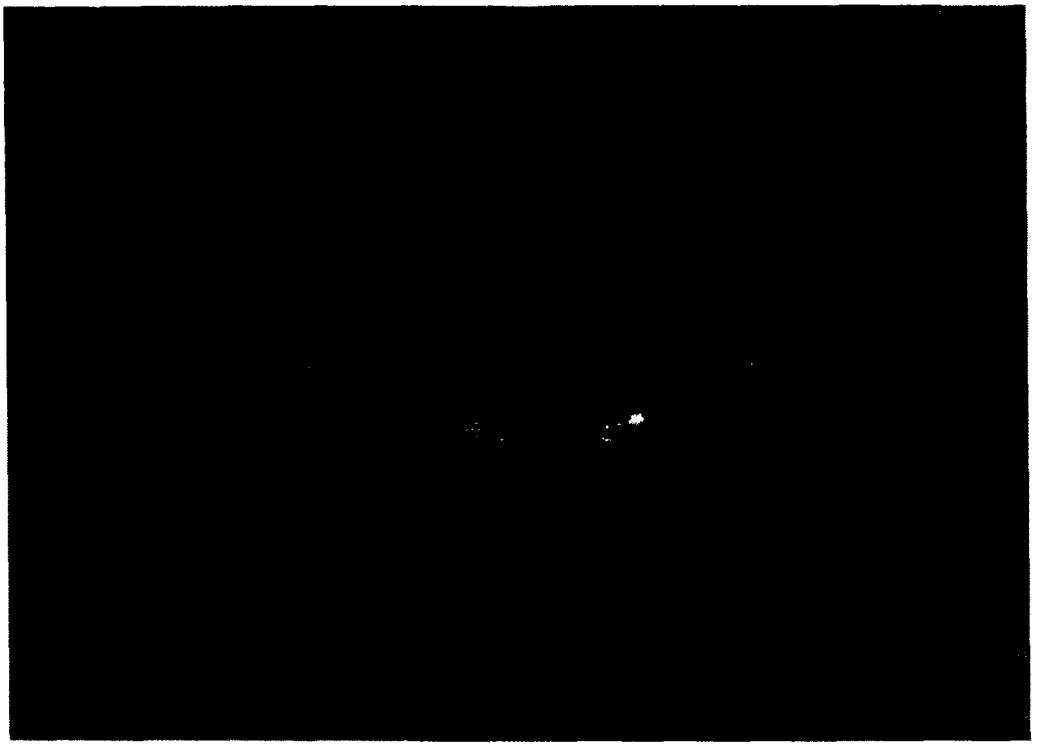

(b)

Figure 3.2: Indentation on a mirror surface sample graded as HF3, (a) 5X objective, (b) 10X objective

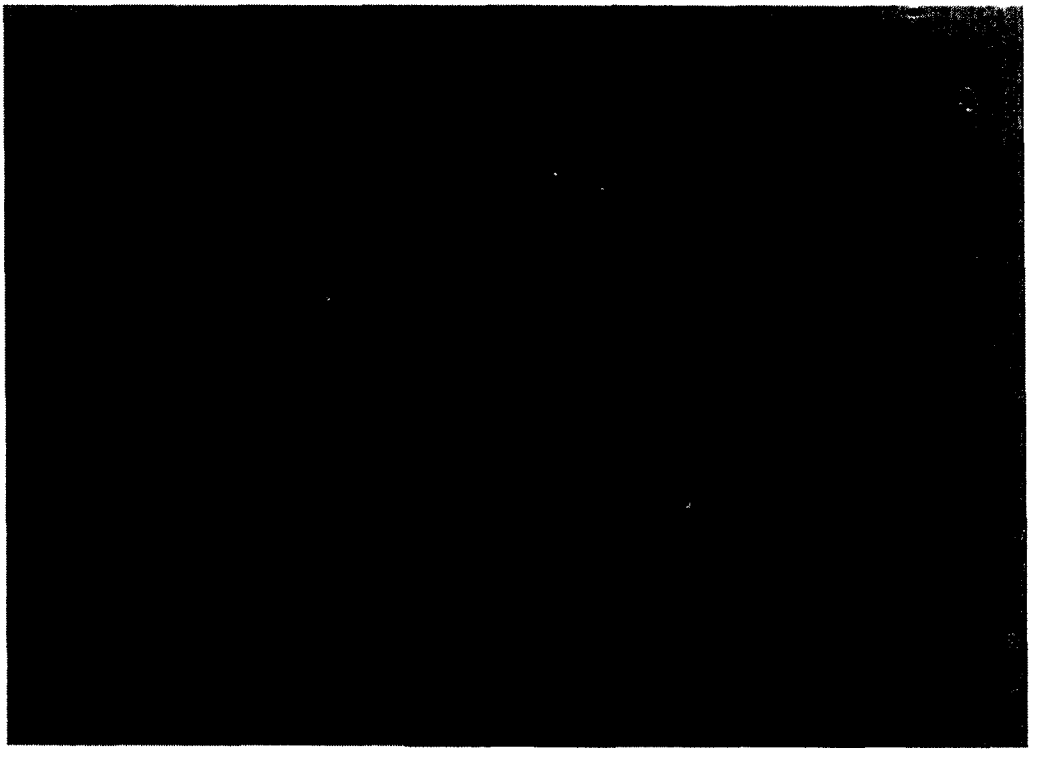

(a)

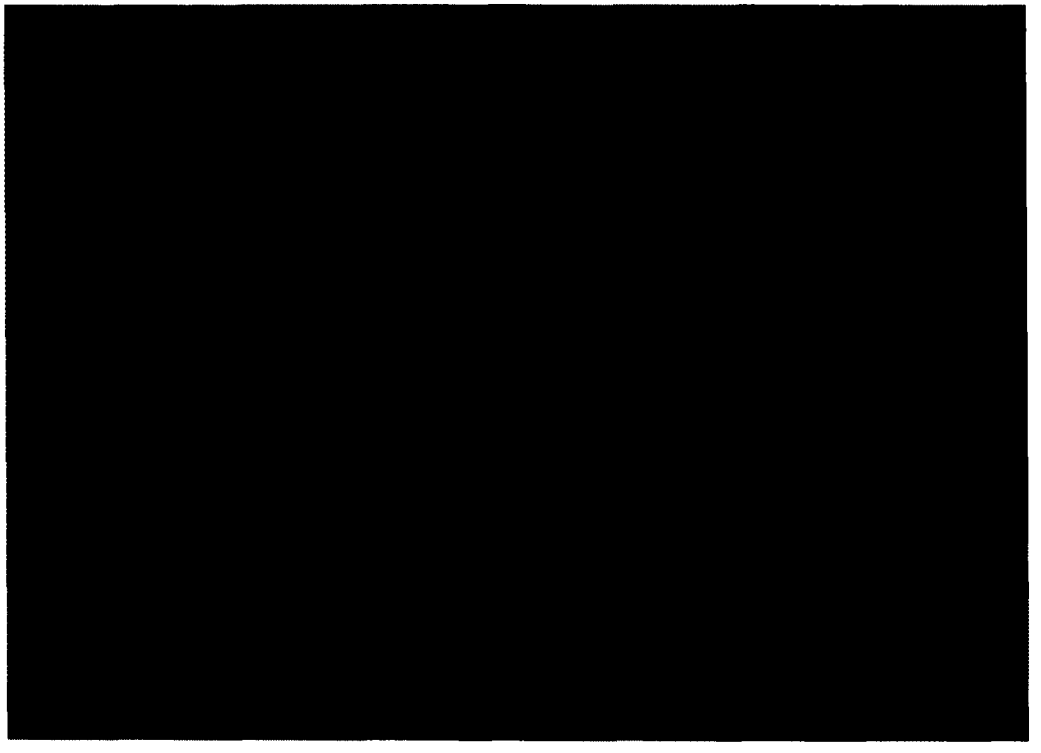

(b)

Figure 3.3: Indentation on a mirror surface sample graded as HF4, (a) 5X objective, (b) 10X objective

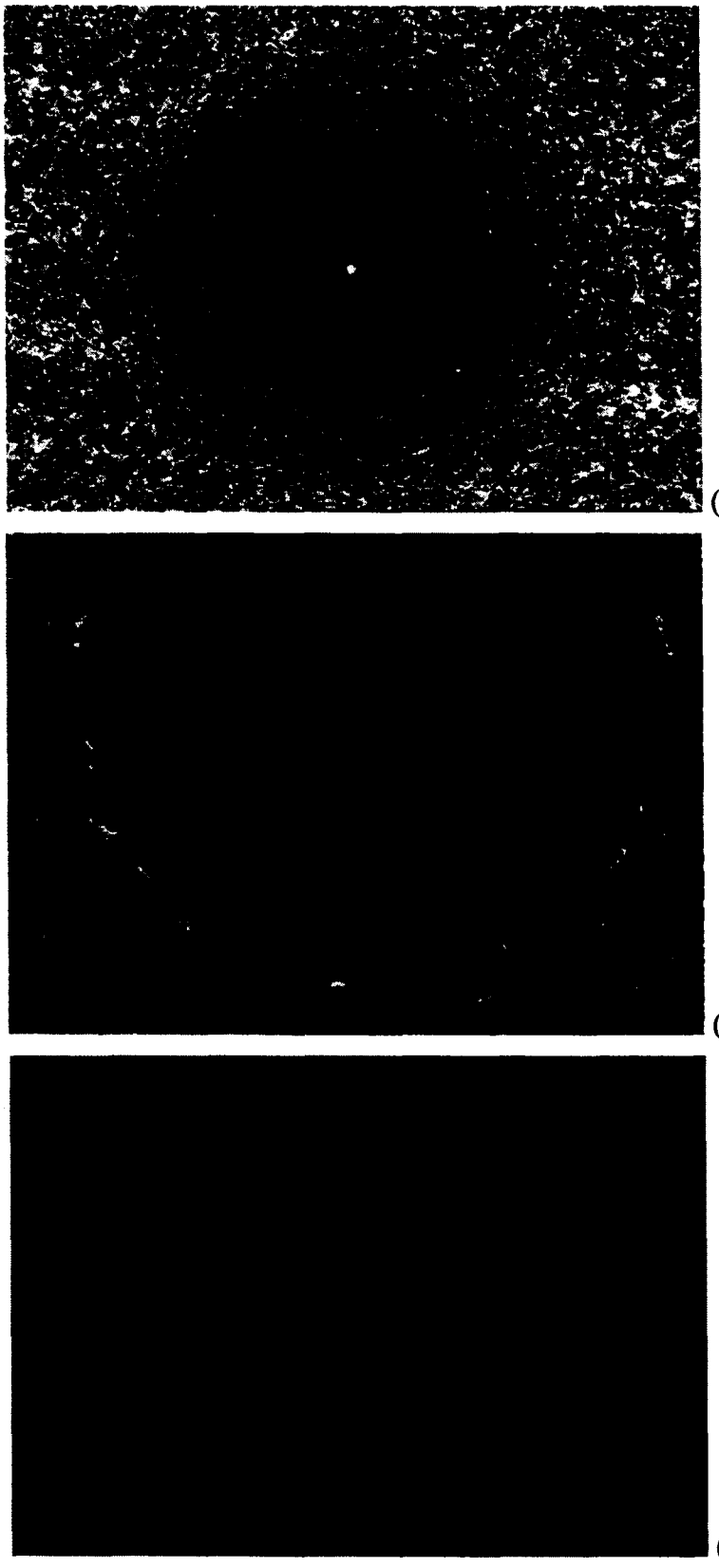

Figure 3.4: Indentation on a Bullion laser frosted sample graded as HF3, (a) 5X objective, (b) 10X objective, (c) 50X objective

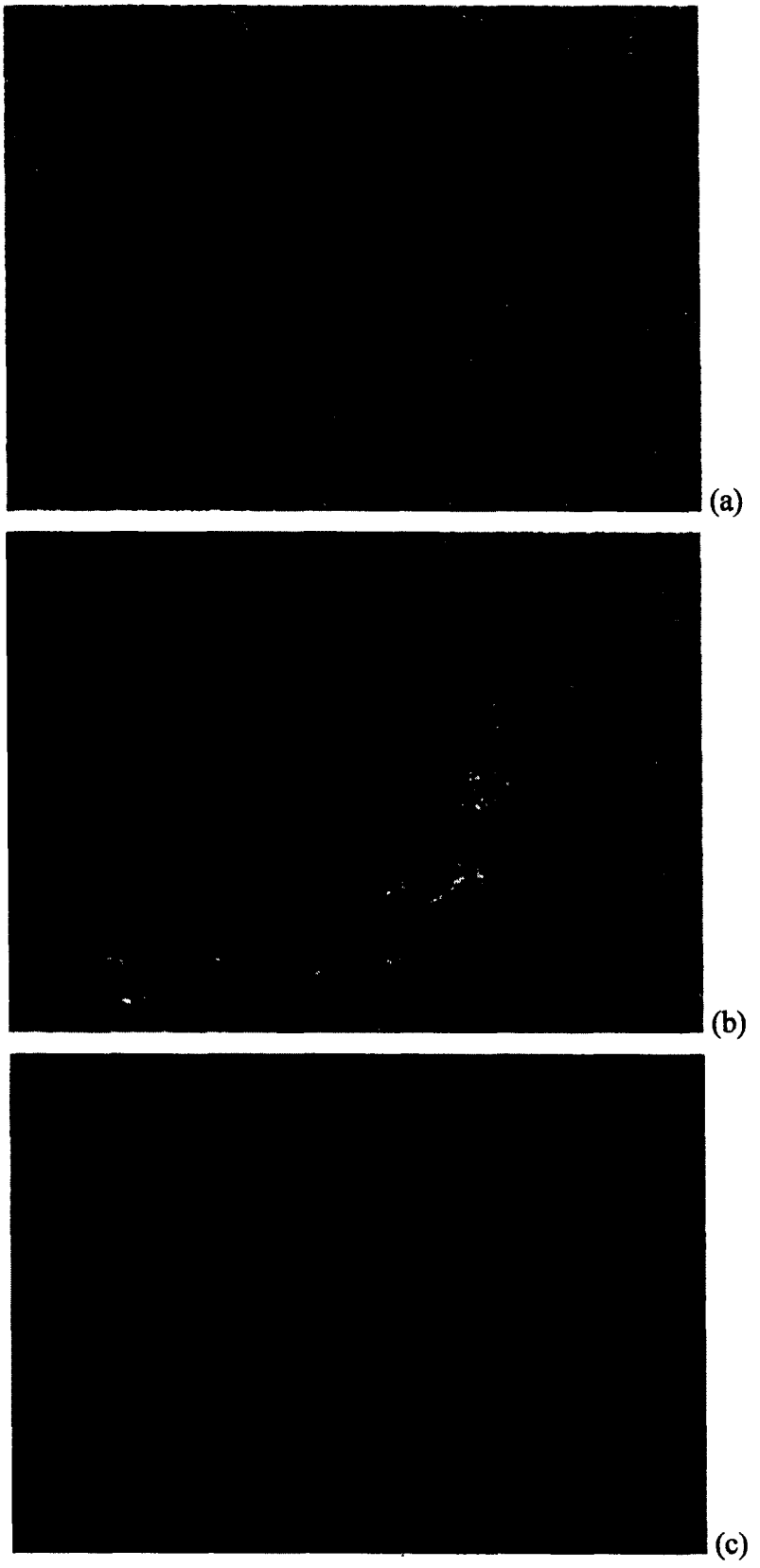

Figure 3.5: Indentation on a Glass Bead laser frosted sample graded as HF3, , (a) 5X objective, (b) 10X objective, (c) 50X objective

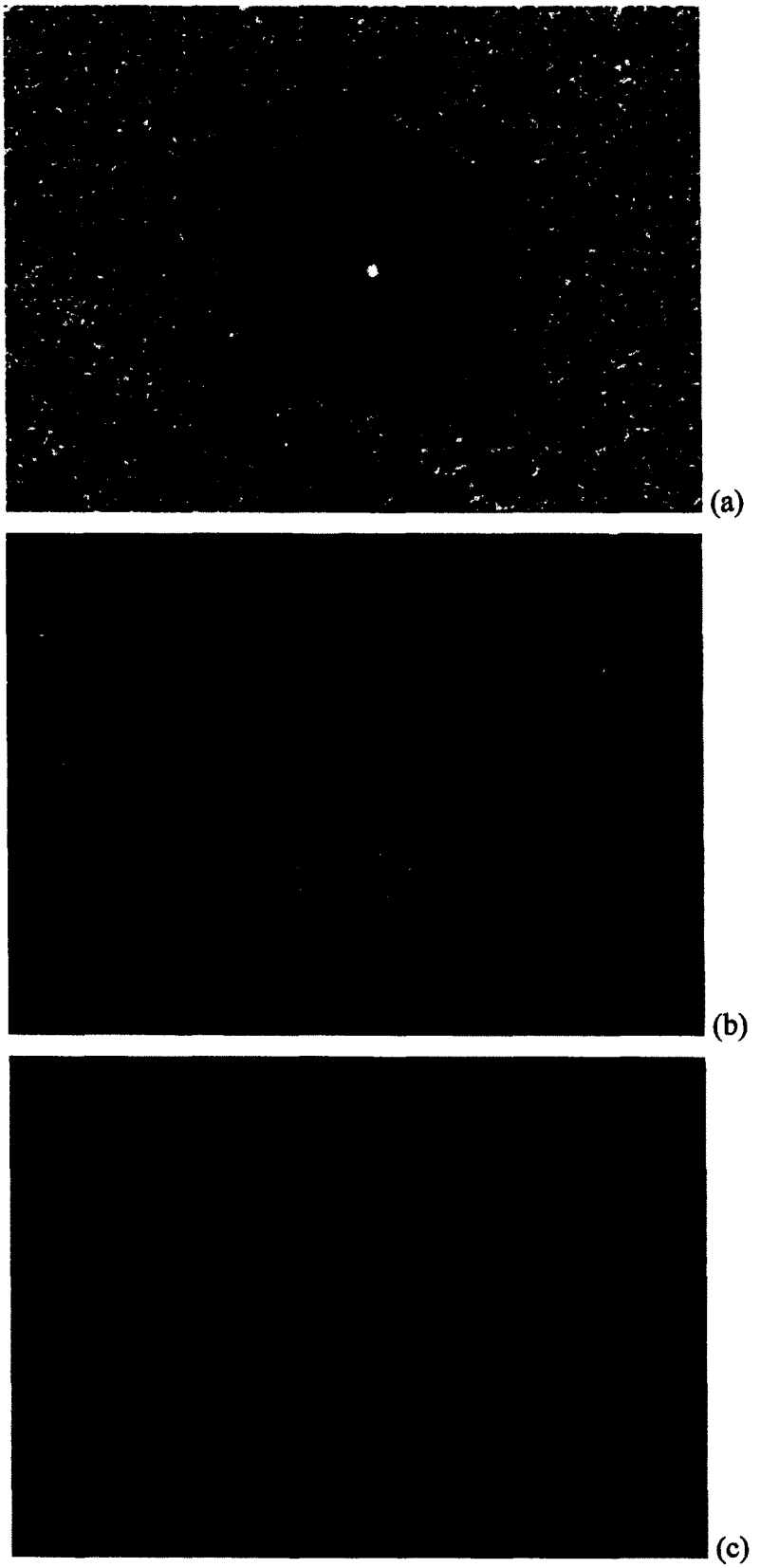

Figure 3.6: Indentation on a Four-to-One laser frosted sample graded as HF6, (a) 5X objective, (b) 10X objective, (c) 50X objective

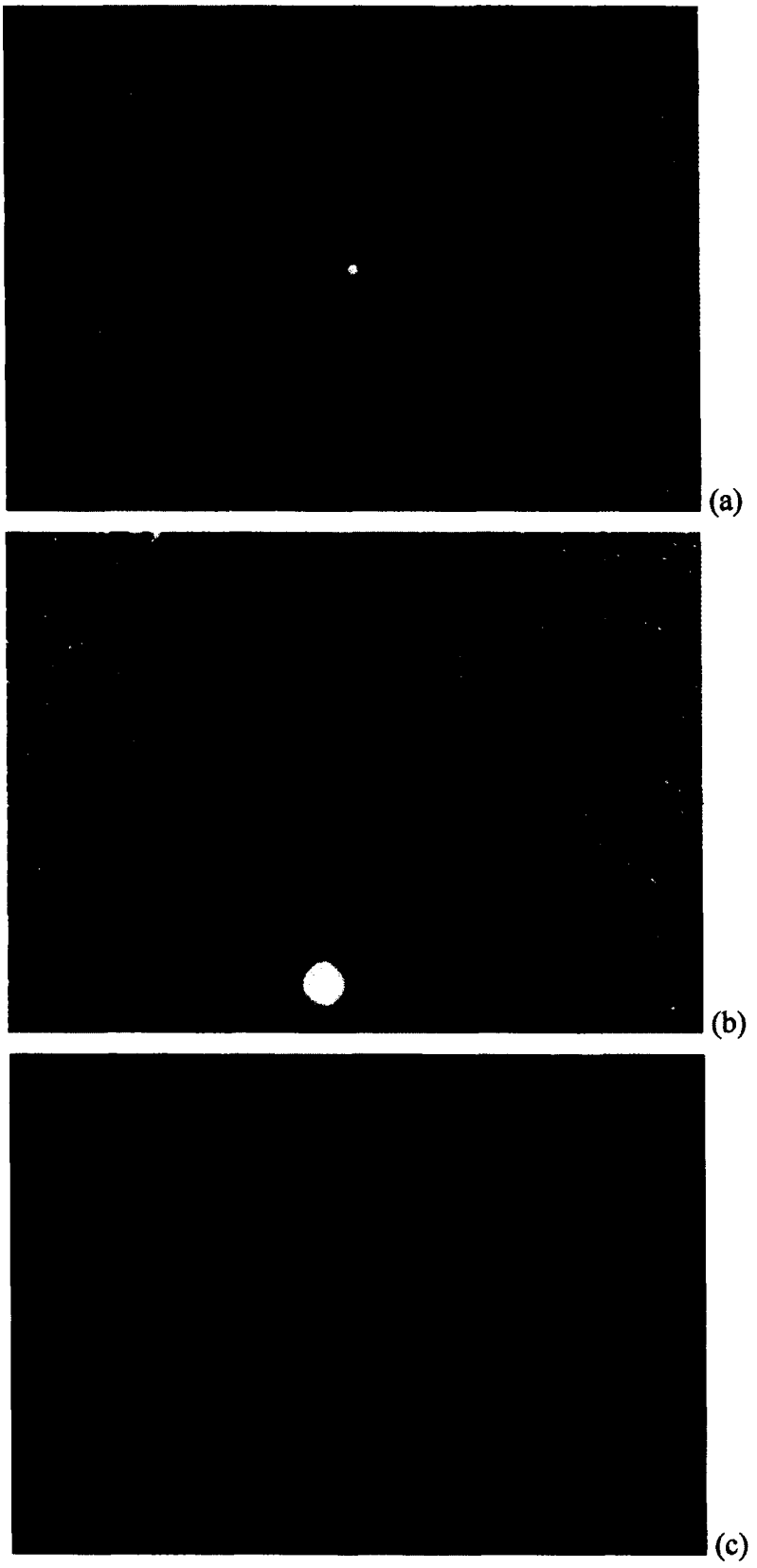

Figure 3.7: Indentation on a Aluminum Oxide laser frosted sample graded as inconclusive due to high surface roughness, (a) 5X objective, (b) 10X objective, (c) 50X objective

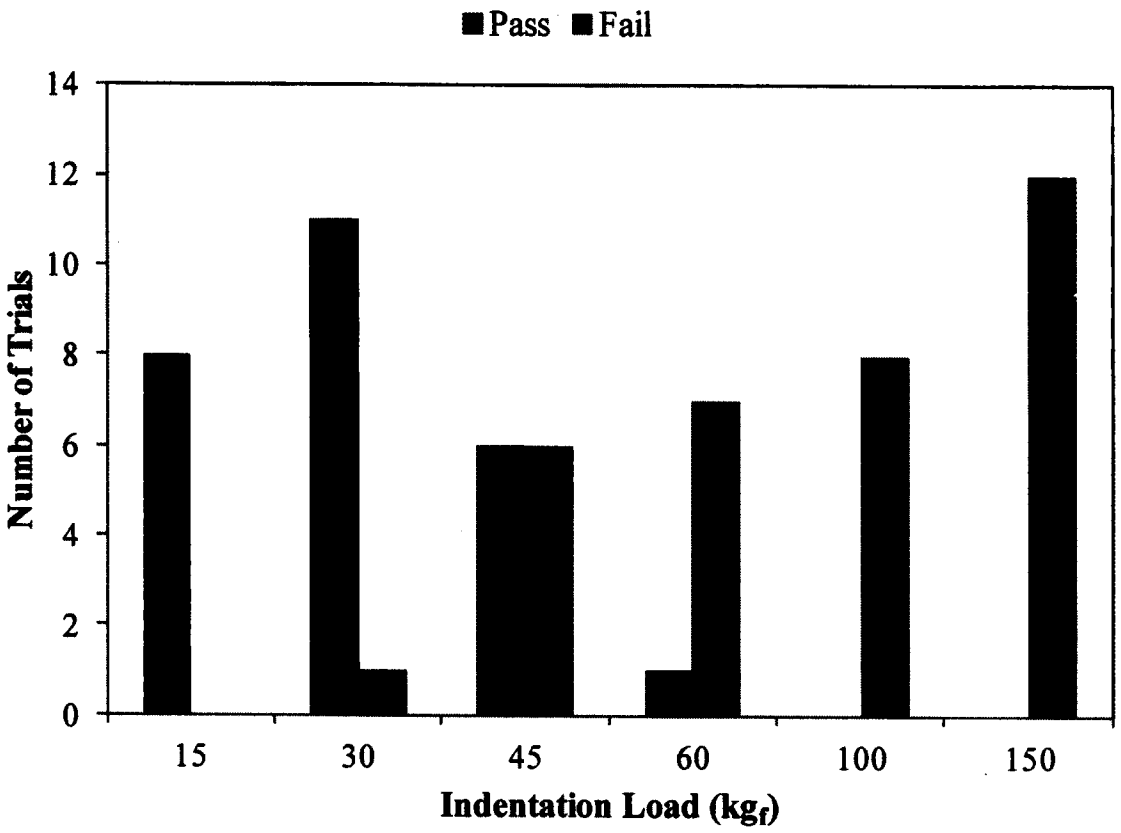

Figure 3.8: Distribution of the stepped indenation results for the PVD coating on a mirror surface

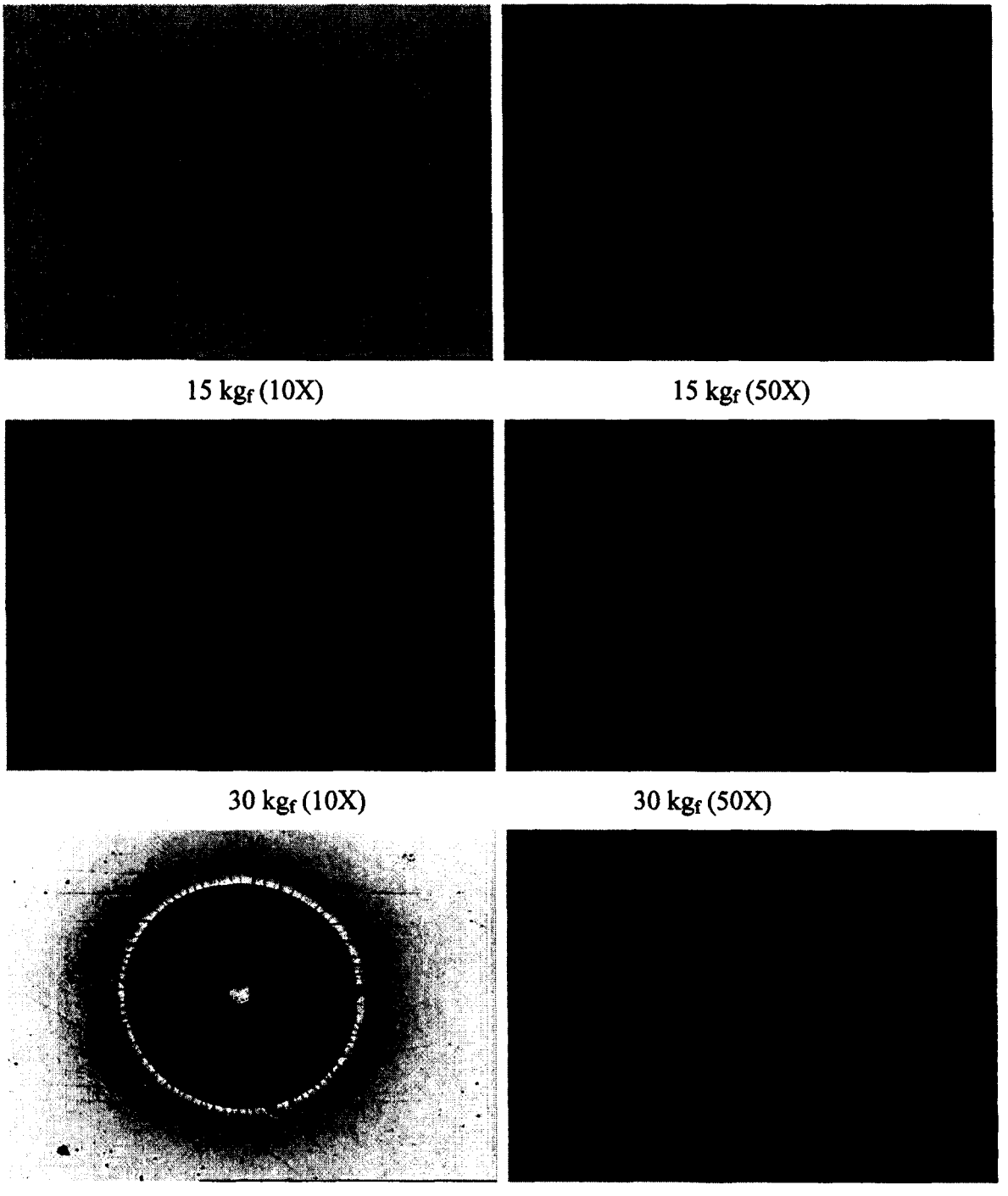

Figure 3.9: Typical results for the Rockwell-C indentation of the PVD coating on a mirror surface for loads of 15, 30, and 45 kg_f

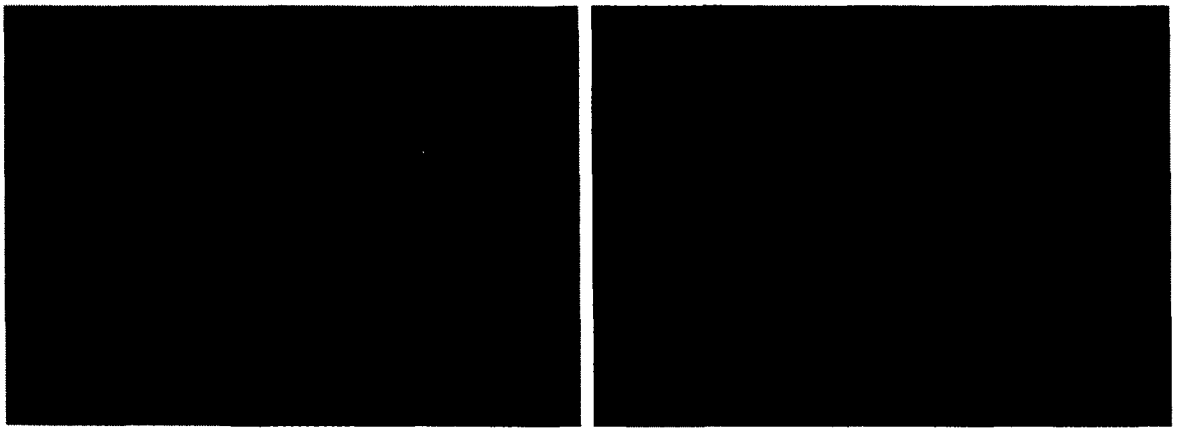

60 kg_f (10X) 60 kg_f (50X)

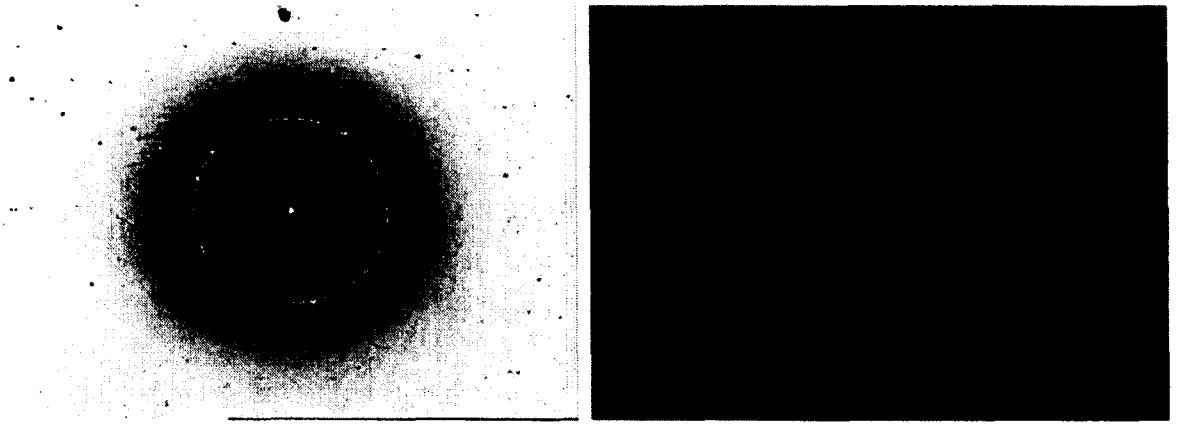

100 kg_f (5X) 100 kg_f (10X)

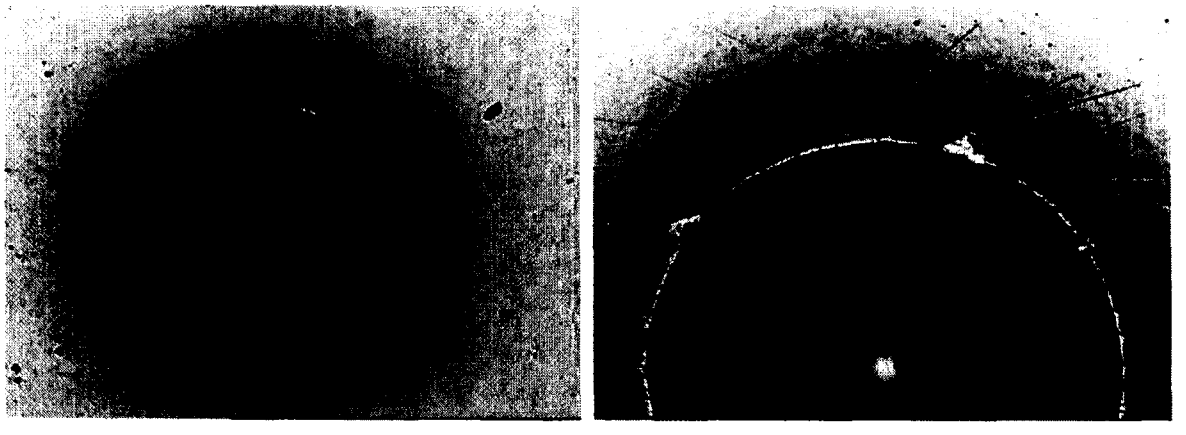

150kg_f (5X) 150 kg_f (10X)

Figure 3.10: Typical results for Rockwell-C indentation of the PVD coating on a mirror surface for loads of 60, 100, and 150 kg_f

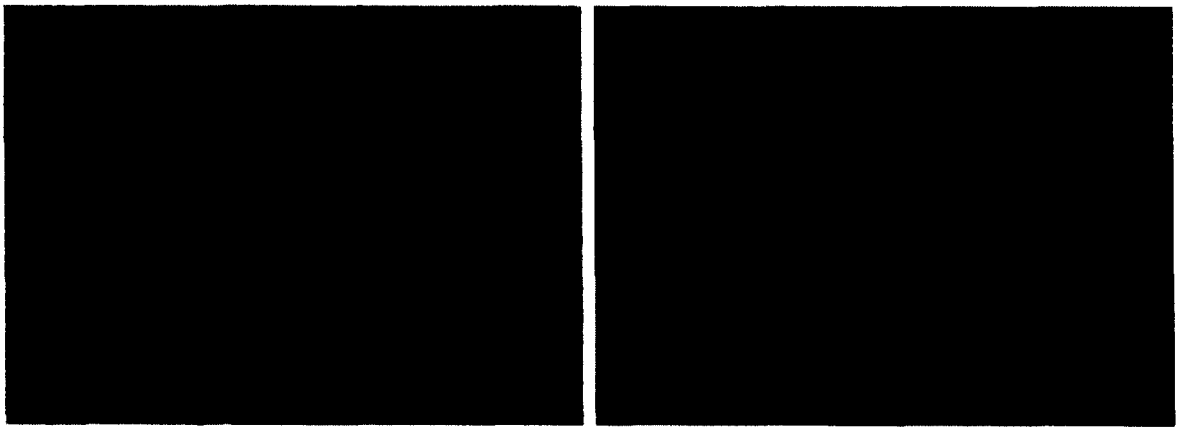

30 kg_f (10X) 30 kg_f (50X)

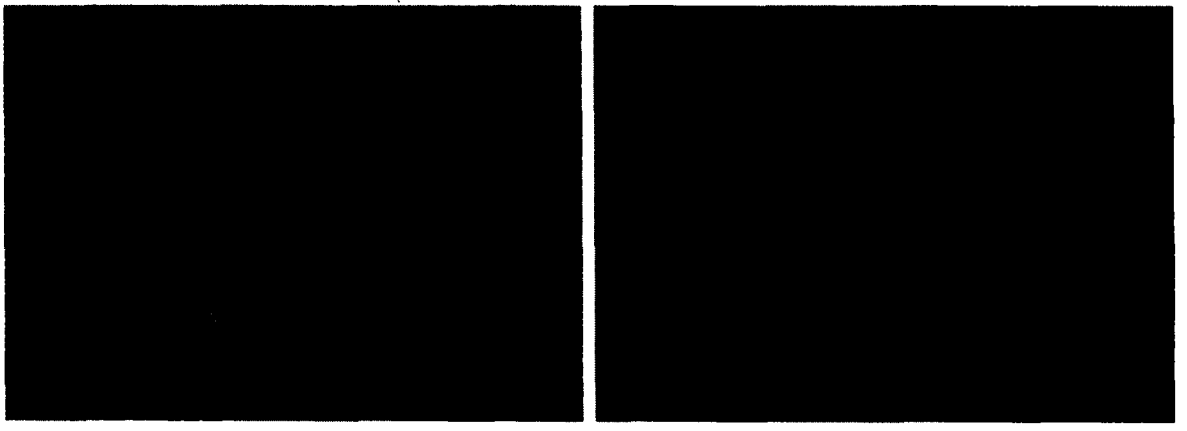

45kg_f (10X) 45 kg_f (50X)

Figure 3.11: Typical results for Rockwell-C indentation of the PVD coating on a Bullion laser frosted surface for loads of 30 and 45 kg_f

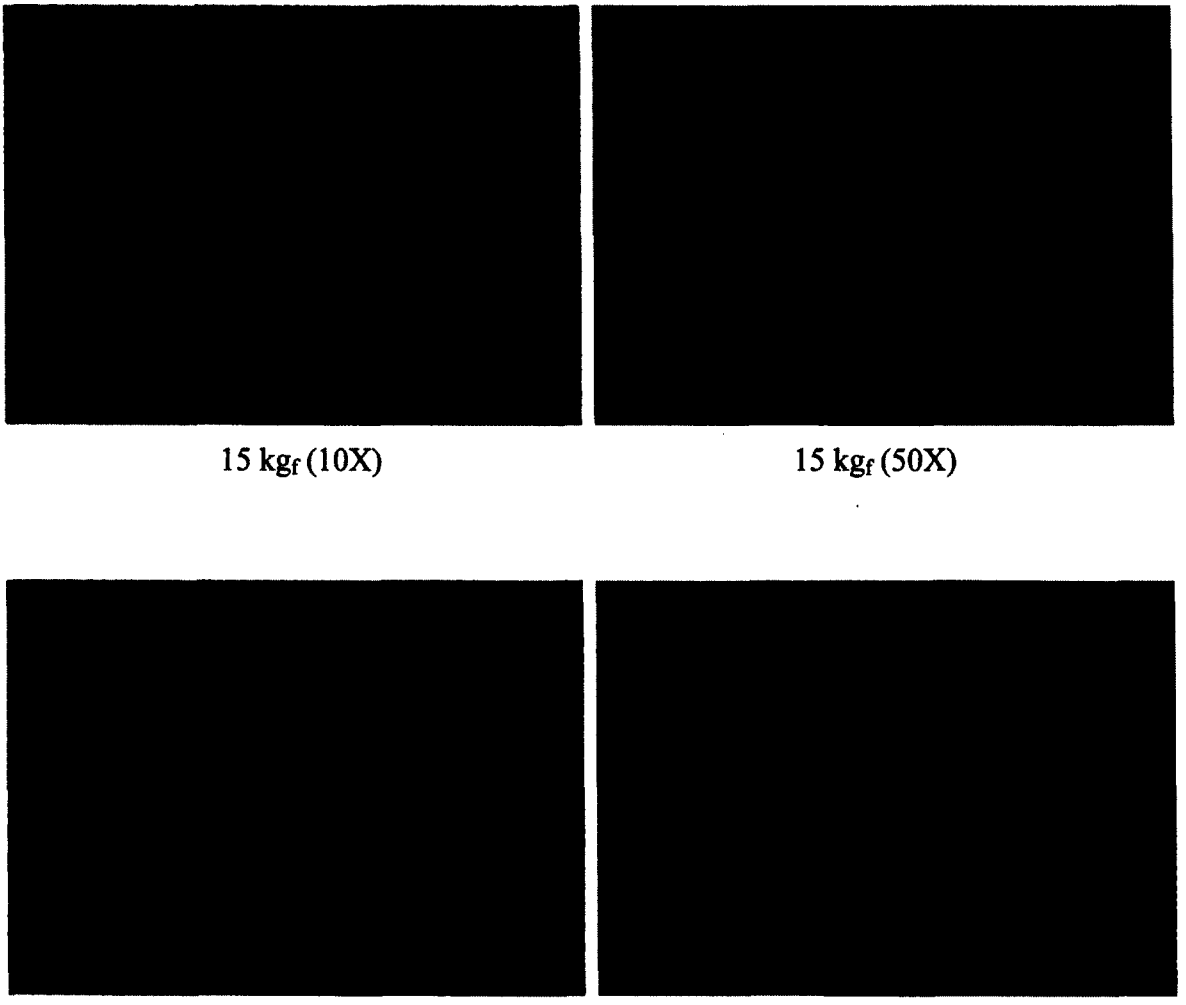

15 kg_f (10X) 15 kg_f (50X)

30 kg_f (10X) 30 kg_f (50X)

Figure 3.12: Typical results for Rockwell indentation of the PVD coating on a Glass Bead laser frosted surface for loads of 15 and 30 kg_f

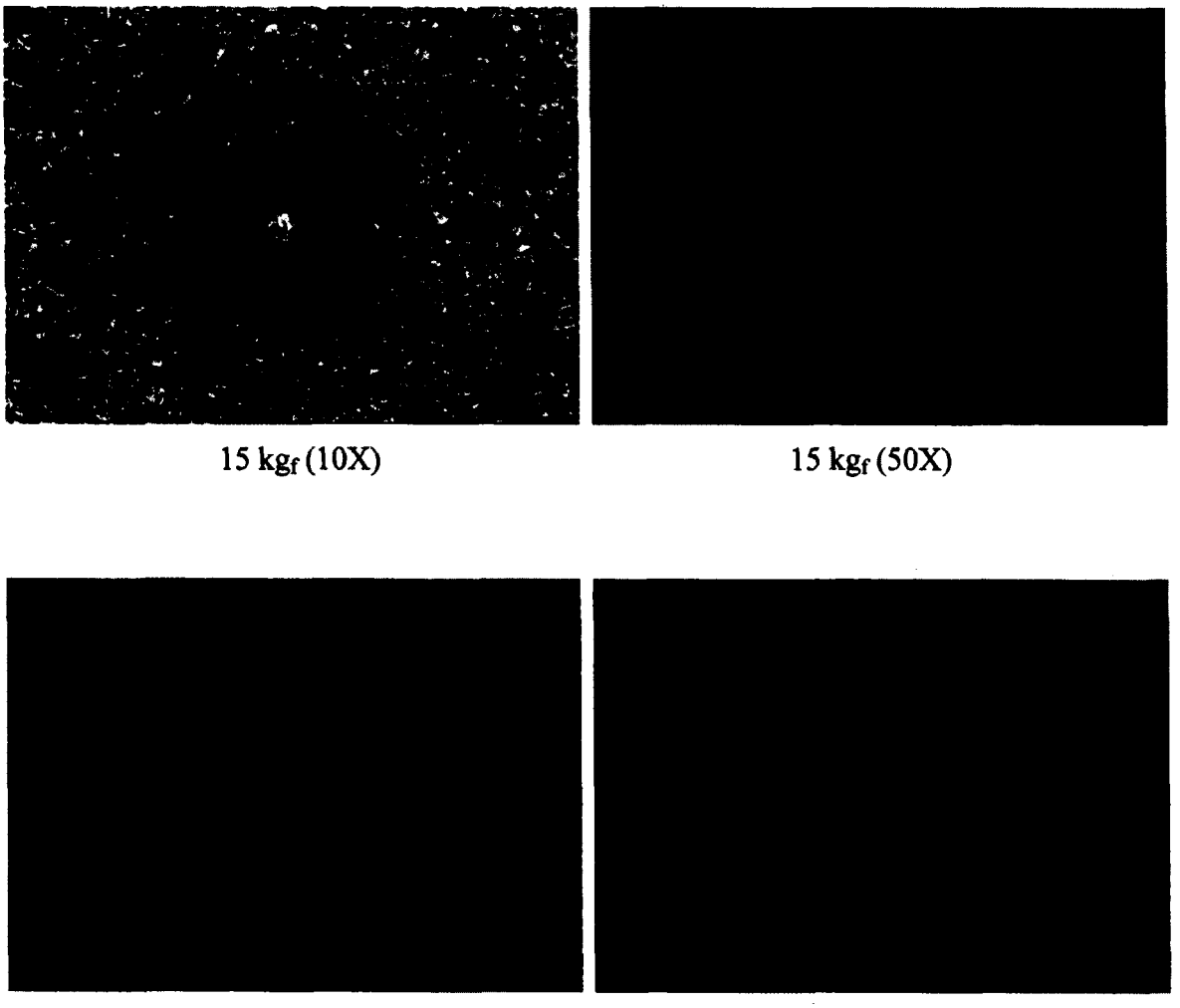

Figure 3.13: Typical results for Rockwell indentation of the PVD coating on a 4 to 1 laser frosted surface for loads of 15 and 30 kg_f

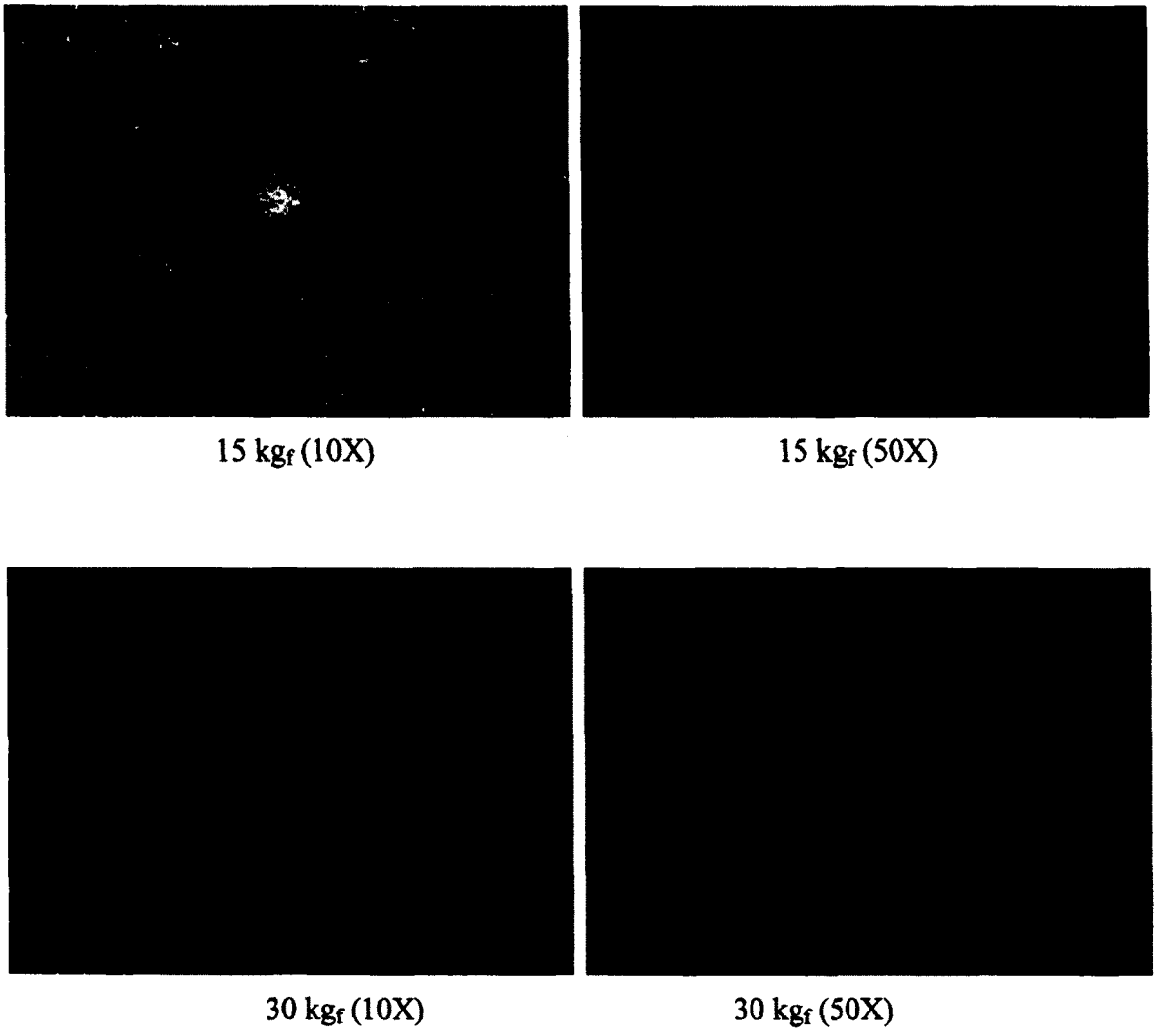

15 kg_f (10X) 15 kg_f (50X)

30 kg_f (10X) 30 kg_f (50X)

Figure 3.14: Typical results for Rockwell indentation of the PVD coating on an Aluminum Oxide laser frosted surface for loads of 15 and 30 kg_f

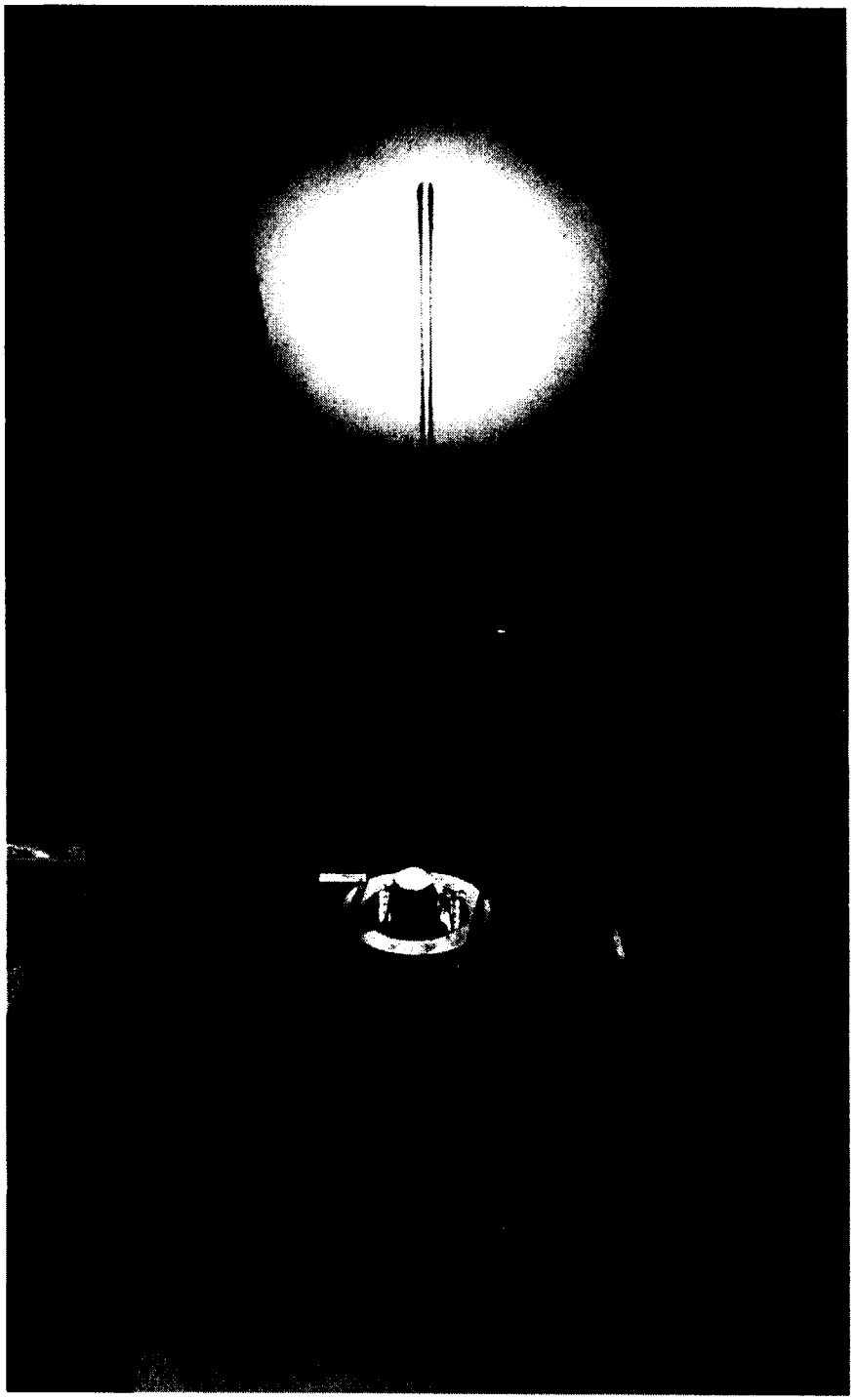

Figure 3.15: Mitutoyo Profile Projector model number PJ-H3000F

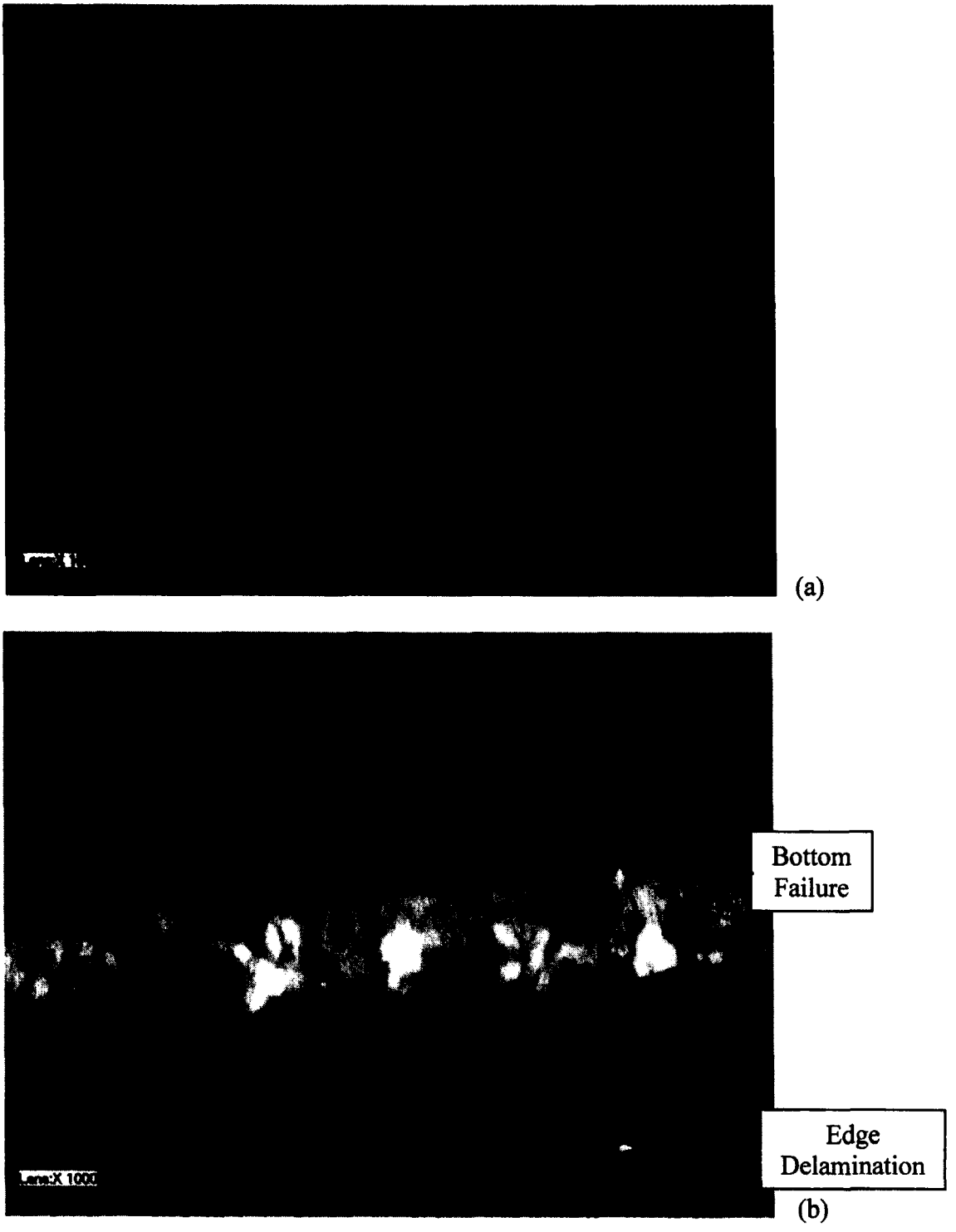

Figure 3.16: Typical scratch results for PVD coated mirror surface (a) 100 X, (b) 1000 X

Chapter 4: Two-dimensional Axisymmetric Indentation Adhesion Test Simulation

This chapter presents the two-dimensional axisymmetric finite element simulation of indentation adhesion tests using ABAQUS (2008). The simulations are used to determine the stress state at the coating-substrate interface prior to coating failure. Focus is placed on the opening stress, the shear stress, and compressive stress at the interface since these stress components are the likely cause of delamination growth. The maximum survivable indentation loads estimated using the stepped indentation adhesion tests in Chapter 3 are used as indentation loads in the simulations. Simulations are completed using 15 and 30 kg_f indentation loads. The 15 kg_f simulation represents the PVD coating deposited on the Glass Bead laser frosted surface and the 30 kg_f represents the PVD coating deposited on the mirror surface and Bullion laser frosted surface. Simulations are not completed for the PVD coating deposited on the Aluminum Oxide and Four-to-One laser frosted surfaces since their maximum survivable indentation load could not be determined during stepped indentation adhesion testing.

The finite element model geometry, boundary conditions, material properties, and mesh design will be outlined below, followed by a presentation of the computed stress state at the coating-substrate interface. The opening, shear, and compressive stresses at the coating-substrate interface will provide a quantification of the PVD coating adhesion strength to the mirror surface and Glass Bead and Bullion laser frosted surfaces.

4.1 FEM Model Setup, Geometry, and Boundary Conditions

The indentation adhesion test is axisymmetric and therefore a simplified axisymmetric finite element model was used to simulate the test. ABAQUS/Standard version 6.8 (2008) was used for the finite element analysis. The indentation adhesion test consists of three steps, first the indenter is lowered to the die surface and then load is applied and ramped up to the maximum load. Finally the load is removed and the indenter is raised off the die surface. The indentation test was modeled as quasi-static and all time-dependant effects were neglected. The indenter and die geometry and boundary conditions are presented below.

4.1.1 Indenter Geometry

The indenter geometry used is that of a Rockwell-C cone indenter as defined by ASTM E18-8b (ASTM E18-8b, 2008). The indenter has a 200 μm radius cone tip and 60° half angle. The axisymmetric indenter model was defined as presented in Figure 4.1 and the geometry was fixed to a reference point. Displacements and loads are applied to the indenter by moving or loading the reference point.

4.1.2 Die Geometry

The die geometry used is shown in Figure 4.2. An axisymmetric boundary condition is placed on the axis of symmetry and vertical displacement is fixed at the bottom of the model. The PVD coating thickness used by the RCM is controlled to be between two and three microns. The average of the thickness range, 2.5 μm, was selected for the model. The overall size of the die segment modeled was one millimetre by one millimetre and was selected after testing different model sizes. Multiple model sizes were tested and the model

size selected was chosen since it minimized the model size while not affecting the stress values at the coating-substrate interface.

4.2 Determination of Material and Interface Properties

The definition of the material properties of the indenter, the coating, and the substrate are outlined below. Internal stresses in the coating and substrate materials induced during machining, heat treating, and coating deposition are not considered in this work. The interactions between the coating and substrate and between the indenter and coating surface are also defined.

4.2.1 Indenter Properties

The Rockwell-C indenter tip is made of diamond which is significantly harder than the die substrate. The deflection of the diamond indenter during loading up to the maximum indentation load used, 30 kg_f, is negligible and therefore it was modeled as an analytical rigid body.

4.2.2 Substrate Properties

The substrate of the die samples used for experimental testing was a tool steel and it was modeled as an elastoplastic material with isotropic strain hardening. The material properties used during indentation simulations are shown in Table 4.1. The elastic modulus and yield strength values were taken from a tool steel material datasheet (Bohler Uddeholm, 2011). The Ramberg-Osgood stress strain relationship was used to define the materials strain hardening as follows (Ramberg and Osgood, 1943):

$$\varepsilon = \frac{\sigma}{E} + \alpha \frac{\sigma_y}{E} \left(\frac{\sigma}{\sigma_y} \right)^n \tag{4.1}$$

where α is the yield offset and n is the strain hardening exponent. Assuming an industry standard strain value of 0.2 % was used when defining the yield strength of the tool steel, α can be calculated as follows:

$$\alpha = 0.2\% \cdot \frac{E_s}{\sigma_{ys}} = 0.002 \cdot \frac{213\ GPa}{2.35\ GPa} = 0.18 \tag{4.2}$$

The strain hardening exponent was determined using a numerical and experimental approach as described by J. Yan et al. (2007). Indentation tests were performed on an uncoated section of the tool steel using 15, 30 45, 60, 100, and 150 kg_f loads to determine the relationship between indentation load and indentation crater radius. Finite element simulations of each loading condition were then performed with the goal of minimizing the difference between the experimental and simulated results by varying the strain hardening exponent used when defining the material plasticity. The indentation crater radii were measured using an optical microscope as shown in Figure 4.3. The measured indentation crater radii are shown in Table 4.2.

A simplified version of the model shown in Figure 4.2 with coating omitted was used for the finite element simulations. The meshes used for the simulations are shown in Figure 4.4 (coarse mesh) and Figure 4.5 (refined mesh). The mesh was refined in the region under the indenter due to the large deformation and stress gradient experienced in this region during indentation. An example of a completed indentation test simulation is shown in Figure 4.6. The indentation crater sizes measured for simulations using strain hardening exponent (n) values equal to 10, 15, and 20 are shown in Table 4.3. The indentation depth is much larger

than the coating thickness (2-3 μm). A comparison between the radius values experimentally measured and radius values determined from simulated results is shown Figure 4.7. The crater sizes for the coarse and refined simulations using n = 15 agreed very well and show that the mesh is adequately refined. A strain hardening exponent value (n) of 15 was found to agree well with the experimental data and therefore n = 15 was used as the strain hardening exponent for the substrate. A comparison of the true stress strain curves defined by the Ramberg-Osgood relationship is shown in Figure 4.8 for the values of n = 10, 15, and 20.

4.2.3 Coating Properties

The material properties used for defining the Cr-Ti-N based hard PVD coating are shown on Table 4.4. The elastic modulus, yield strength, and Poisson's ratio values for the PVD coating were determined using nano-indentation testing completed by McLean (2010). As recommended by Piana et. al (2005), Ramberg-Osgood strain hardening parameters of $\alpha = 1$ and n = 100 were chosen to produce a material with minimal strain hardening. The true stress-strain curve defined by the Ramberg-Osgood relationship for the coating is shown in Figure 4.9.

4.2.4 Interface Properties

Interface between the coating and substrate

The loading conditions used during the indentation test simulations are below the failure load of the coating-substrate interface, therefore the interface between the coating and substrate was modeled as being in perfect adhesion.

Interaction between the indenter and the coating surface

The interaction between the indenter and the coating surface was defined using the "Interaction Module" built into ABAQUS (ABAQUS, 2008). A contact pair was defined, with indenter being the master surface and the coating surface being the slave surface. The indenter is ideal for the master surface because it is an analytical rigid body and is accurately defined without discretization using an arc and a line. To complete the interaction definition the tangential and normal behaviour between the two surfaces must be defined. The tangential behaviour was defined as frictionless as recommended by Piana et al. (2005). Neglecting friction has an insignificant effect on the results of indentation test simulations (Piana, et al. 2005). The normal behaviour was defined as "hard contact", which does not allow the coating top surface nodes to pass through the indenter geometry. Separation after contact was permitted to allow for unloading of the indenter.

4.2.5 Mesh Design

The mesh was refined towards the indentation location to properly model the large deformation and steep stress gradient. Due to the large deformation in the region of the indentation, it is important to enable non linear geometry in ABAQUS (2008). The finite element models were discretized using 4-node bilinear axisymmetric quadrilateral elements, which are defined as CAX4R in the ABAQUS element library (ABAQUS, 2008). This element type is a first order continuum element and uses reduced integration. Reduced integration lowers the number of constraints introduced by the elements, thus decreasing the CPU time and storage requirements and also preventing volumetric locking. The "hourglass control" is enabled to address the potential zero energy deformation modes (hourglass modes) introduced when using reduced integration (ABAQUS, 2008). The mesh design of

the coating-substrate system is shown in Figure 4.10. The shown model uses 4 element layers to discretize the coating, 8, 16 and 25 layered meshes were also used for mesh refinement analysis. A node set is defined along the coating-substrate interface for easy retrieval of displacement and stress data during post processing.

4.3 Stress Transformation

In order to properly evaluate the stresses at the coating-substrate interface, the global stress components obtained from ABAQUS (2008) must be transformed into local coordinate stress components. Figure 4.11 shows how the global coordinates axes (x-y-z) relate to the local coordinates axes (x'-y'-z'). The x' local coordinate axis is parallel to the coating-substrate interface and the y' local coordinate axis is perpendicular to the coating-substrate interface. The following equations show how the global stress components were transformed into local stress components (Benham et al., 1996):

$$\sigma_{x'x'} = \frac{\sigma_{xx}+\sigma_{yy}}{2} + \frac{\sigma_{xx}-\sigma_{yy}}{2}\cos 2\theta + \tau_{xy}\sin 2\theta \tag{4.3}$$

$$\sigma_{y'y'} = \frac{\sigma_{xx}+\sigma_{yy}}{2} - \frac{\sigma_{xx}-\sigma_{yy}}{2}\cos 2\theta - \tau_{xy}\sin 2\theta \tag{4.4}$$

$$\sigma_{z'z'} = \sigma_{zz} \tag{4.5}$$

$$\tau_{x'y'} = \frac{\sigma_{xx}-\sigma_{yy}}{2}\sin 2\theta + \tau_{xy}\cos 2\theta \tag{4.6}$$

Going forward, $\sigma_{x'x'}$, $\sigma_{y'y'}$, $\sigma_{z'z'}$, and $\tau_{x'y'}$ will be called the radial stress, the opening stress, the hoop stress and the shear stress. Note that the stress component ($\sigma_{x'x'}$) named radial stress is not perfectly radial once x' is not aligned with x, but the name is still used for

simplicity. The two out of plane shear stress components, τ_{xz} and τ_{yz}, are zero due to the problem being axisymmetric.

4.4 Results

The stress state at the coating-substrate interface was examined at two times during the simulations, first when the maximum indentation load is applied and second after unloading of the indenter. A convergence analysis is presented below, followed by plots of the von Mises stress, radial stress ($\sigma_{x'x'}$), hoop stress ($\sigma_{z'z'}$), opening stress ($\sigma_{y'y'}$), and shear stress ($\tau_{x'y'}$) along the coating-substrate interface for both the maximum load and after unloading states. The stress in the coating material and substrate material at the interface are both included in the presented stress results.

4.4.1 Convergence Analysis

A convergence analysis was completed on the indentation model using the 30 kg_f indentation load. The maximum opening and shear stresses along the coating-substrate can be used to define the coating adhesion strength since the two stress components can cause delamination growth and coating adhesion failure. For this reason, the convergence of the maximum values of these two stress components were analyzed using increasingly refined models. The opening and shear stresses experienced in the coating material and in the substrate material at the interface must be equal during perfect adhesion to satisfy equilibrium (Ramalingam, 1995). With increasing mesh refinement, the maximum opening and shear stress values in the coating and substrate should converge.

Figure 4.12 shows the convergences of maximum opening and shear stress values on both sides of the coating-substrate interface with increasing mesh refinement. The maximum

opening stress converges well before the maximum shear stress. A comparison of the maximum stress values in the coating and the substrate at the interface for the most refined model is presented in Table 4.5 (15 kg_f) and Table 4.6 (30 kg_f). The convergence of the maximum opening stress was achieved to less than a 3% difference and convergence of the maximum shear stress was achieved to less than 20% difference. The large difference between the coating and substrate maximum shear stresses is due to a sharp peak which will be presented in section 4.4.7, the difference is much smaller at all other locations along the interface.

The deformation and stress results from the most refined model are presented in the following sections for both the 15 and 30 kg_f simulations.

4.4.2 Deformed Geometry

The deformed geometry of the coating-substrate interface is shown in Figure 4.13 and Figure 4.14 for the 15 and 30 kg_f loading conditions respectively. The indentation radius values are approximately 80 and 110 μm for the 15 and 30 kg_f loading conditions. Coating adhesion failure was observed around the crater circumference during experimental testing and therefore large opening and/or shear stresses are expected in this region.

4.4.3 Von Mises Stress Results

Von Mises stress contour plots are shown in Figure 4.15 (maximum load case) and Figure 4.16 (after unloading) for the 30 kg_f indentation case. At maximum load, large von Mises stresses occur in the coating under the indenter and extend outward past the indentation radius. After unloading, the von Mises stress is significantly reduced inside the crater region, but large values are still present outside the indentation radius. Very low von Mises stress

gradients are present near the bottom and right edges of the model, which shows that the model was properly sized.

Figure 4.17 (15 kg_f) and Figure 4.18 (30 kg_f) show the von Mises stress distribution along the coating-substrate interface at both the maximum load condition and after unloading. The maximum von Mises stress experienced in the coating is 8.31 GPa and 8.39 GPa for the 15 and 30 kg_f loading conditions respectively. The maximum von Mises stress experienced in the substrate is 3.10 GPa and 3.23 GPa for the 15 and 30 kg_f loading conditions respectively. All the maximum von Mises stresses occur at the maximum load condition.

4.4.4 Radial Stress Results

The radial stress ($\sigma_{x'x'}$) distributions along the coating-substrate interface for the 15 and 30 kg_f loading cases are plotted in Figure 4.19 and Figure 4.20 respectively. A sharp compressive stress peak is present in the coating at the edge of the indentation craters (80 and 110 μm) at the maximum loading condition. This compressive stress could be responsible for coating buckling which could lead to circumferential cracking or coating spallation if delaminations are present at the coating-substrate interface. The maximum compressive radial stress occurs at maximum loading, the values for the 15 and 30 kg_f loading conditions are 11.29 GPa and 12.69 GPa.

4.4.5 Hoop Stress Results

The hoop stress ($\sigma_{z'z'}$) distributions for the 15 and 30 kg_f loading cases are plotted in Figure 4.21 and Figure 4.22. The hoop stress in the coating reaches a maximum after unloading at a location a few microns outside the indentation crater. This tensile hoop stress is the cause of radial through thickness coating cracking observed during experimental testing. The

maximums values occur after unloading and are equal to 4.41 GPa and 5.17 GPa for the 15 and 30 kg_f loading cases respectively.

4.4.6 Opening Stress Results

The opening stress ($\sigma_{y'y'}$) distribution along the interface is shown in Figure 4.23 (15 kg_f) and Figure 4.24 (30 kg_f). The coating and substrate opening stress distribution match very well as expected to do stress equilibrium perpendicular to the interface (Ramalingam, 1995). The maximum opening stress occurs near the indentation crater edge after unloading with values of 0.896 GPa (coating) and 0.872 GPa (substrate) for the 15 kg_f loading case and of 1.18 GPa (coating) and 1.16 GPa (substrate) for the 30 kg_f loading case. These simulated opening stresses provide a measure of the coating adhesion strength for the mirror surface and Bullion and Glass Bead laser frosted surface.

4.4.7 Shear Stress Results

The shear stress ($\tau_{x'y'}$) distribution along the interface for the 15 and 30 kg_f loading cases are plotted in Figure 4.25 and Figure 4.26. To satisfy equilibrium conditions along the coating-substrate interface, the shear stress in the coating and substrate materials must be equal and the results agree well with this equilibrium condition (Ramalingam, 1995). The difference between the coating and substrate shear stress value is minimal except near the indentation crater edge where a nearly 20% difference occurs. The maximum shear stress values along the interface are 1.89 GPa (coating) and 1.67 GPa (substrate) for the 15 kg_f loading case and of 2.16 GPa (coating) and 1.78 GPa (substrate) for the 30 kg_f loading case. These maximum shear stress values occur at maximum loading of the indenter and provide a measure of the coating adhesion strength for the simulated surface types.

4.5 Summary

The stress state at the coating-substrate interface during 15 and 30 kg_f indentation tests has been simulated. Peak stress values were found in the region near the indentation crater edge, which is where failure was observed during experimental testing. Using finite element simulations, the PVD coating deposited on a mirror surface and Glass Bead and Bullion laser frosted surfaces was found to be capable of surviving the loads presented in Table 4.7. The peak opening and shear stresses at the coating-substrate interface provide a characterization of the coating adhesion strength since these two stress components are capable of directly causing delamination growth and coating adhesion failure. Significant compressive radial stress is present in the coating outside the indentation crater. In the presence of coating adhesion defects, this compressive stress can lead to coating buckling and spallation.

The three stress components (opening, shear, and radial compressive) reach their peak near the indentation crater edge, which is the location where coating delamination was occurred during experimental testing at higher loads. Now that the stress state at the coating-substrate interface produced during indentation adhesion tests has been simulated and analyzed, a similar process can be performed for the scratch adhesion tests and the results can be compared.

Property	Symbol	Value
Elastic Modulus	E_s	213 GPa
Yield Strength	σ_{ys}	2.35 GPa
Poisson's Ratio	ν_s	0.3
Strain hardening exponent	n_s	15
Yield offset	α_s	0.18

Table 4.1: Material properties of the simulated substrate

Load (kg_f)	Indentation crater radius (μm)			
	Trial Number			Average
	1	2	3	
15	93.83	94.56	94.91	94.4
30	122.1	121.8	121.8	121.9
45	143.6	144.2	144.1	144.0
60	155.3	155.4	155.4	155.4
100	201.7	201.7	200.8	201.4
150	247.1	248.8	247.2	247.7

Table 4.2: Experimental indenation crater size

Load (kg_f)	n = 10		n = 15		n = 15 refined		n = 20	
	Radius (μm)	Depth (μm)	Radius (μm)	Depth (μm)	Radius (μm)	Depth (μm)	Radius (μm)	Depth (μm)
15	80	16.7	80	16.7	80	16.7	82	17.6
30	107	30.8	114	34.9	112	33.7	115	35.5
45	132	45.3	138	48.7	137	48.2	142	51.0
60	151	56.2	158	60.3	159	60.9	164	63.7
100	194	81.1	203	86.3	206	88.0	212	91.5
150	238	106.5	250	113.4	253	115.1	260	119.2

Table 4.3: Simulated indentation crater size using ABAQUS and multiple strain hardening exponent values

Property	Symbol	Value
Elastic Modulus	E_c	300 GPa
Yield Strength	σ_{yc}	8.2 GPa
Poisson's Ratio	ν_c	0.15
Strain hardening exponent	n_c	100
Yield offset	α_c	1

Table 4.4: Material properties of the simulated coating

Stress Type	Coating	Substrate	% Difference
Maximum Opening stress (GPa)	0.8956	0.8720	2.7%
Maximum Shear stress magnitude (GPa)	1.890	1.674	12.1%

Table 4.5: Convergence of the coating and substrate maximum opening and shear stresses for the 15 kg_f indentation simulation using the most refined model

Stress Type	Coating	Substrate	% Difference
Maximum Opening stress (GPa)	1.180	1.155	2.1%
Maximum Shear stress magnitude (GPa)	2.161	1.778	19.4%

Table 4.6: Convergence of the coating and substrate maximum opening and shear stresses for the 30 kg_f indentation simulation using the most refined model

Stress Component *[material]*	**15 kg_f (Glass Bead)**	**30 kg_f (mirror and Bullion)**
Maximum Opening stress (GPa) *[average of coating and substrate value]*	0.884	1.17
Maximum Shear stress (GPa) *[average of coating and substrate value]*	1.78	1.97
Maximum Compressive stress (GPa) *[coating value]*	-11.3	-12.7

Table 4.7: Important stress values for coating adhesion strength characterisation

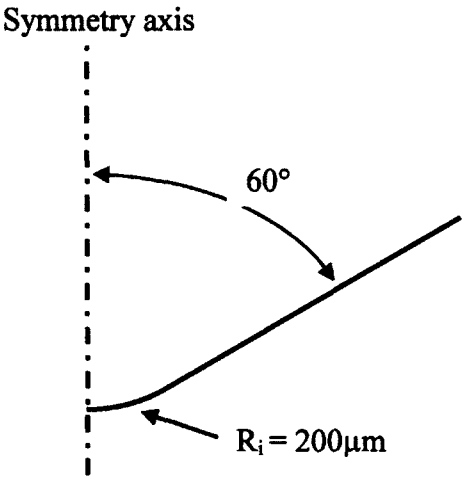

Figure 4.1: Rockwell C indenter tip geometry

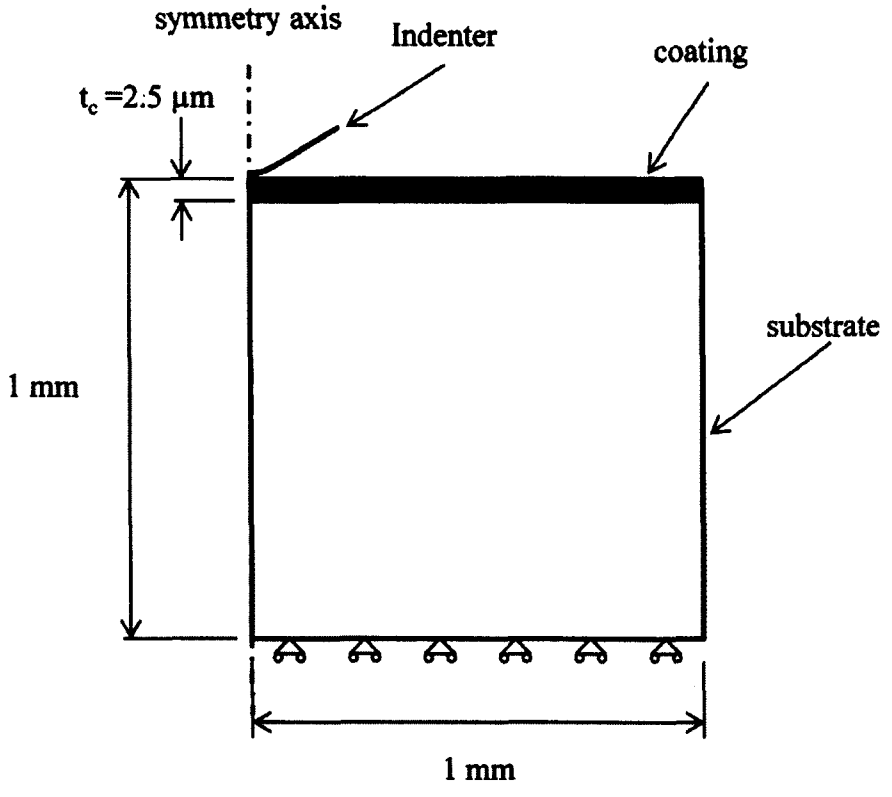

Figure 4.2: Die geometry and boundary conditions (not to scale)

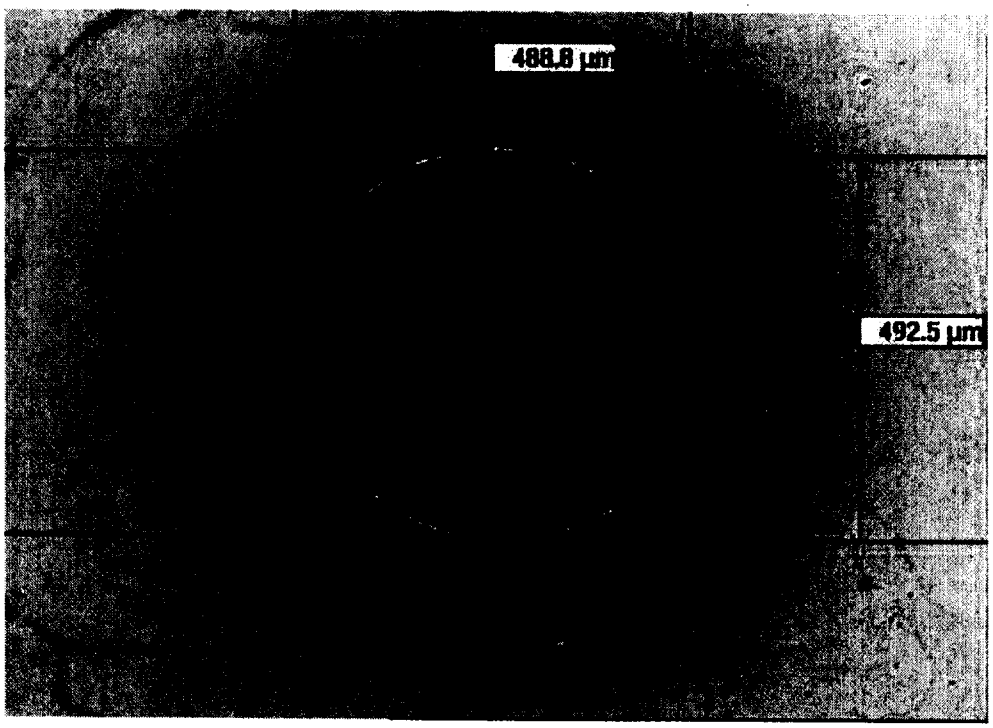

Figure 4.3: Example of indantation size measurement

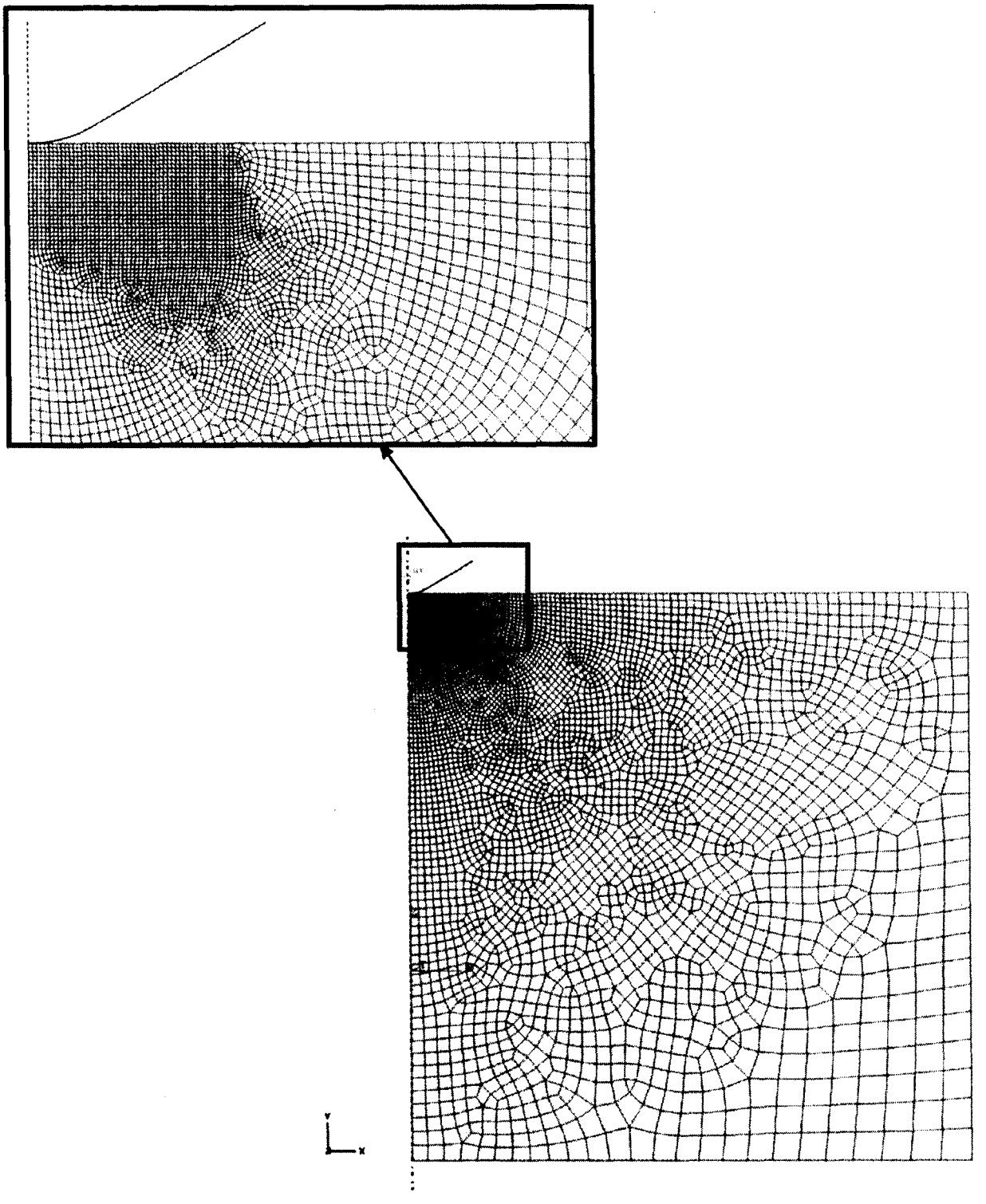

Figure 4.4: Coarse mesh used for simulation of the indentation test performed on the uncoated substrate

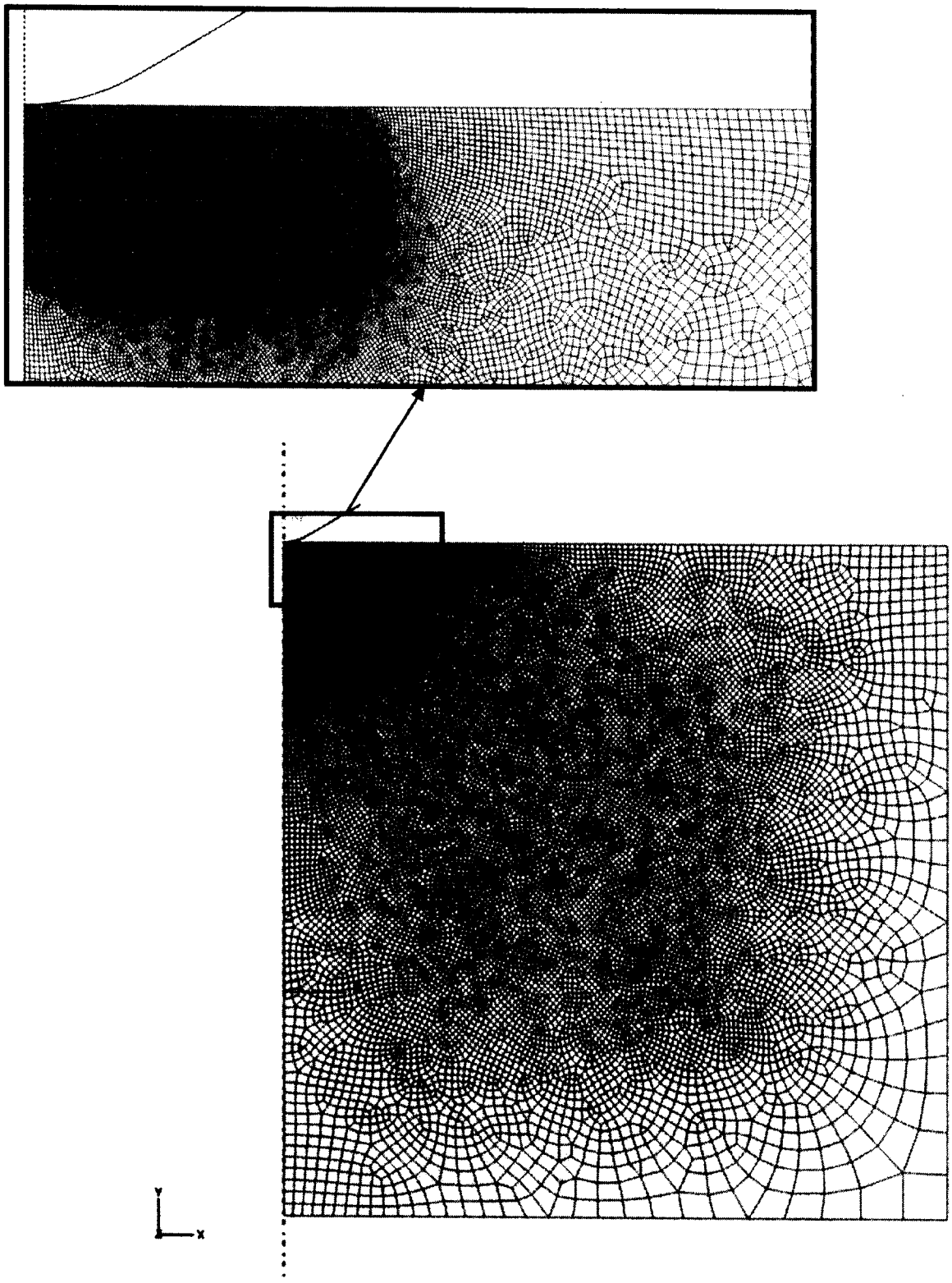

Figure 4.5: Refined mesh used for simulation of the indentation test performed on the uncoated substrate

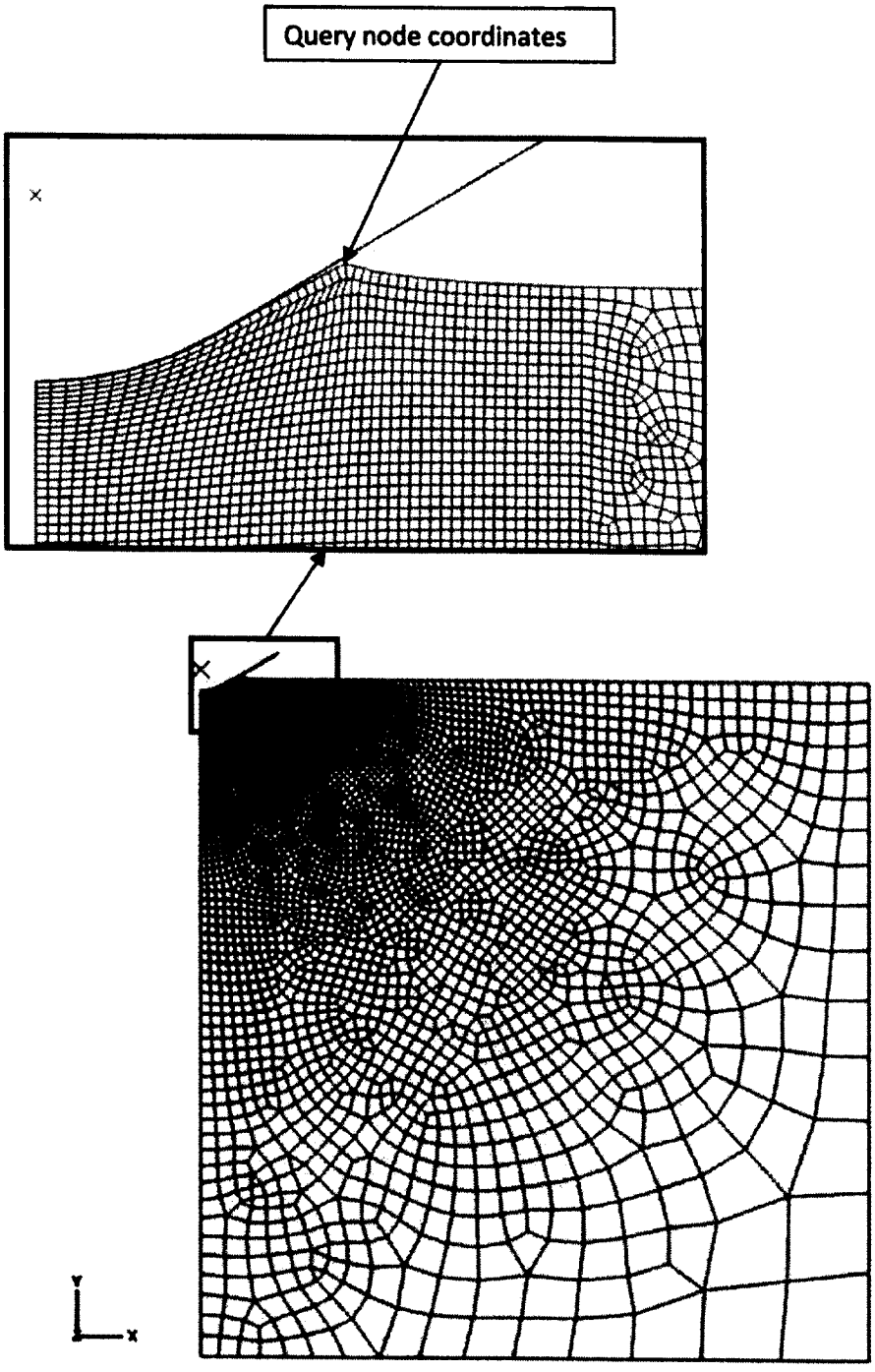

Figure 4.6: Example of completed indentation simulation with crater sizing

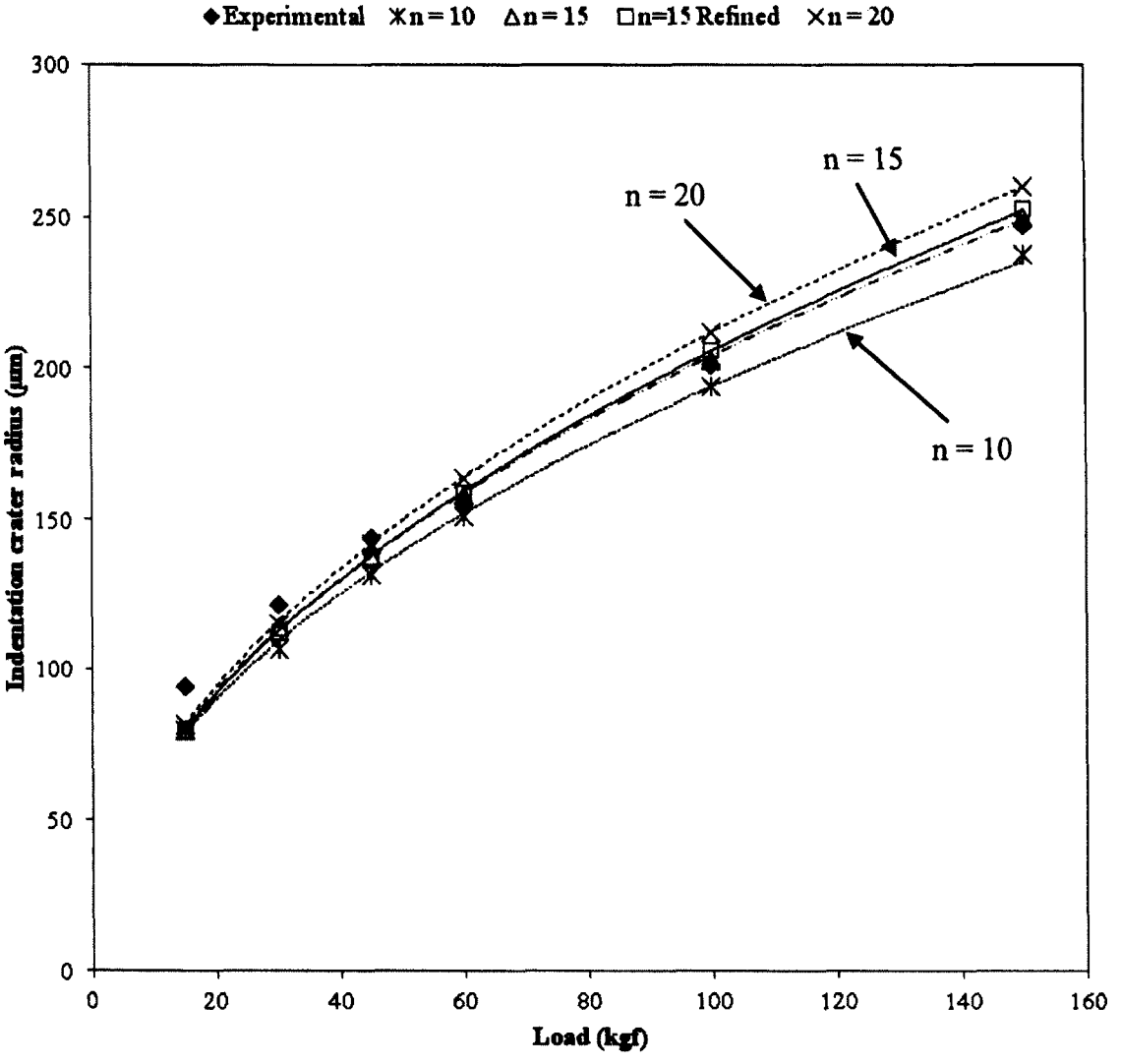

Figure 4.7: Comparison of the experimentally measured indentation crater size and the ABAQUS results using the Ramberg-Osgood formulation

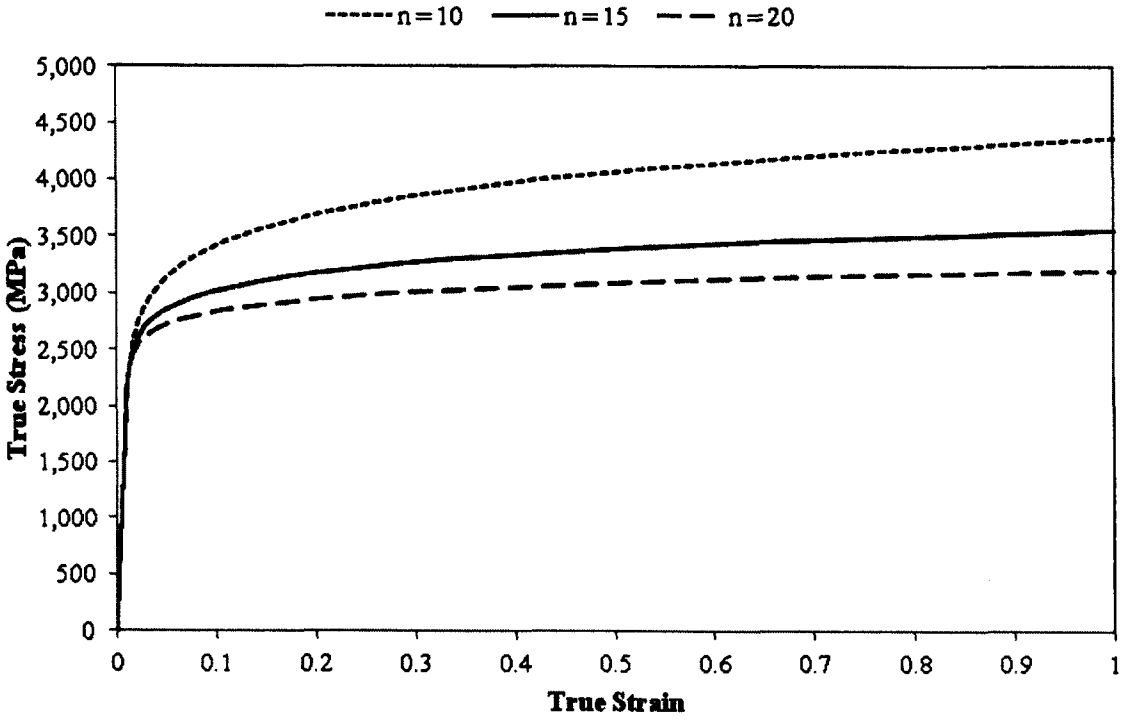

Figure 4.8: True stress strain curve of the substrate Ramberg-Osgood formulation with α = 0.18 and multiple values of n

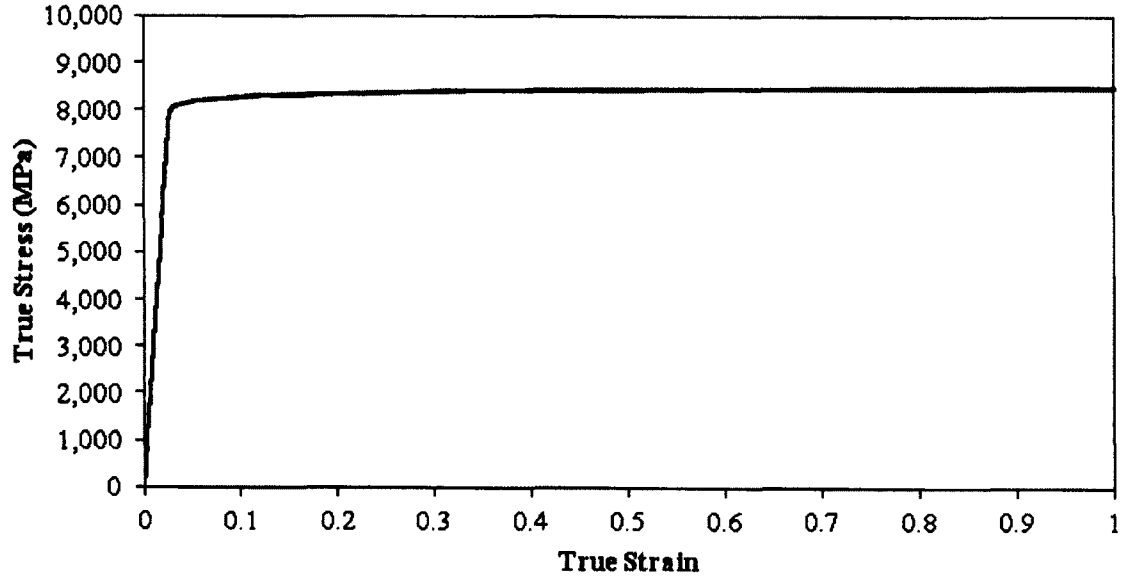

Figure 4.9: True stress strain curve of the coating Ramberg-Osgood formulation with α = 1 and n = 100

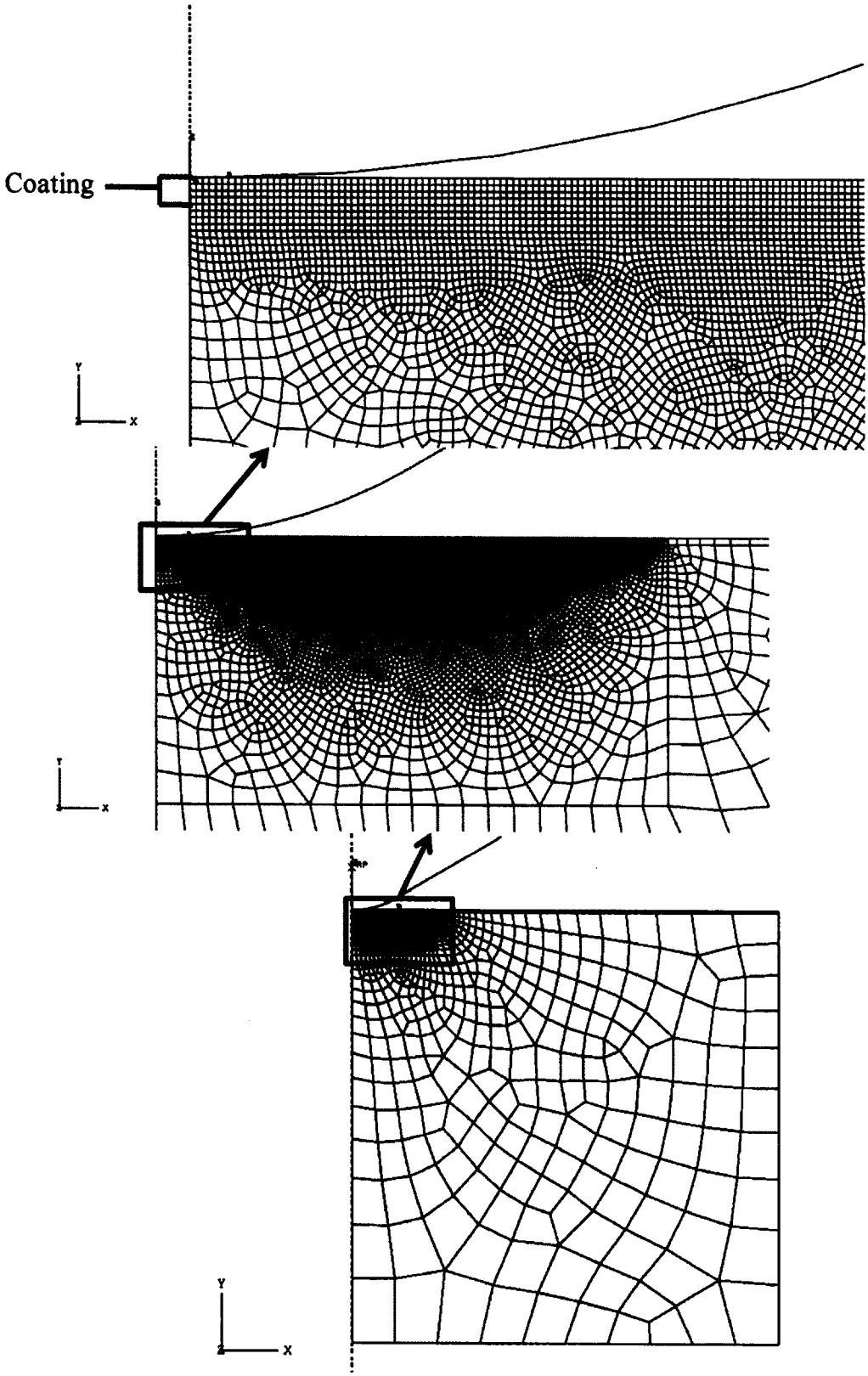

Figure 4.10: Coating substrate mesh design, 4 element layer coating

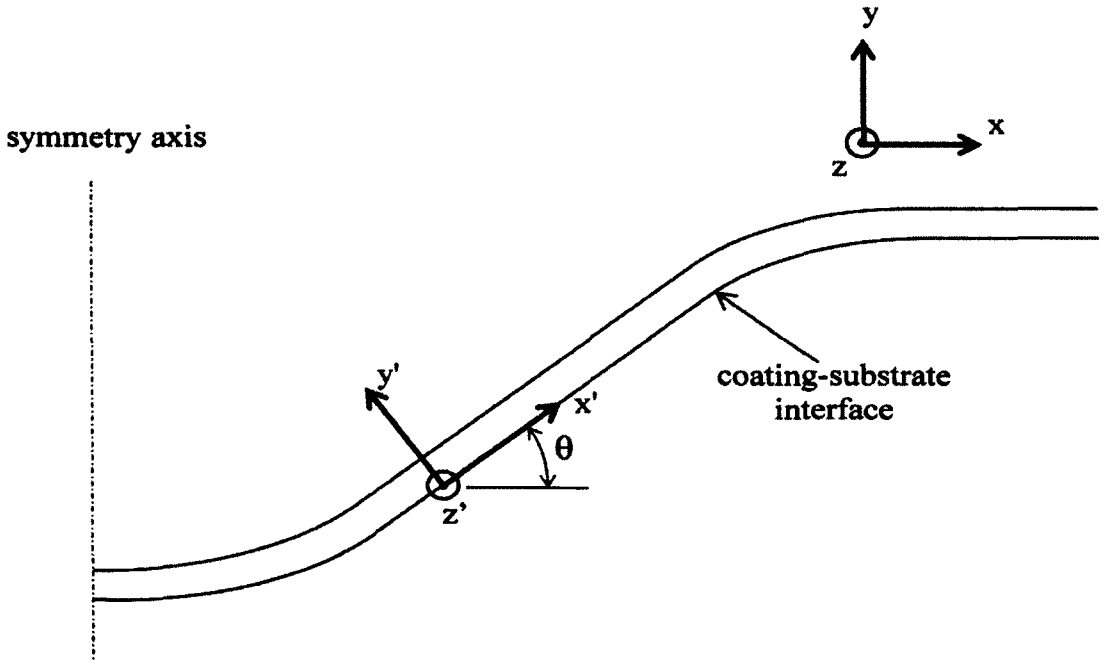

Figure 4.11: Local coordinate system at the coating-substrate interface

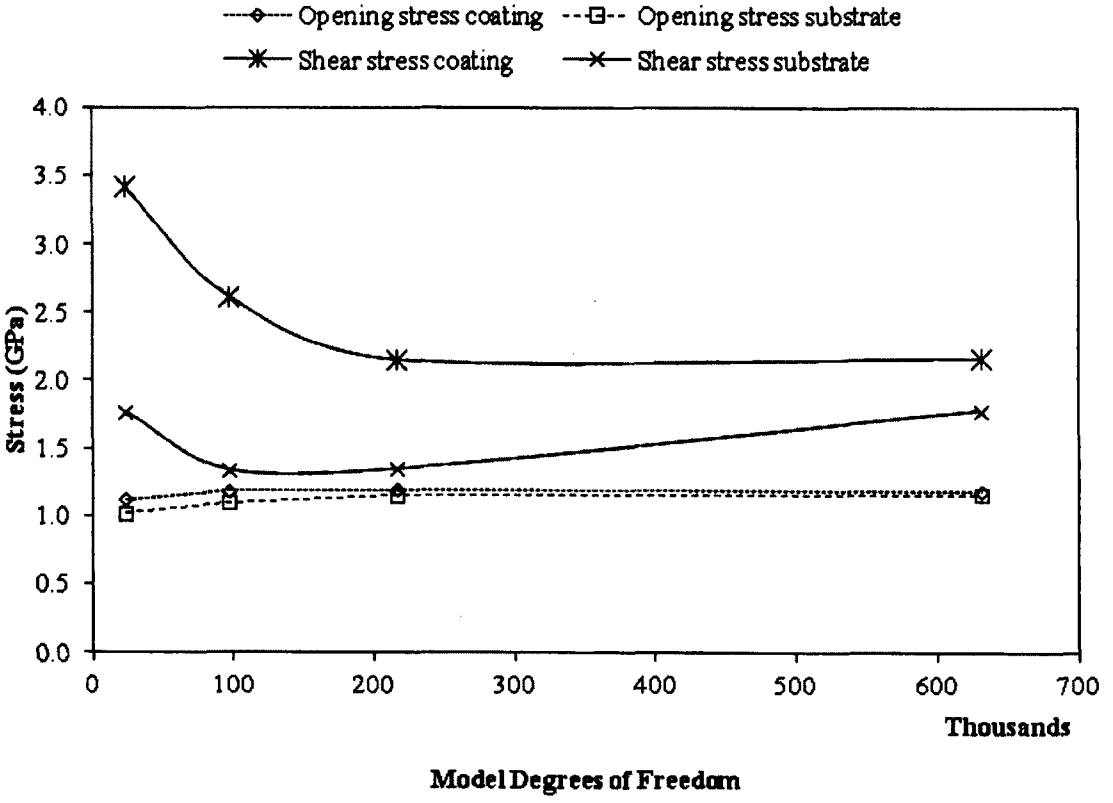

Figure 4.12: Convergence of the maximum opening and shear stress for the 30 kg_f loading simulation

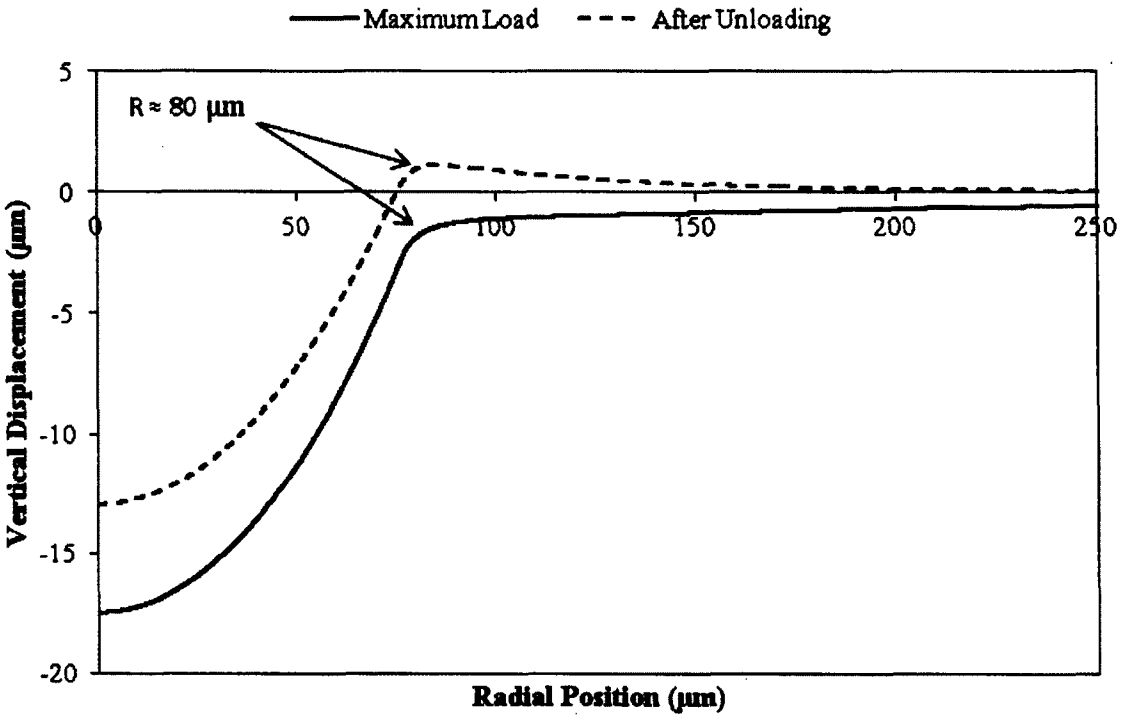

Figure 4.13: Indentation geometry for the 15 kg_f simulation

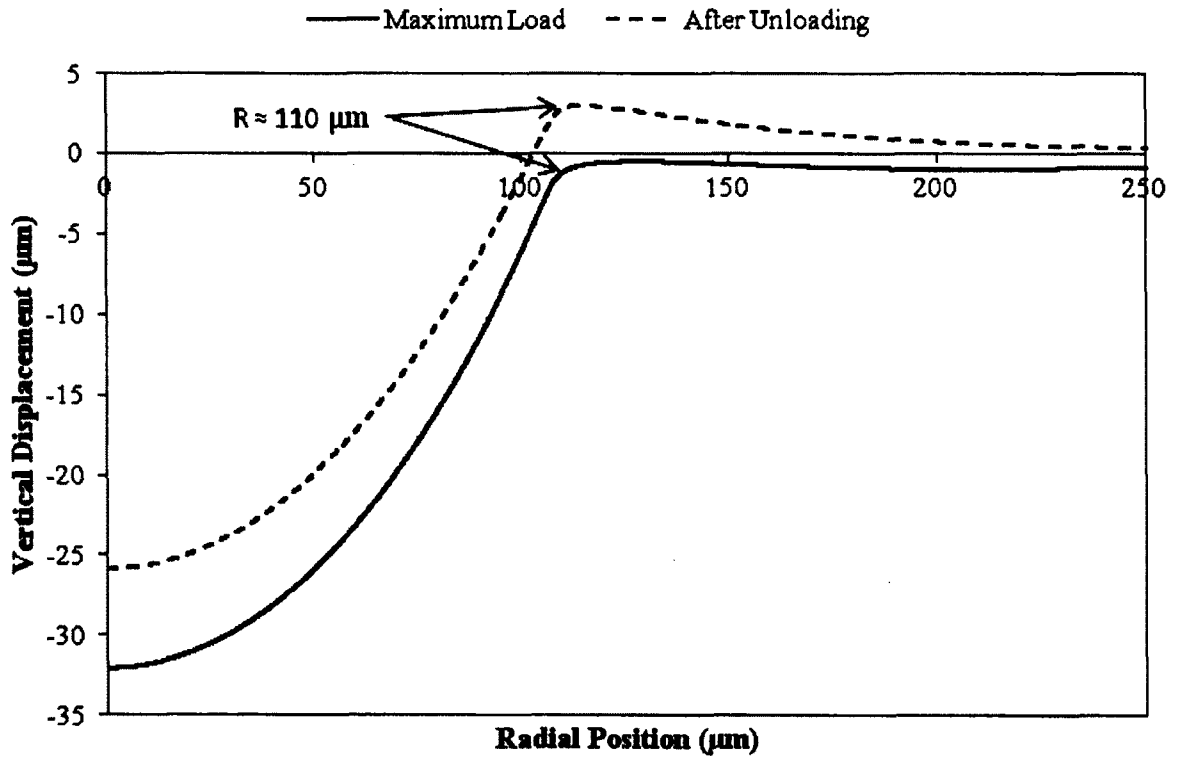

Figure 4.14: Indentation geometry for the 30 kg_f simulation

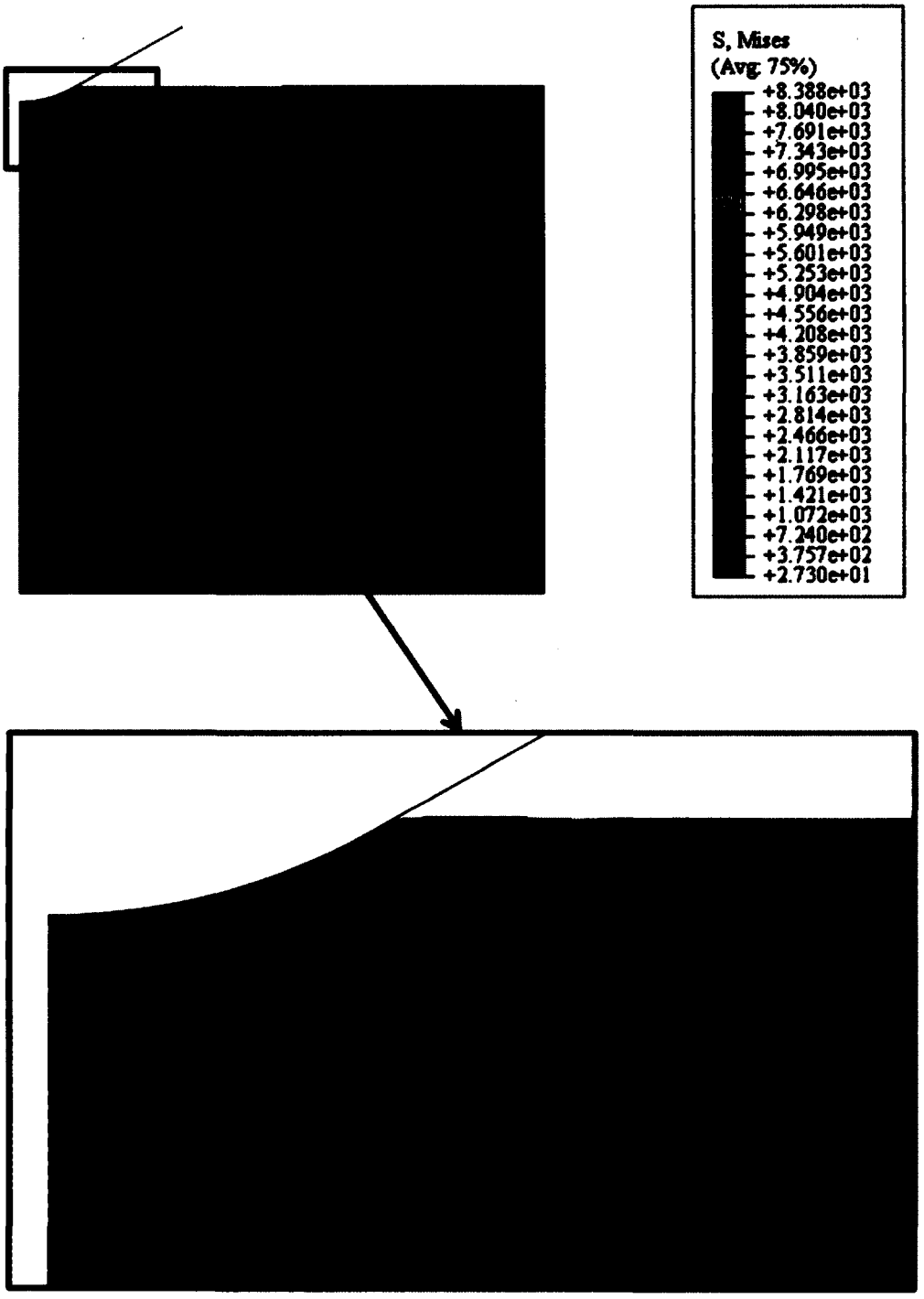

Figure 4.15: von Mises Stress contour at the 30 kg_f loading condition

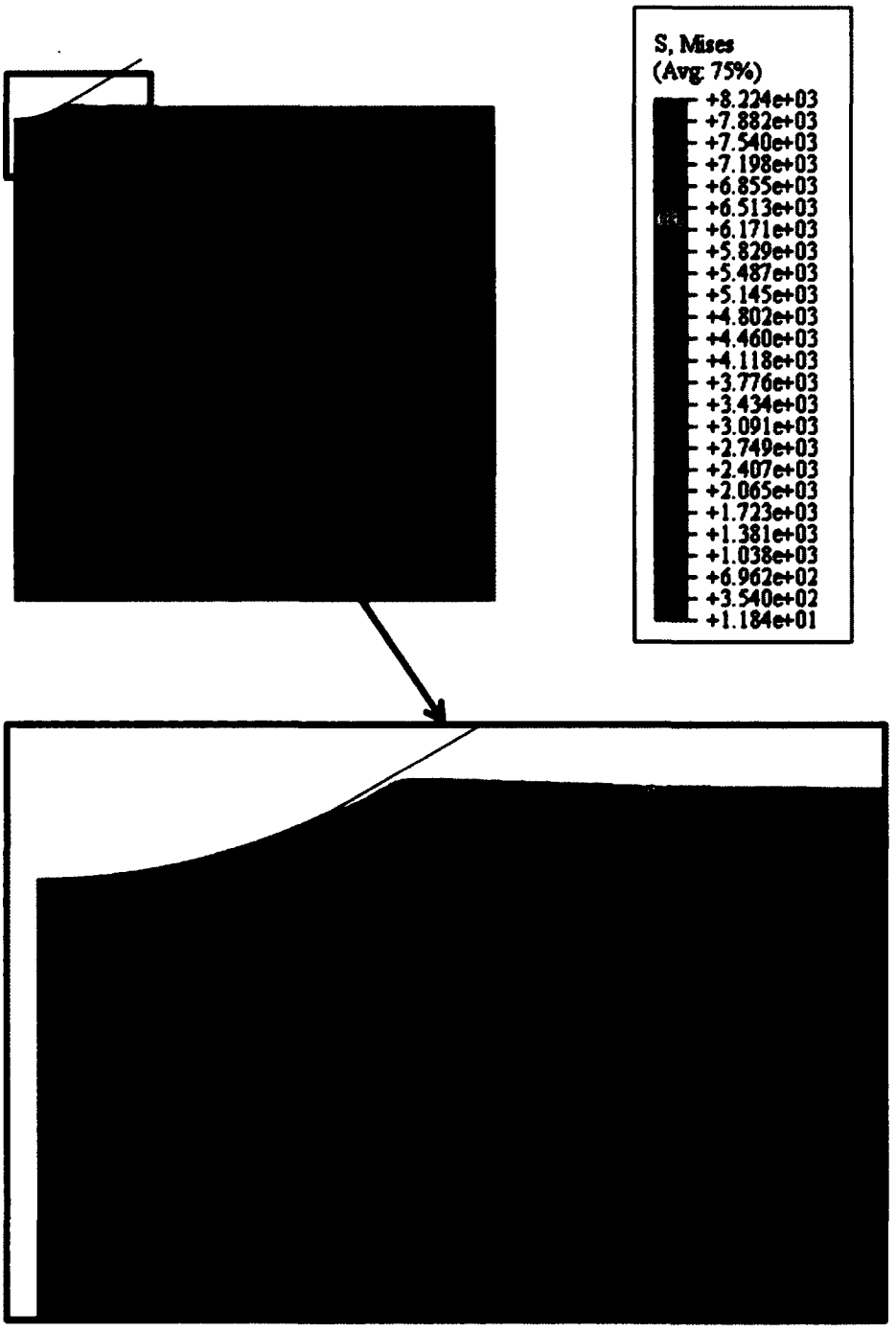

Figure 4.16: von Mises Stress contour after unloading the 30 kg_f load

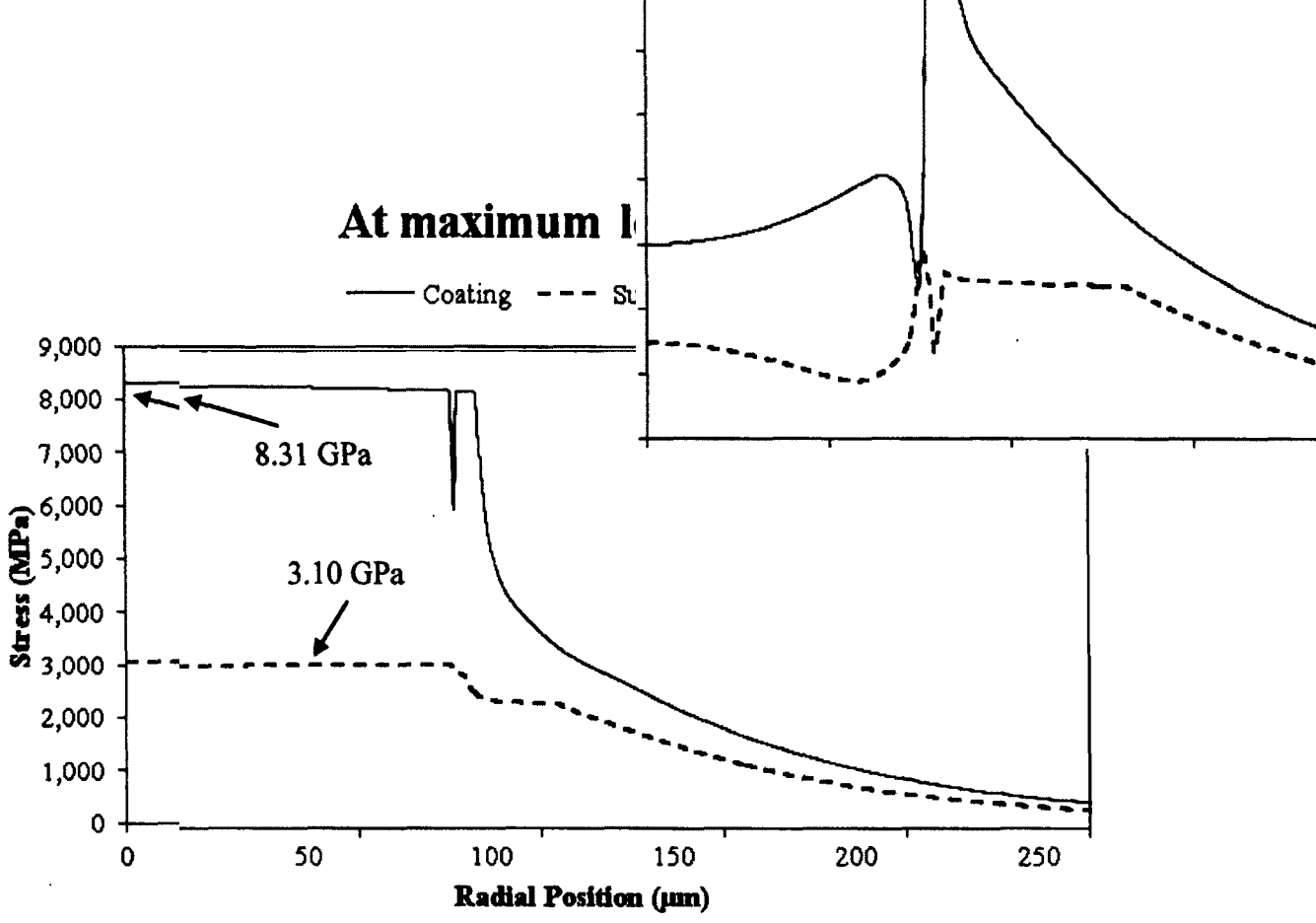

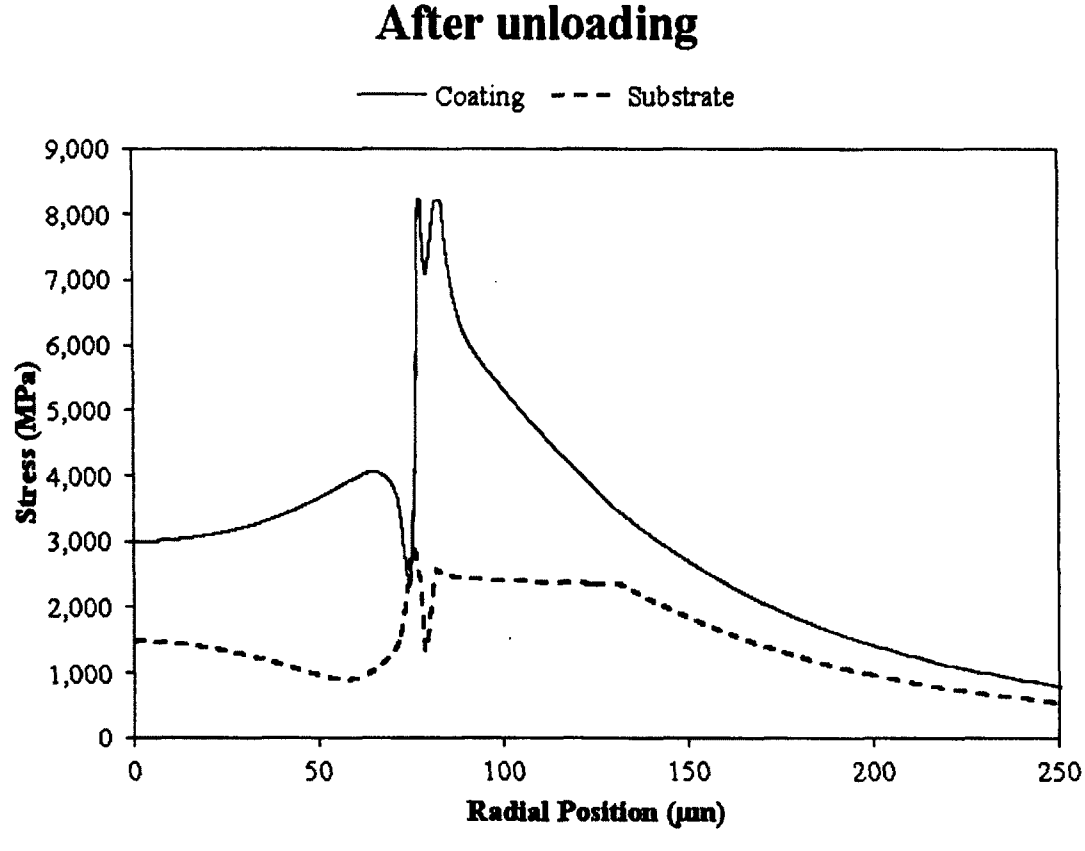

Figure 4.17: von Mises stresses at the coating-substrate interface for the 15 kg_f case

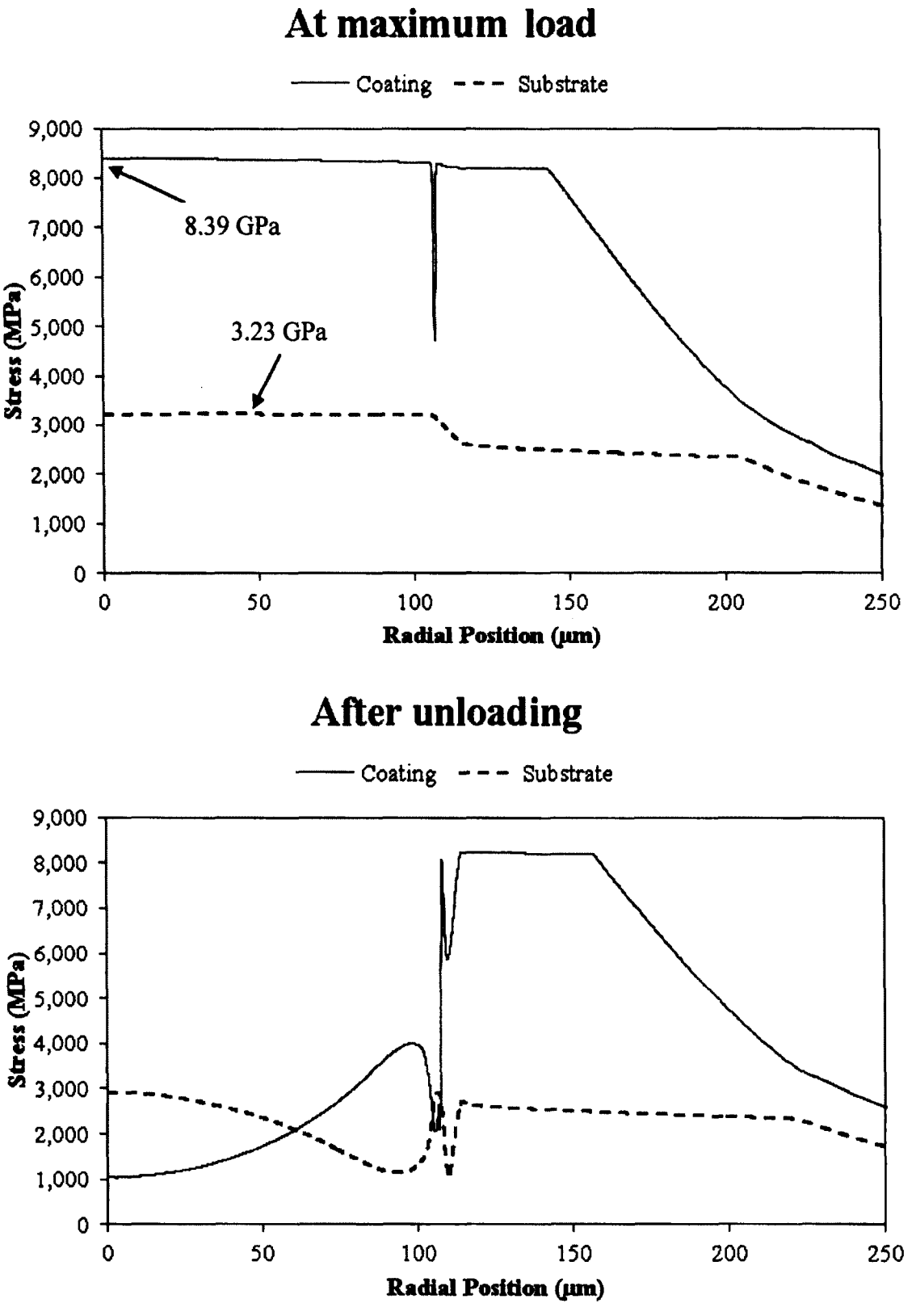

Figure 4.18: von Mises stresses at the coating-substrate interface for the 30 kg_f case

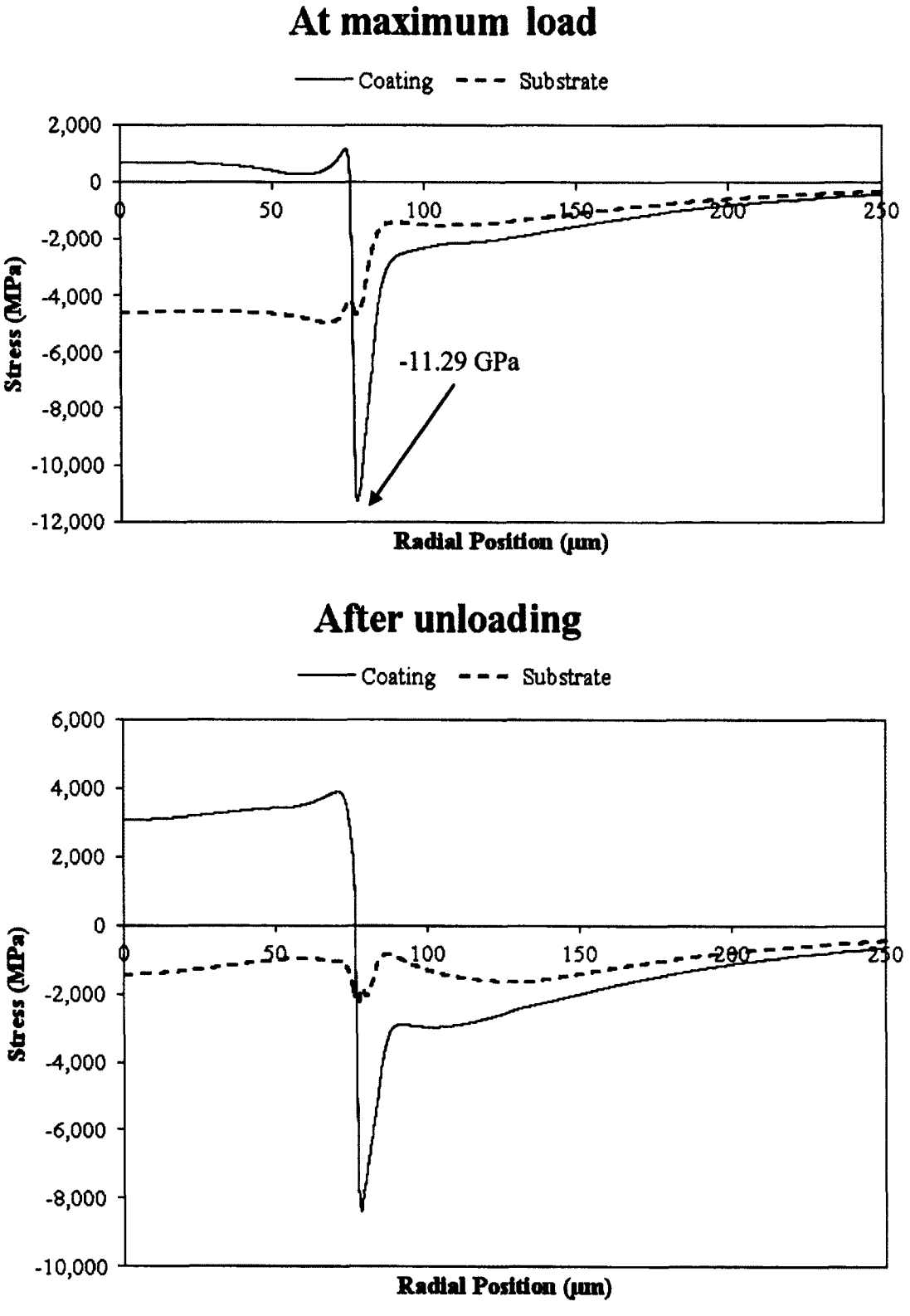

Figure 4.19: Radial stress at the coating-substrate interface for the 15 kg_f case

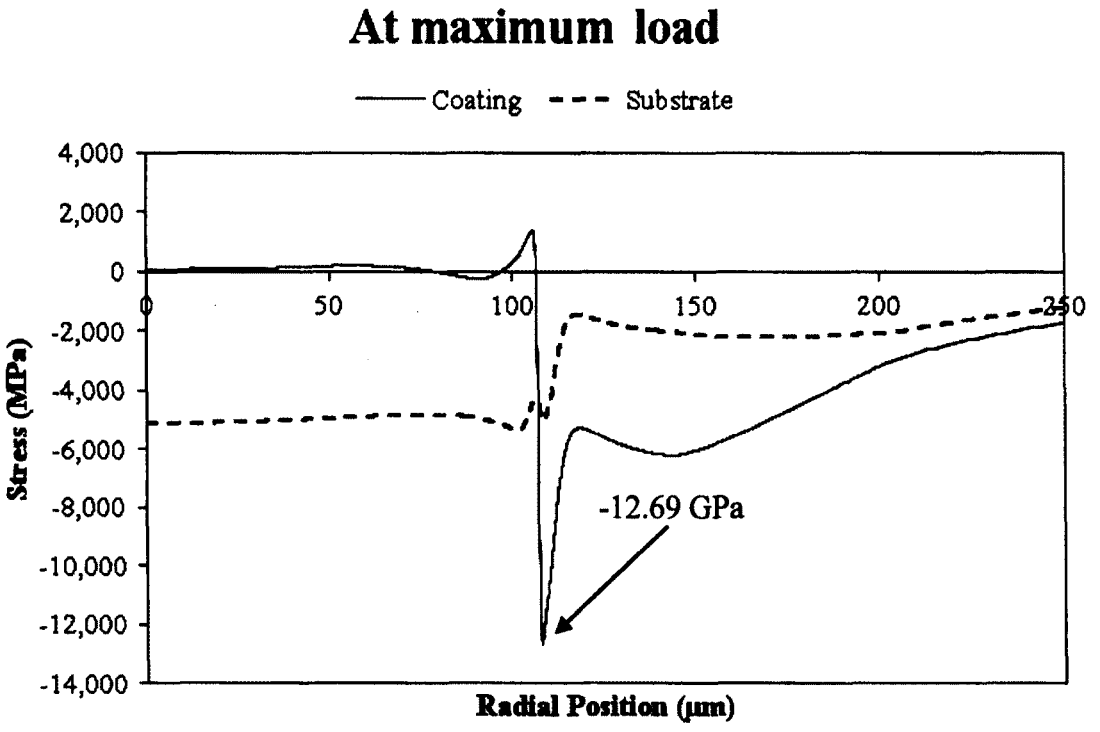

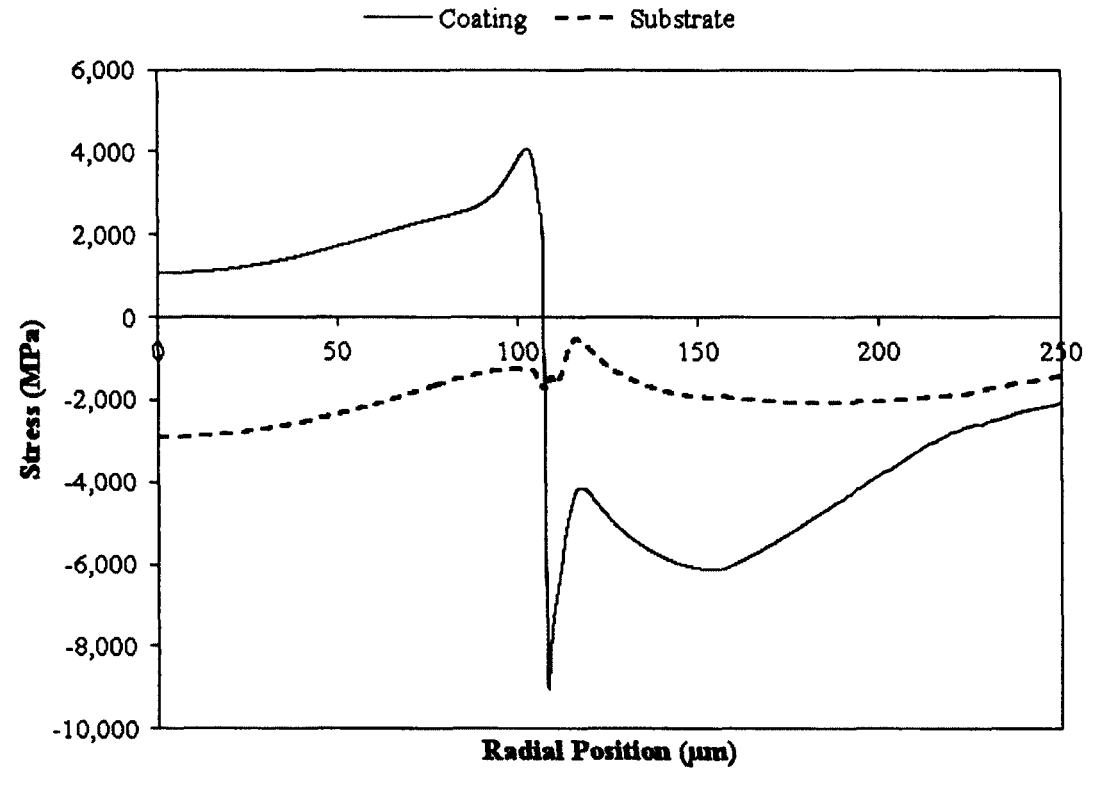

Figure 4.20: Radial stress at the coating-substrate interface for the 30 kg_f case

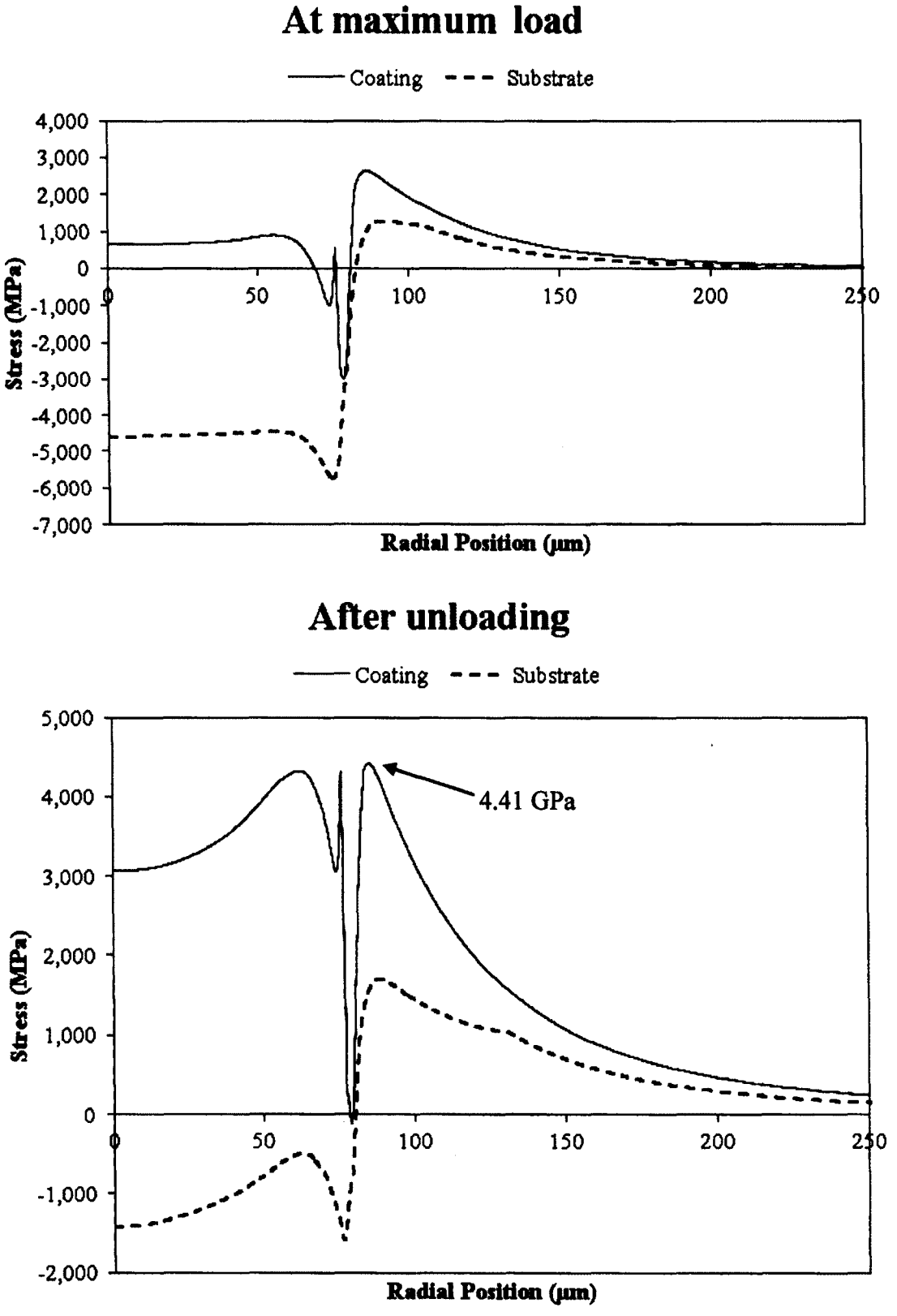

Figure 4.21: Hoop stress at the coating-substrate interface for the 15 kg_f case

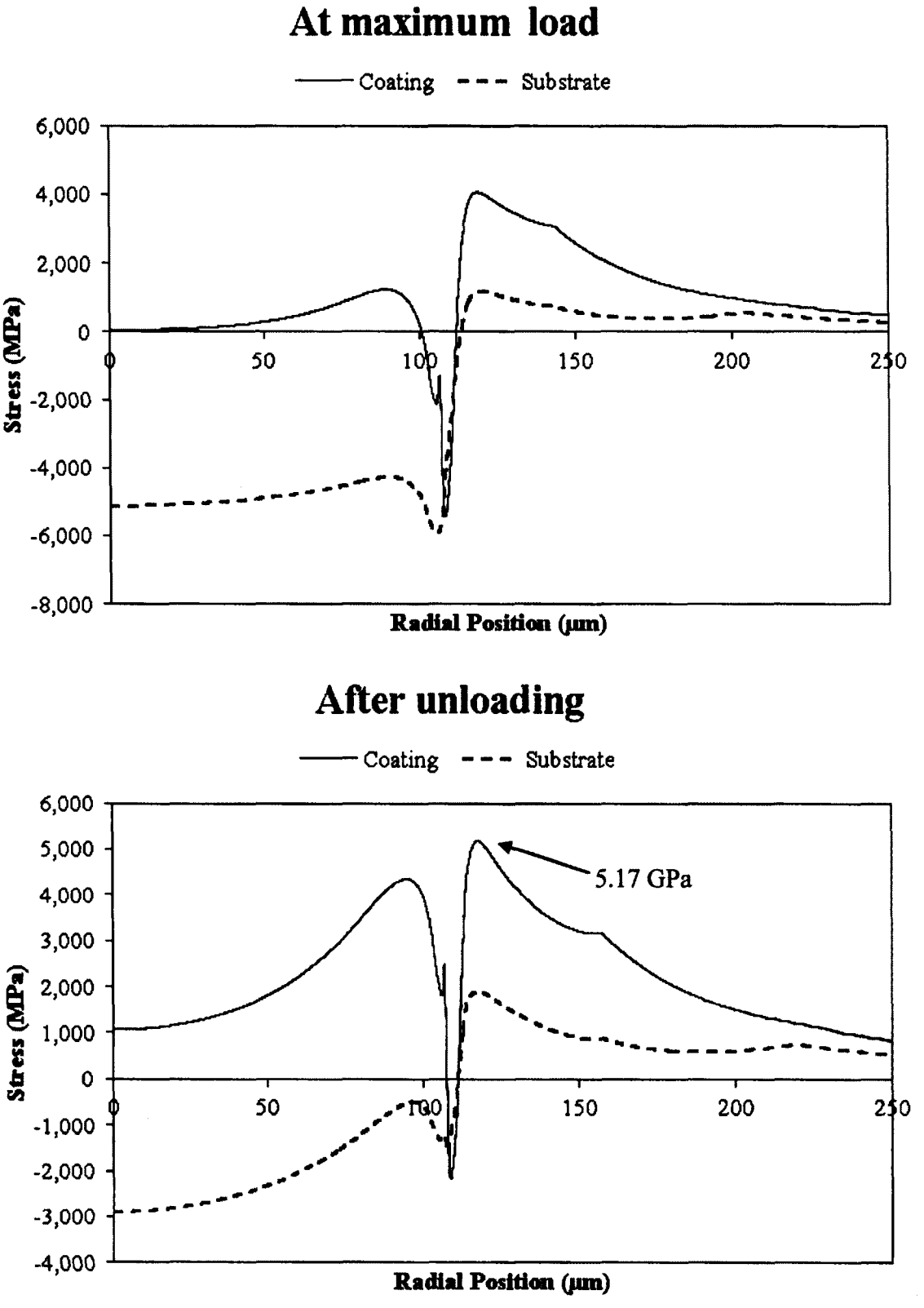

Figure 4.22: Hoop stress at the coating-substrate interface for the 30 kg_f case

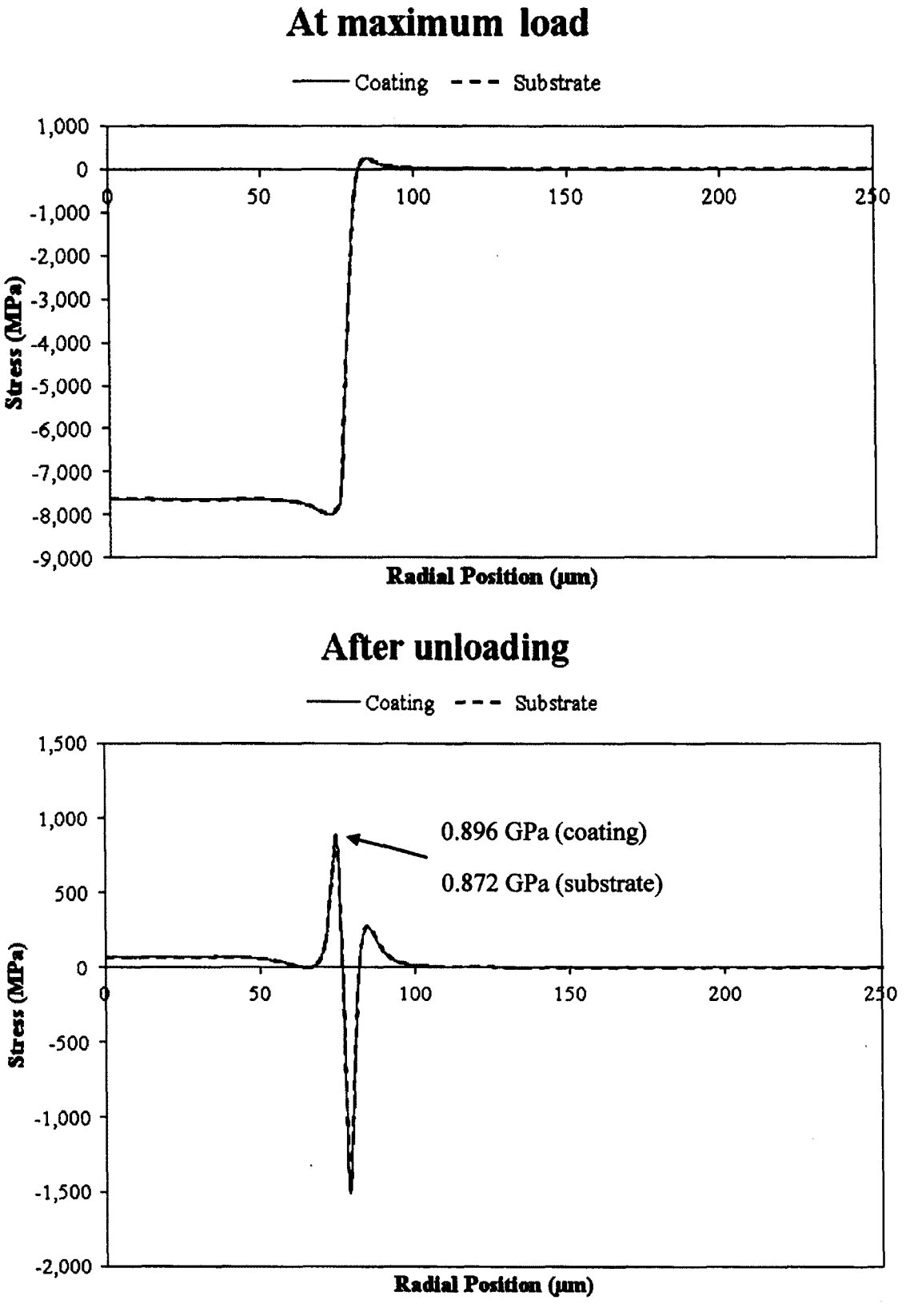

Figure 4.23: Opening stress at the coating-substrate interface for the 15 kg_f case

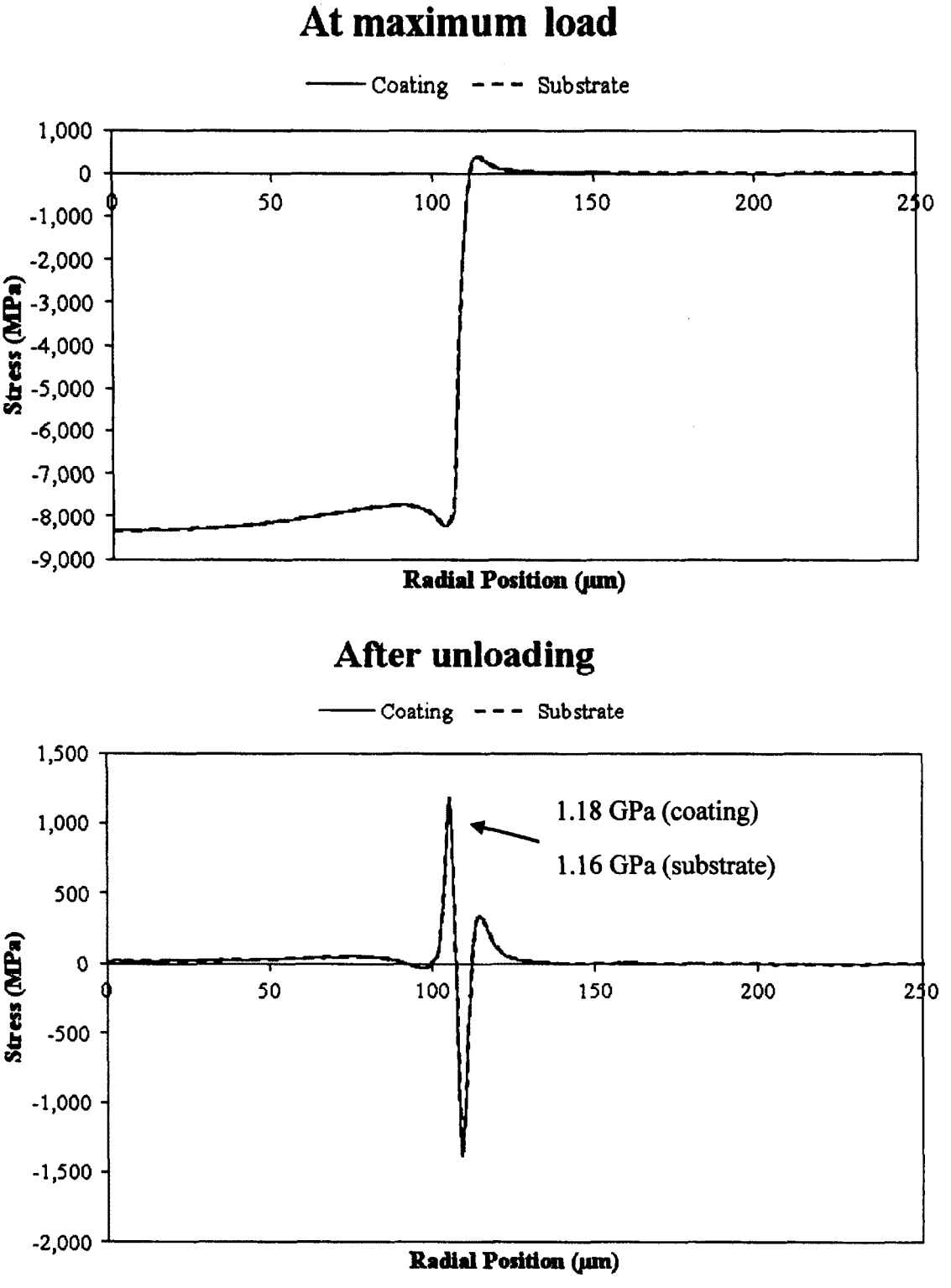

Figure 4.24: Opening stress at the coating-substrate interface for the 30 kg_f case

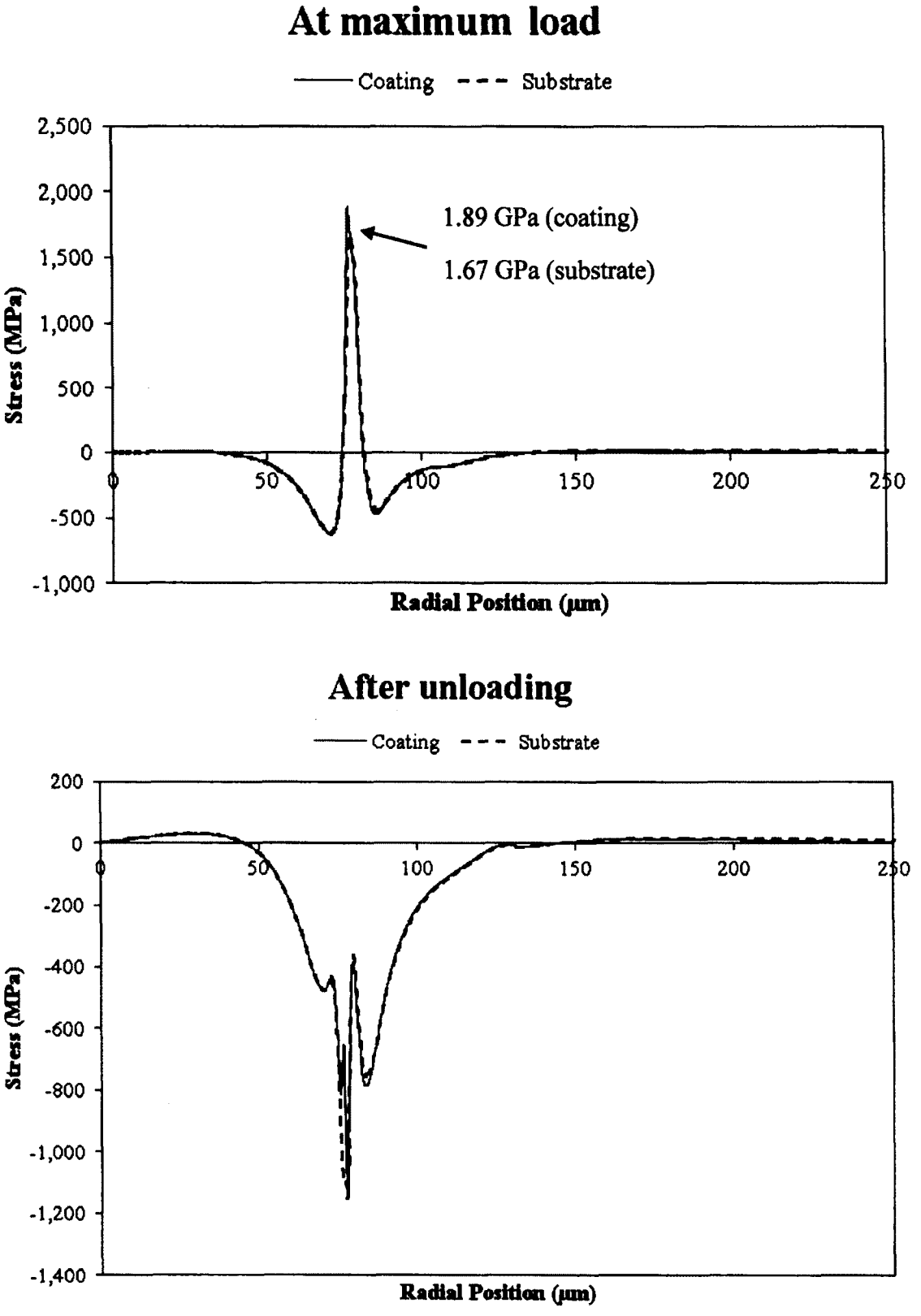

Figure 4.25: Shear stress at the coating-substrate interface for the 15 kg_f case

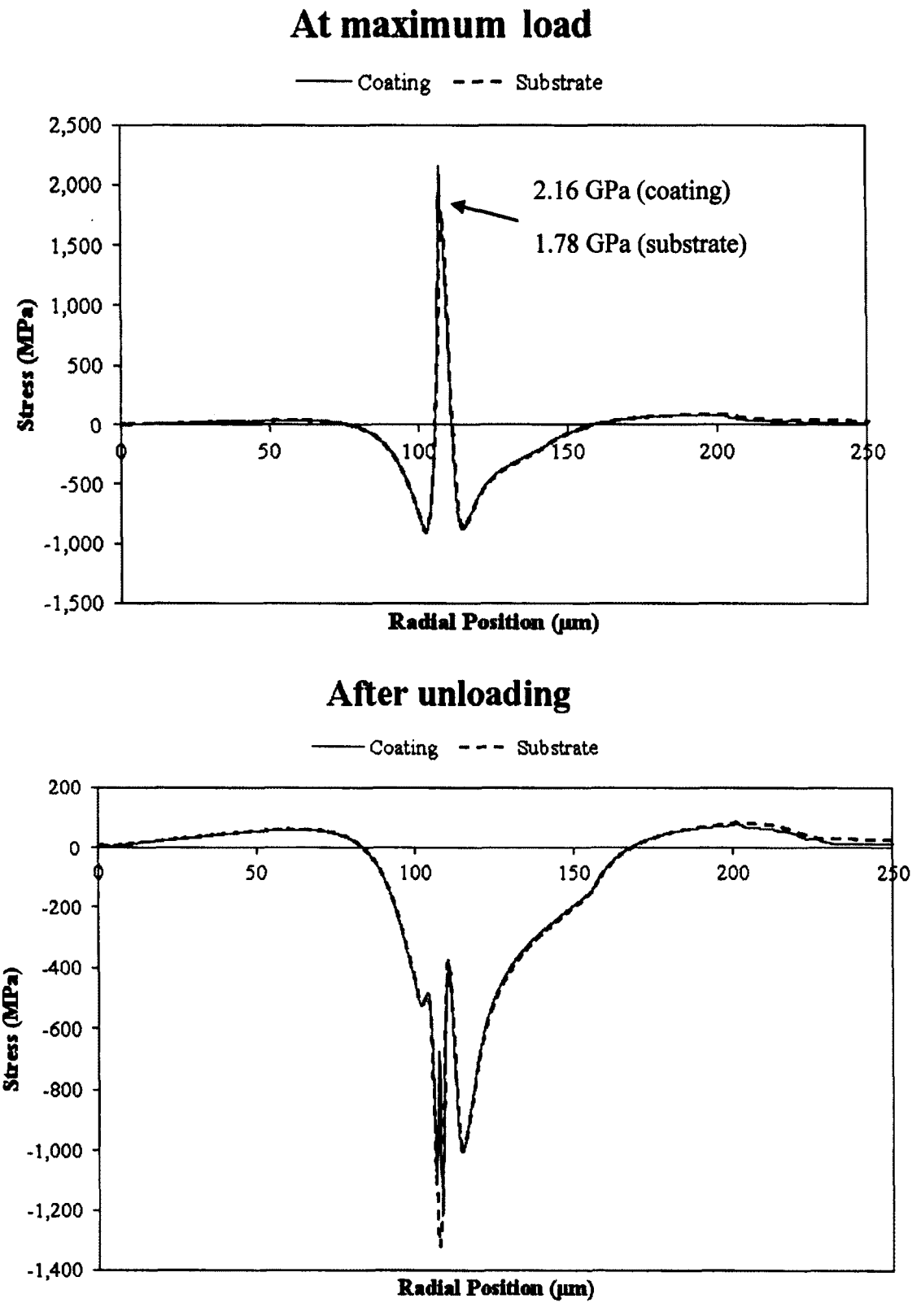

Figure 4.26: Shear stress at the coating-substrate interface for the 30 kg_f case

Chapter 5: Three-dimensional Scratch Adhesion Test Simulation

This chapter presents the simulations of scratch adhesion tests using ABAQUS (2008). The estimated failure load found in Chapter 3 for the scratch test is used as the input load to the simulations. Due to the large variability of the scratch test results and the computational costs of three-dimensional scratch test simulation, only a scratch test simulating the PVD coating failure on a mirror surface was completed with a failure loading of 30 N.

The following sections discuss the finite element model geometry, boundary conditions, material properties, and mesh design. A summary of the stress state at the coating-substrate interface is then presented. The computed stresses help to quantify the coating adhesion and will also be compared to the results for the indentation test simulations from Chapter 4.

5.1 FEM Model Geometry and Setup

The scratch test simulation consists of four separate steps. First the indenter is lowered to the die surface. A load is then applied, followed by a translation of the indenter, and finally an unloading step. The scratch test was modeled as quasi-static since the indenter translates slowly and therefore, time-dependant effects were neglected. To simplify the analysis, the load on the indenter during the translation was not increased linearly up to the critical load (30 N), but instead the indenter load was first loaded up to the critical load and then held constant during translation. A schematic of the scratch test model is shown in Figure 5.1. F_N represents the normal load placed on the indenter during translation. Since the scratch test

has a plane of symmetry, only half of the system was modeled. ABAQUS /Standard version 6.8 (2008) was used for the finite element analysis.

5.1.1 Indenter Geometry and Properties

The indenter geometry is the same as the Rockwell-C indenter used in the indentation simulation. Instead of simply being defined by a curve as in the axisymmetric case, the scratch test indenter is defined by a revolution. The indenter is again defined as an analytical rigid body due to its high hardness compared to that of the die substrate.

5.1.2 Die Geometry and Properties

The die geometry, shown in Figure 5.2, is defined by a 0.5 mm long extrusion of a 0.2 mm radius quarter circle. As labeled in Figure 5.2, an x-plane of symmetry boundary condition is placed on the plane of symmetry, z displacement is fixed at both ends of the extrusion, and the curved back surface is fixed. The indenter is offset by 0.05 mm from one end face and translates a total of 0.4 mm along the z-axis to finish at a distance of 0.05 mm from the other end face. The size used is large enough that the localized stress field is not affected by edge effects except near the start and end of the scratch path. The coating and substrate properties used are the same as those presented in Chapter 4 for the indentation simulations.

5.1.3 Interface Properties

Coating-substrate interface

The interface between the coating and substrate is modeled as perfect adhesion since the loading condition used simulates a scratch test where the coating-substrate interface has yet to suffer adhesion failure.

Coating-Indenter interface

The interaction between the coating and indenter is defined using the same procedure as during the indentation simulation. The exceptions are that the master and slaves surfaces are now two-dimensional surfaces instead one-dimensional lines. The friction between both surfaces is insignificant and cannot be neglected as was done during the indentation simulations. From literature, a friction coefficient of 0.1 was selected to estimate the friction between the diamond indenter tip and the PVD coating (Feild, 1996).

5.1.4 Mesh Design

The mesh was refined towards the scratch path where more elements are required to accurately simulate the deformation and stress distribution. Four-node tetrahedral continuum elements, defined as C3D4 in the ABAQUS element library, were used to discretize the model (ABAQUS, 2008). Tetrahedral elements were chosen over hexahedral and wedge elements due to their superior ability to produce a locally refined mesh, while minimizing element count. Large deformation in the region of the scratch path is expected and therefore non linear geometry was enabled in ABAQUS. Figure 5.3 shows the coarse mesh used, with only one element layer in the coating. The refined mesh used for the final results is shown in Figure 5.4. This mesh has two element layers to discretize the coating.

To facilitate post processing, two node sets are defined along the coating-substrate interface as shown in Figure 5.3. A longitudinal node set runs along the z-axis, while a transverse set runs parallel to the x-axis offset by 300 μm from one end of the extrusion. Displacement and stresses at these node sets were measured and post processing was done to transform the stress results from global to local coordinates.

5.2 Results

As presented earlier in the indentation simulation results, the stresses which are critical to coating adhesion failure are the maximum opening stress, maximum in-plane shear stress, and maximum compressive stress at the coating-substrate interface. Every few increments the critical stress values were calculated in the transverse and longitudinal node sets to determine the maximum critical stresses induced during the scratch test simulation. A von Mises stress contour of the simulation partway through the translation step is in Figure 5.5. The indenter surface is hidden to provide a view of the surface under the indenter, but the center line profile is included to show the indenter location. The stress variation near the extremities of the model is minimal, showing that the model is adequately sized.

5.2.1 Stress Transformation

The stresses returned in ABAQUS are global stresses and they must be transformed into local coordinate components to properly examine the stresses present at the coating-substrate interface. The stress transformations are very similar to those completed during the indentation simulations, but are more complex since the model is no longer axisymmetric.

Stress transformation for the longitudinal node set

Given that the longitudinal node set is on a plane of symmetry a simple two-dimensional rotation can be used to transform the stresses state from global to local coordinates. Figure 5.6 shows the global and local coordinate systems. The following equations show how the global stress components were transformed into local stress components with θ being the angle between the z-axis and z'-axis (Benham et al., 1996):

$$\sigma_{x'x'} = \sigma_{xx} \tag{5.1}$$

$$\sigma_{y'y'} = \frac{\sigma_{zz}+\sigma_{yy}}{2} - \frac{\sigma_{zz}-\sigma_{yy}}{2}\cos 2\theta - \tau_{yz}\sin 2\theta \tag{5.2}$$

$$\sigma_{z'z'} = \frac{\sigma_{zz}+\sigma_{yy}}{2} + \frac{\sigma_{zz}-\sigma_{yy}}{2}\cos 2\theta + \tau_{yz}\sin 2\theta \tag{5.3}$$

$$\tau_{x'y'} = \tau_{xy}\cos\theta + \tau_{xz}\cos(90+\theta) \tag{5.4}$$

$$\tau_{x'z'} = \tau_{xz}\cos\theta + \tau_{xy}\cos(90-\theta) \tag{5.5}$$

$$\tau_{y'z'} = \sigma_{yy}\cos\theta\cos(90-\theta) + \sigma_{zz}\cos\theta\cos(90+\theta)$$

$$+\tau_{yz}[\cos^2\theta + \cos(90+\theta)\cos(90-\theta)] \tag{5.6}$$

$$\tau_{max} = \sqrt{\tau_{x'y'}^2 + \tau_{y'z'}^2} \tag{5.7}$$

Here τ_{max} is the maximum shear stress in the plane of the coating-substrate interface and will be used to determine the overall maximum shear stress experienced at the coating-substrate interface.

Stress transformation for the transverse node set

The stress transformation for the transverse node set converts the global coordinate system into the local coordinate system (see Figure 5.7). The node set is not on a plane of symmetry therefore the transformation requires a more involved transformation to account for the nine direction cosines. Examining the displaced model during simulation, it was found that the angle between the x and x' was the most significant. Therefore a simplified transformation was used as follows (Benham et al, 1996):

$$\sigma_{x'x'} = \frac{\sigma_{xx}+\sigma_{yy}}{2} + \frac{\sigma_{xx}-\sigma_{yy}}{2}\cos 2\alpha + \tau_{xy}\sin 2\alpha \quad (5.8)$$

$$\sigma_{y'y'} = \frac{\sigma_{xx}+\sigma_{yy}}{2} - \frac{\sigma_{xx}-\sigma_{yy}}{2}\cos 2\alpha - \tau_{xy}\sin 2\alpha \quad (5.9)$$

$$\sigma_{z'z'} = \sigma_{zz} \quad (5.10)$$

$$\tau_{x'y'} = \sigma_{xx}\cos\alpha\cos(90+\alpha) + \sigma_{yy}\cos\alpha\cos(90-\alpha)$$

$$+\tau_{xy}[\cos^2\alpha + \cos(90+\alpha)\cos(90-\alpha)] \quad (5.11)$$

$$\tau_{x'z'} = \tau_{xz}\cos\alpha + \tau_{yz}\cos(90-\alpha) \quad (5.12)$$

$$\tau_{y'z'} = \tau_{yz}\cos\alpha + \tau_{xz}\cos(90+\alpha) \quad (5.13)$$

$$\tau_{max} = \sqrt{\tau_{x'y'}^2 + \tau_{y'z'}^2} \quad (5.14)$$

Again, τ_{max} is the maximum shear stress in the plane of the coating-substrate interface.

5.2.2 Convergence Analysis

The same stress components (opening and shear stress) as the indentation test were used to examine the convergence of the scratch test simulation. The maximum opening and in-plane shear stresses were determined for two separate simulations. The first used a coarse mesh with only one element layer used to discretize the coating and the second used a more refined mesh with two element layers for the coating. Table 5.1 and Table 5.2 show the convergence of the maximum opening and in-plane shear stresses in the coating and substrate materials at the interface. The maximum percent difference between both simulations is approximately 9%.

To further examine convergence of the scratch test simulation, the difference between the coating and substrate opening and in-plane shear stresses has been included in Table 5.3 for two layer simulation. As stated during the indentation test simulation results, the equilibrium at the interface dictates that these values should agree, but a large difference is present (as large of 85%). Good convergence has not been achieved in the most refined simulation results. The mesh was not further refined due to the large computational costs associated with doing so.

The following sections discuss the stress state at the coating-substrate interface at different points during the indenter translation. All results were determined using the refined model. The stress state along the longitudinal node set is examined after 200 and 300 μm of translation of the indenter. Figure 5.8 shows the vertical displacement along the longitudinal node set. After 200 and 300 μm of translation the indenter centerline is located at 250 and 350 μm along the longitudinal axis (z-axis). The stress state along the longitudinal axis is examined at two different points during the simulation to show that a steady state has been reached and the stress values for both agree. The stress state in the transverse node set is examined after 200, 250, and 300 μm of translation (indenter centerline at 250, 300, and 350 μm). These three test points were selected to show the stress state ahead of the indenter in the pile up region (200 μm), directly under the indenter (250 μm), and behind the indenter (300 μm). The vertical displacement along the transverse node set for these three points during the simulation is shown in Figure 5.9.

5.2.3 Von Mises Stress Results

The von Mises stress results in the coating and substrate at the coating-substrate interface is shown in Figure 5.10 and Figure 5.11 for the longitudinal and transverse node sets

respectively. The longitudinal data shows that the von Mises stress reaches a peak approximately under the indenter centerline. The von Mises stress results in the transverse node set are highest after 250 μm of translation (indenter above the transverse node set). The peak von Mises stresses experienced at the interface during the scratch test was 8.4 GPa in the coating and 2.8 GPa in the substrate.

5.2.4 Opening Stress Results

The opening stress ($\sigma_{y'y'}$) at the coating-substrate interface plane is shown in Figure 5.12 and Figure 5.13 for the longitudinal and transverse node sets. As expected due to equilibrium conditions, the substrate and coating opening stress values agree well. Exceptions exist near the peak values where sharp changes in opening stress are observed. The longitudinal plot shows a large compressive stress region under the indenter and a very small tensile (opening) stress in front and behind the indenter. The transverse plot shows the peak opening stress near the centerline for the results after 200 μm of translation. The overall maximum opening stress experienced during the scratch test was 390 MPa in the coating and 714 MPa in the substrate.

5.2.5 Shear Stress Results in the Interface Plane

The maximum shear stress in the coating-substrate plane for each node in the longitudinal and transverse node sets is plotted in Figure 5.14 and Figure 5.15. The shear stress in the interface plane reaches a peak in the longitudinal node set in the pile up region in front of the indenter. The maximum in-plane shear stress experienced during the scratch test calculated was 3.7 GPa in the coating and 1.5 GPa in the substrate. The coating and substrate values should be equal due to equilibrium, but the sharp peak in shear stress near

the maximum value introduces a significant discrepancy due to insufficient mesh refinement.

5.2.6 Normal Stresses Results in the Interface Plane

The maximum tensile and compressive normal stresses in the coating-substrate interface plane occur in the longitudinal direction (z'). The longitudinal stress ($\sigma_{z'z'}$) in the coating is plotted in Figure 5.16 and Figure 5.17 for the longitudinal and transverse node sets.

The maximum tensile stress (7.8 GPa) occurs behind the indenter in the longitudinal node set and the maximum compressive stress (-11.6 GPa) occurs in the pile up region in front of the indenter. The large tensile stresses in the coating can cause tensile through thickness cracking of the coating behind the indenter, while the large compressive stresses can lead to coating buckling and spallation in front of the indenter.

5.3 Summary

The stress state at the coating-substrate interface during a 30 N load scratch test has been simulated. The stresses found are representative of the stress values the PVD coating deposited on a mirror surface can survive without coating adhesion failure. The peak stresses were found primarily in the pile up region in front of the indenter. Table 5.4 provides a summary of the maximum stress values which are important to coating adhesion characterization. The average value between the coating and substrate was used for the maximum opening and shear stresses. Similar to the indentation simulation results, the opening, shear, and compressive stresses reach their peak in regions where coating failure was observed during experimental scratch testing, which is along the scratch path centerline.

The compressive stress in the coating in front of the indenter explains the compressive spallation failures observed during experimental scratch testing at higher loads.

Similar to the indentation test, the combined effect of the opening and shear stresses is most likely responsible for initiation of delamination growth and compressive stresses are responsible for coating spallation. The stress results from the scratch simulation and the corresponding results from the indentation simulation for the mirror surface are presented in Table 5.5. The maximum compressive stress values are very similar for both simulations. The opening and shear peak stresses are also quite similar with the opening stress being larger for the indentation test and the shear stress being larger for the scratch test. The indentation and the scratch adhesion tests are two different adhesion tests conducted using different set ups and loading conditions (almost 10x larger normal load for the indentation test), but the critical stress levels produced at the coating-substrate interface for both tests are quite similar. This similarity in the stress levels indicates that both tests are a good indicator of coating adhesion strength.

Stress Type	Stress [MPa]		% Difference
	1 layer	2 layer	
Maximum Opening stress (MPa)	523	390	8.6%
Maximum Shear stress magnitude (MPa)	3436	3730	7.9%

Table 5.1: Convergence of maximum critical stress in the coating side of the interface

Stress Type	Stress [MPa]		% Difference
	1 layer	2 layer	
Maximum Opening stress (MPa)	677	714	5.1%
Maximum Shear stress magnitude (MPa)	1628	1504	8.2%

Table 5.2: Convergence of maximum critical stress in the substrate side of the interface

Stress Type	Coating	Substrate	% Difference
Maximum Opening stress (GPa)	0.390	0.714	59%
Maximum Shear stress magnitude (GPa)	3.73	1.50	85%

Table 5.3: Convergence of coating and substrate maximum stress value for the 2 layer simulation

Stress Type *[material]*	**Maximum Value (GPa)**
Opening stress *[average of coating and substrate value]*	0.552
Shear stress *[average of coating and substrate value]*	2.60
Compressive stress *[coating]*	-11.6

Table 5.4: Important stress values for coating adhesion strength characterisation

Stress Type *[material]*	**30 kg_f [294 N] Indentation test (GPa)**	**30 N Scratch (GPa)**
Opening stress *[average of coating and substrate value]*	1.17	0.552
Shear stress *[average of coating and substrate value]*	1.97	2.60
Compressive stress *[coating]*	-12.7	-11.6

Table 5.5: Comparison of maximum stress results for the indentation and scratch simulation of the PVD coating adhesion to a mirror surface

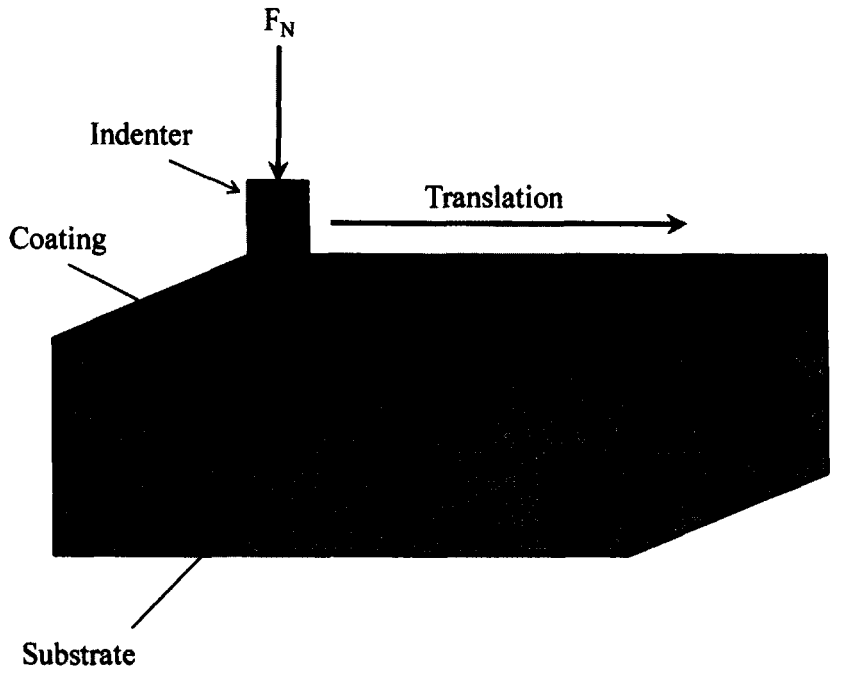

Figure 5.1: Schematic of the scratch adhesion test

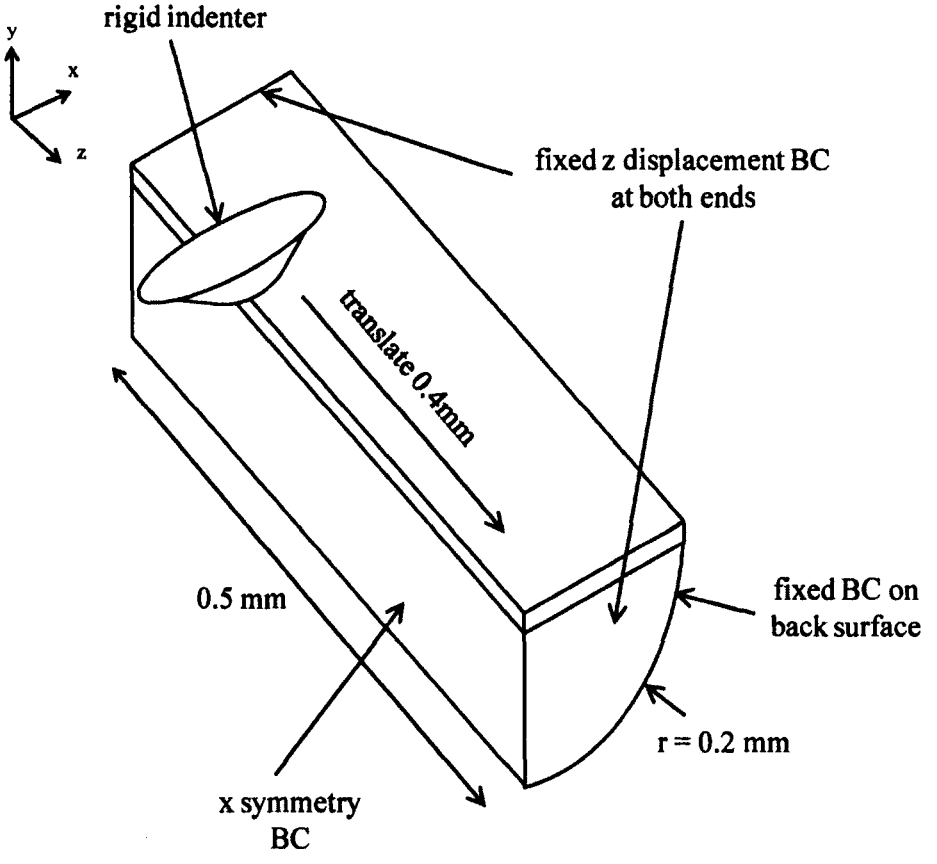

Figure 5.2: Scratch test model size and boundary conditions, coating thickness = 2.5 μm (not to scale)

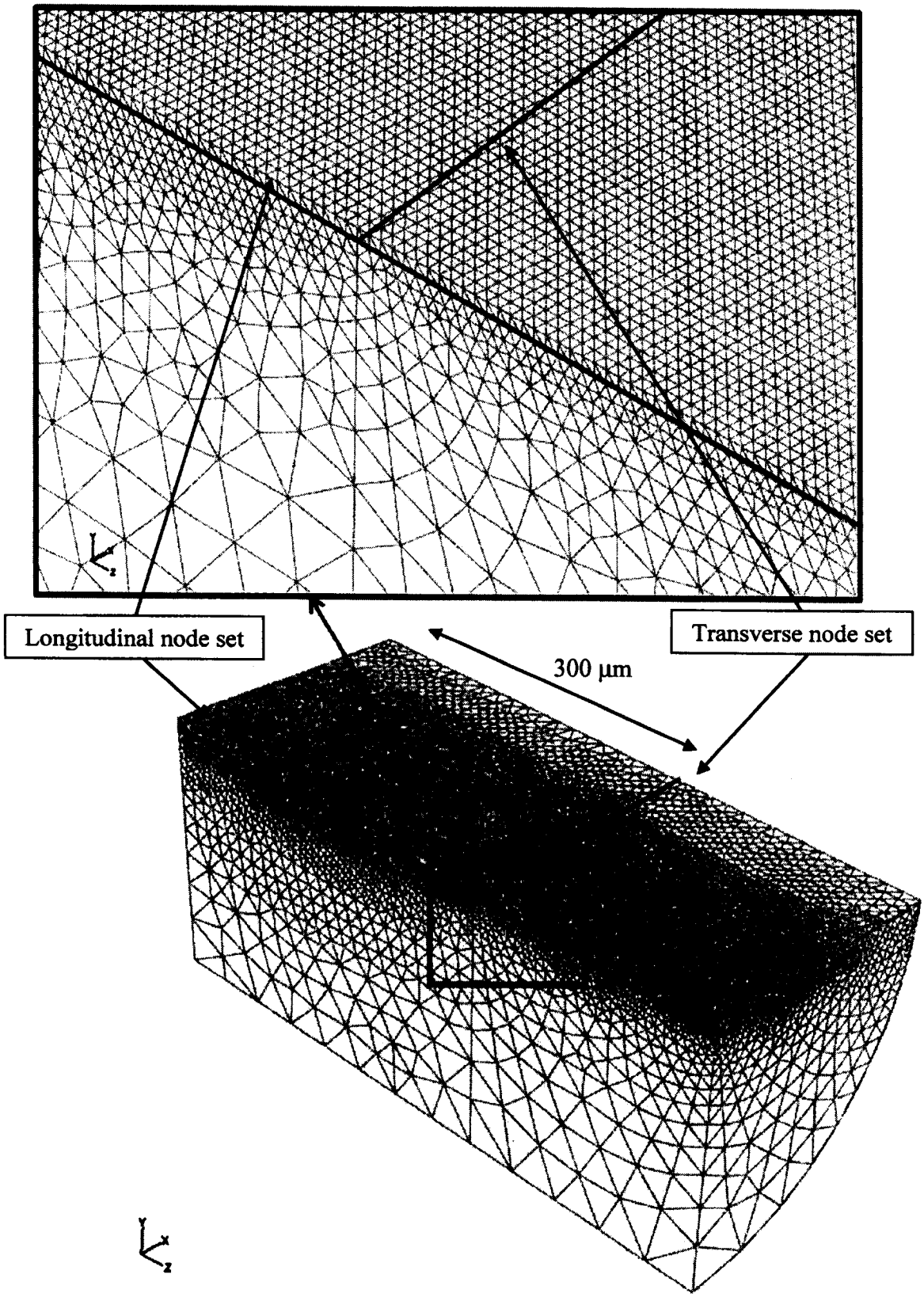

Figure 5.3: Coating substrate mesh design, 1 element layer coating

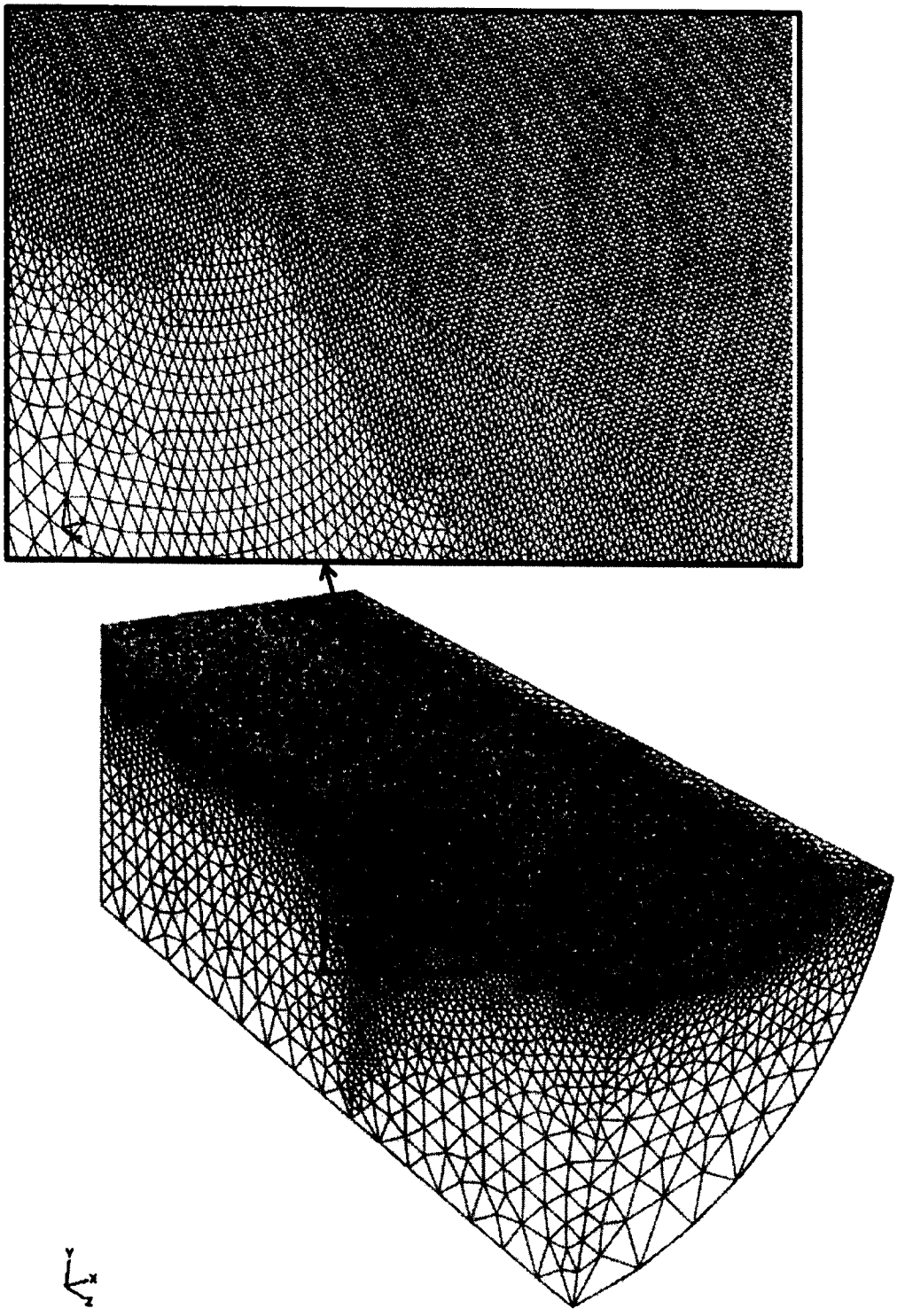

Figure 5.4: Coating substrate mesh design, 2 element layer coating

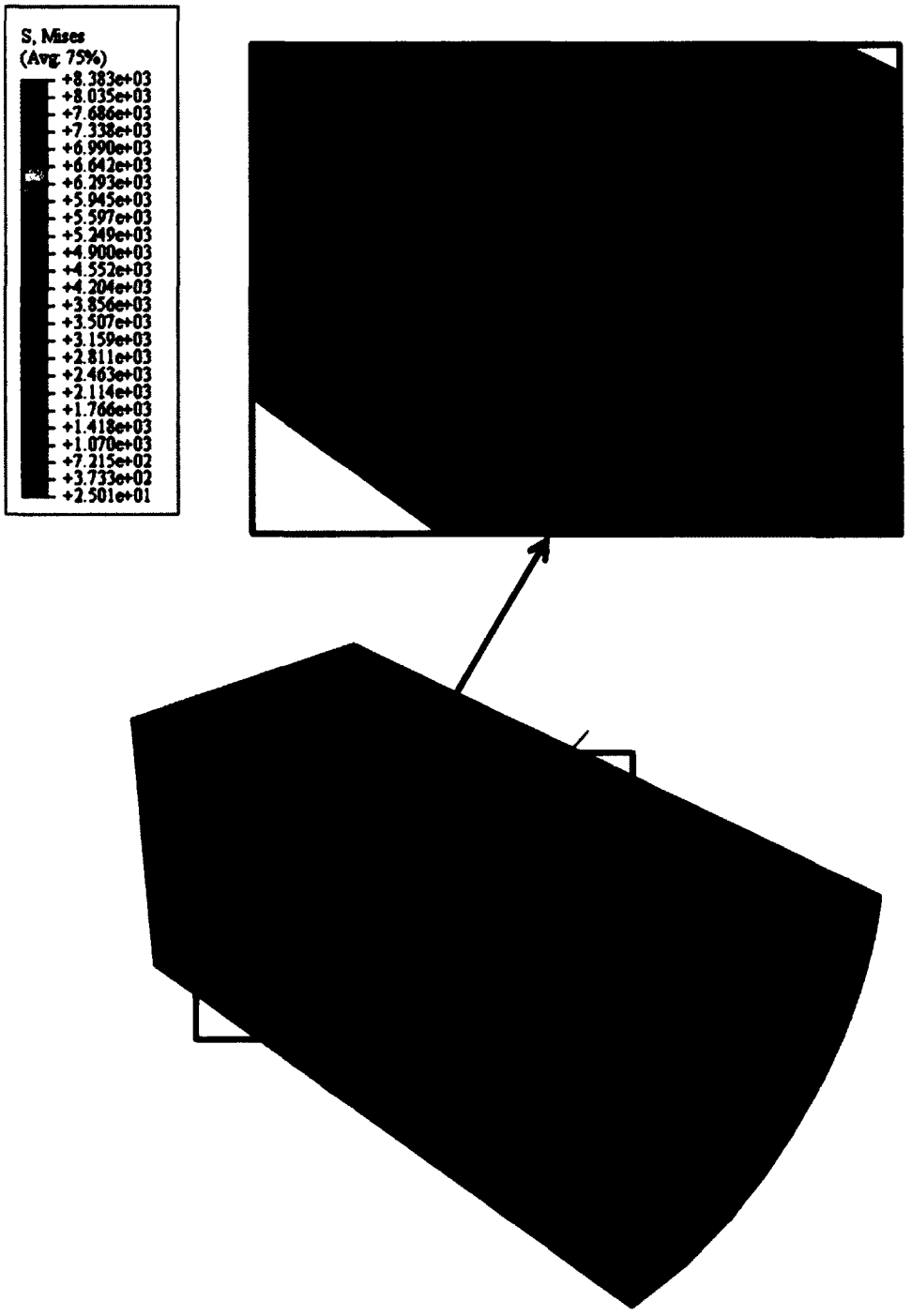

Figure 5.5: Von Mises Stress contour of the scratch simulation during translation step for the refined model

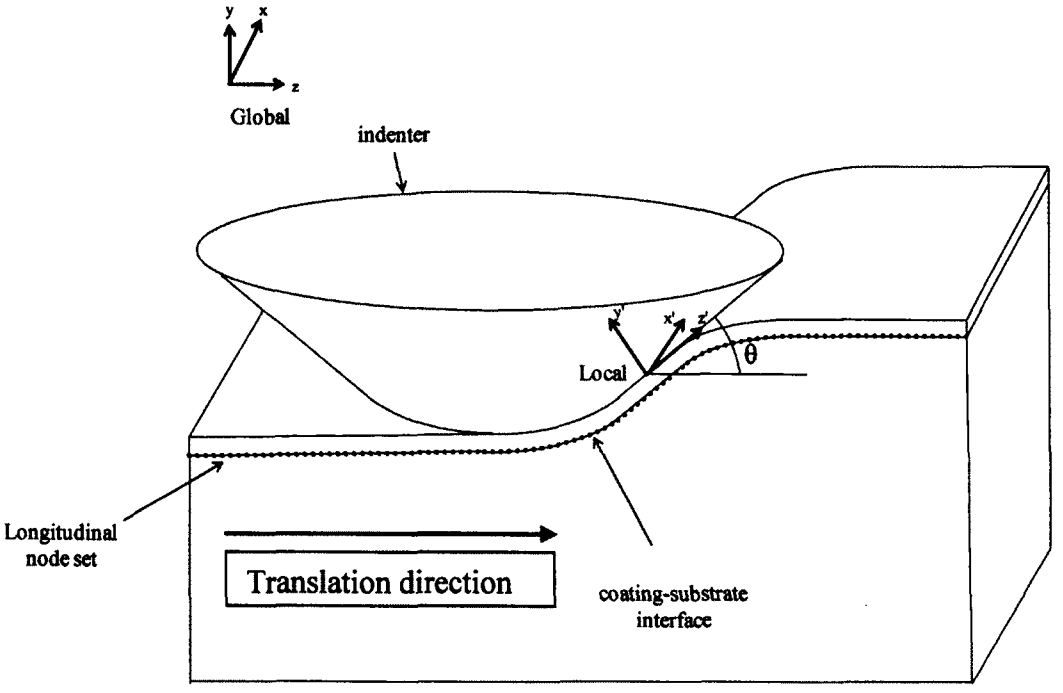

Figure 5.6: Scratch test global and local coordinate system for longitudinal node set

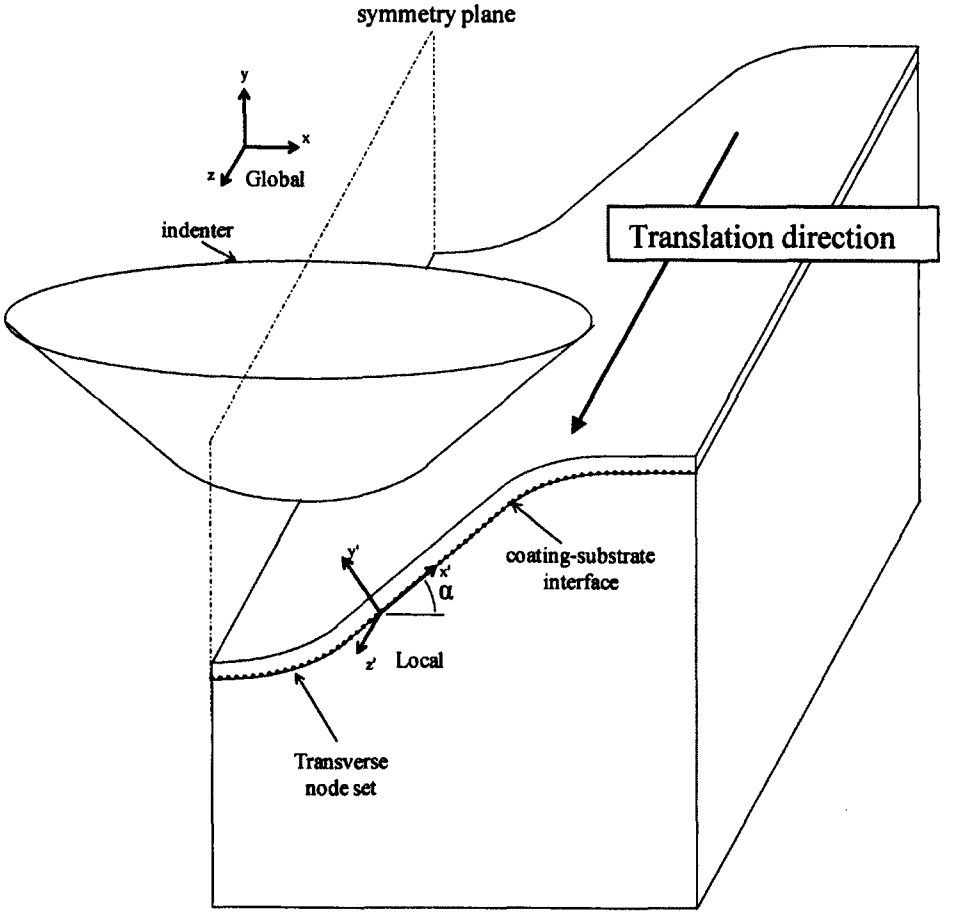

Figure 5.7: Scratch test global and local coordinate system for transverse node set

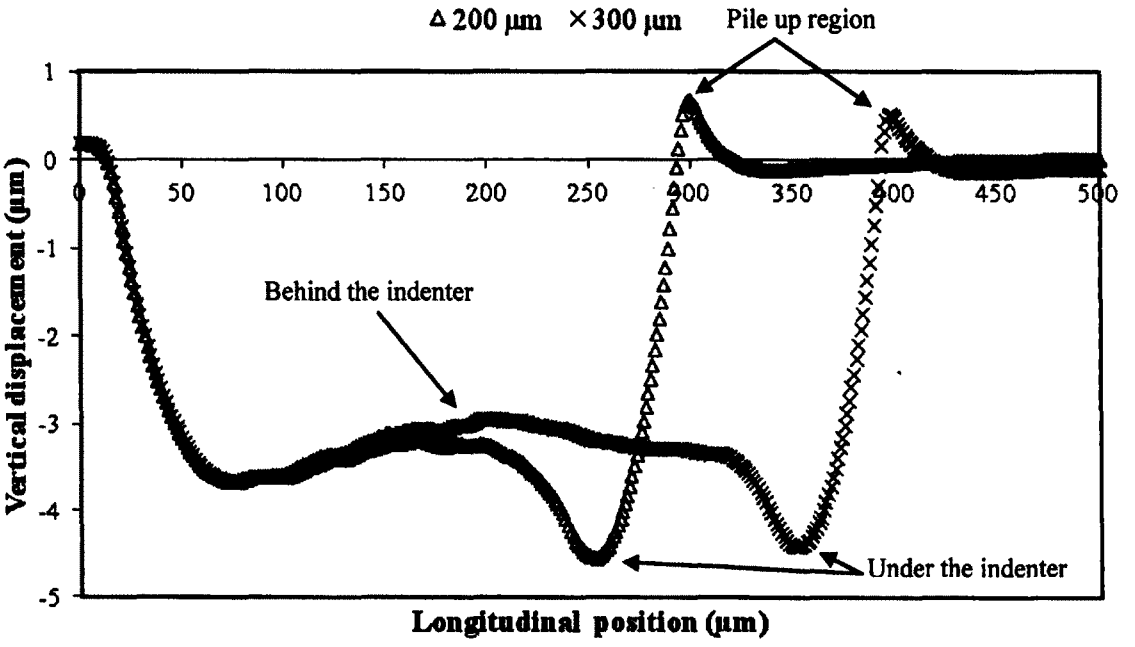

Figure 5.8: Vertical displacement along the longitudinal node set after 200 and 300 μm of translation

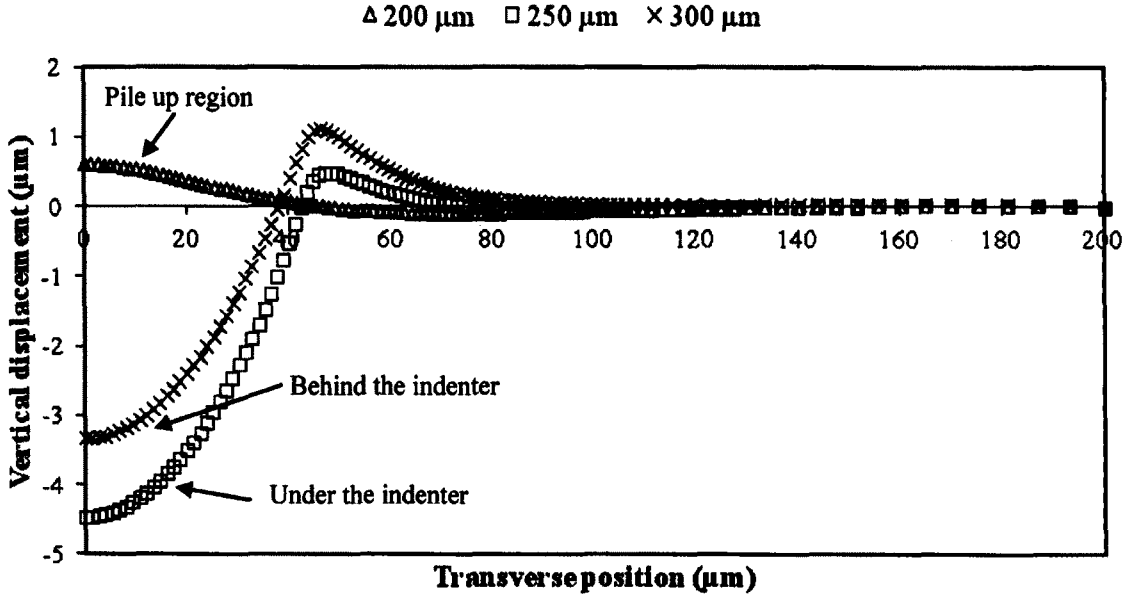

Figure 5.9: Vertical displacement along the transverse node set after 200, 250 and 300 μm of translation

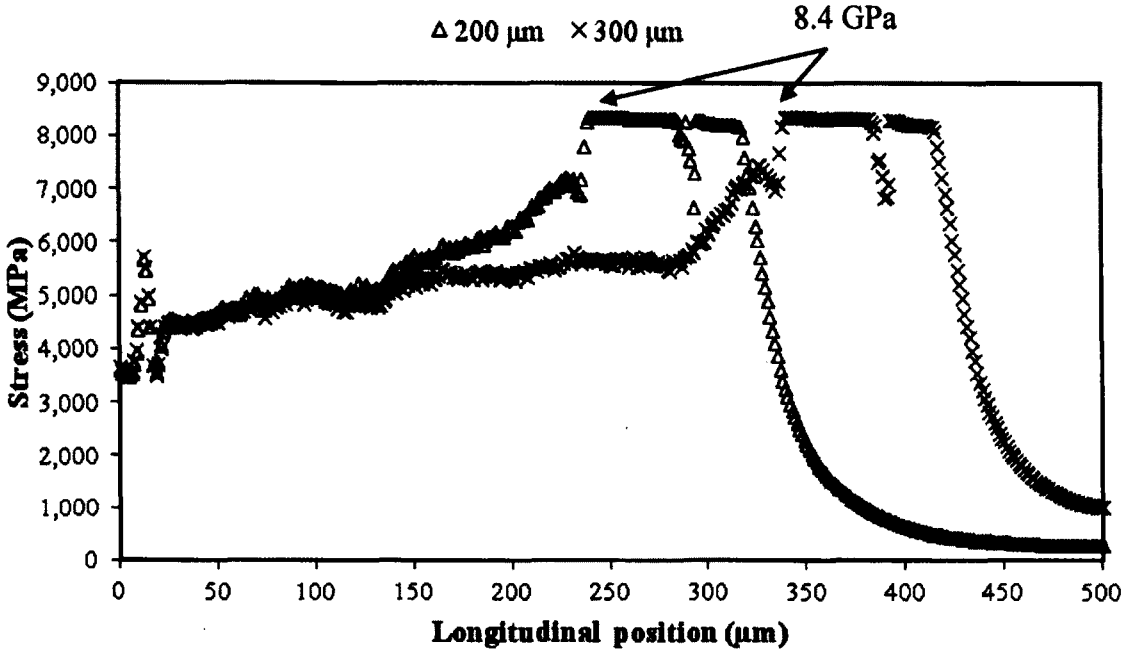

(a) coating

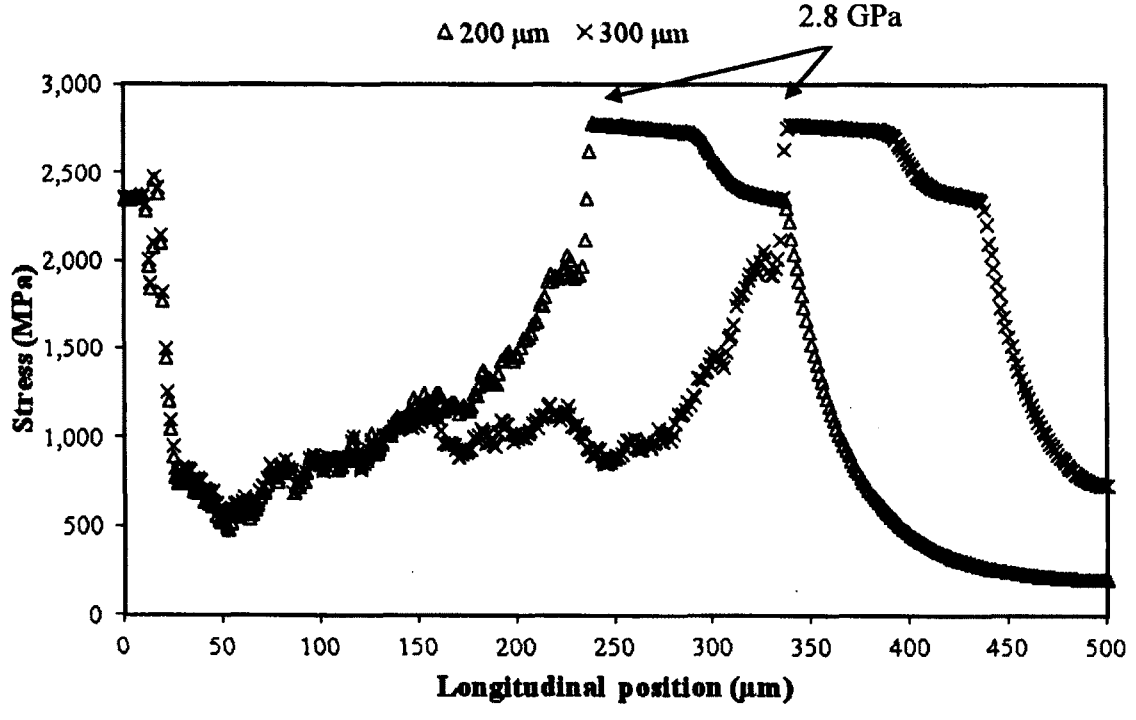

(b) substrate

Figure 5.10: von Mises stress along the longitudinal node set after 200 and 300 μm of translation; (a) in coating, (b) in substrate

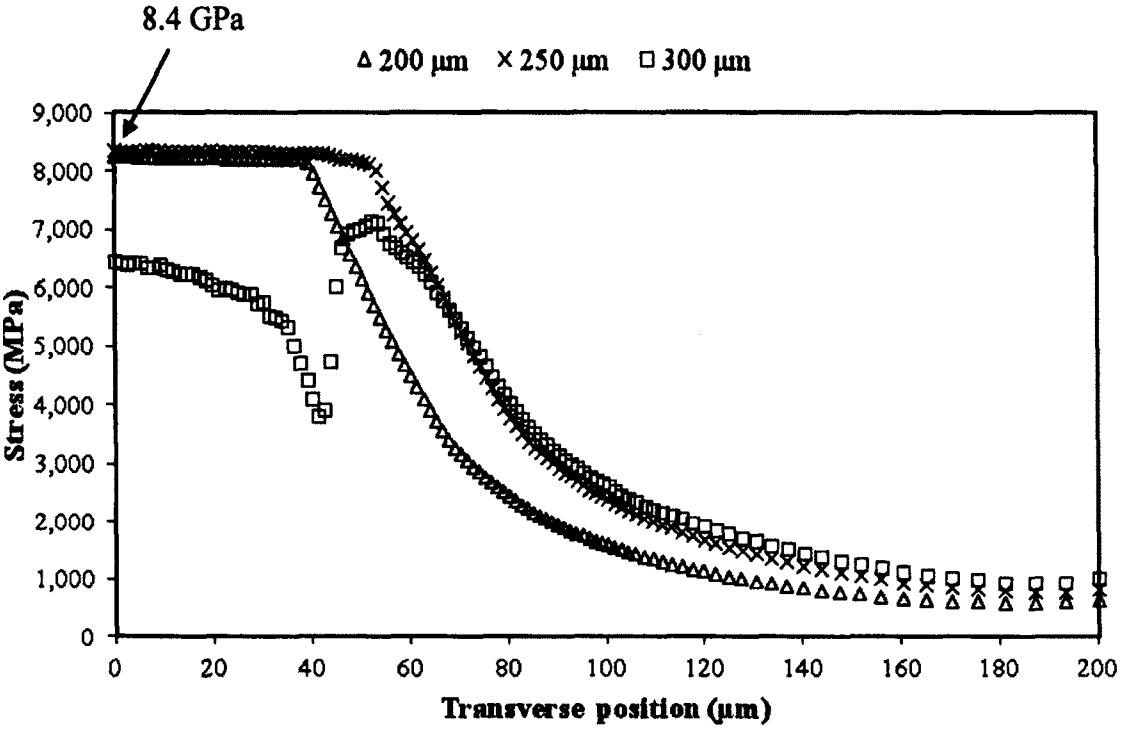

(a) coating

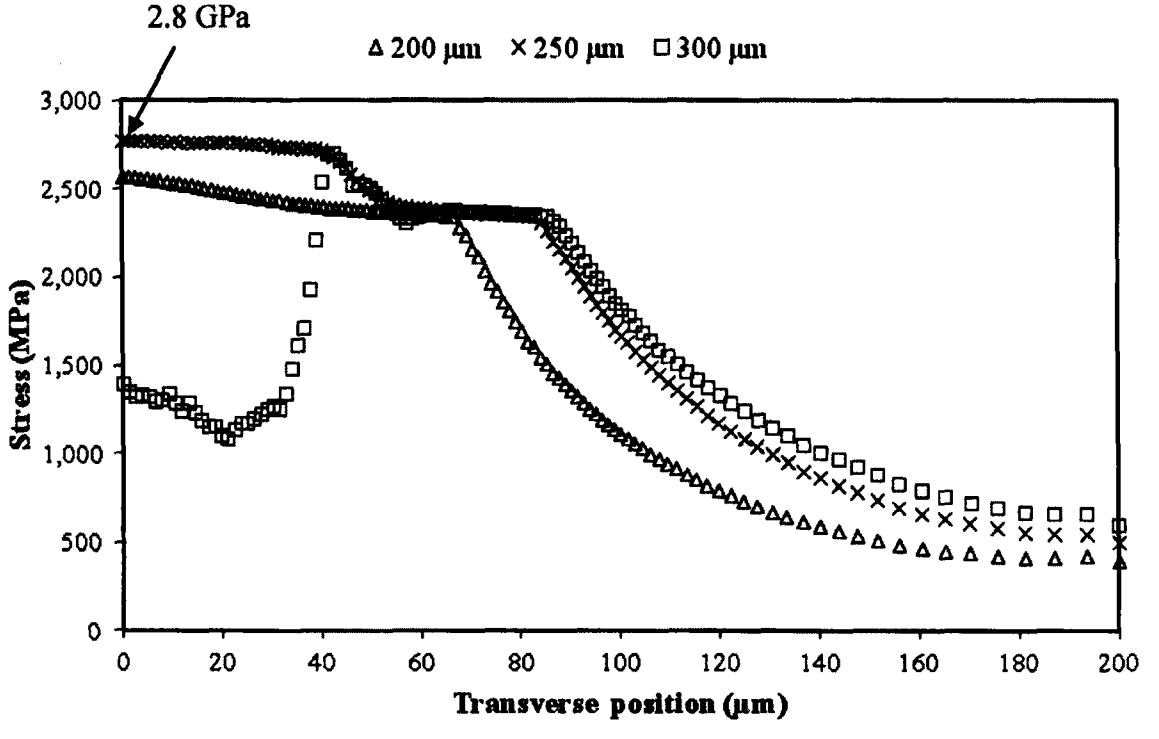

(b) substrate

Figure 5.11: von Mises stress along the transverse node set after 200, 250, and 300 μm of translation; (a) in coating, (b) in substrate

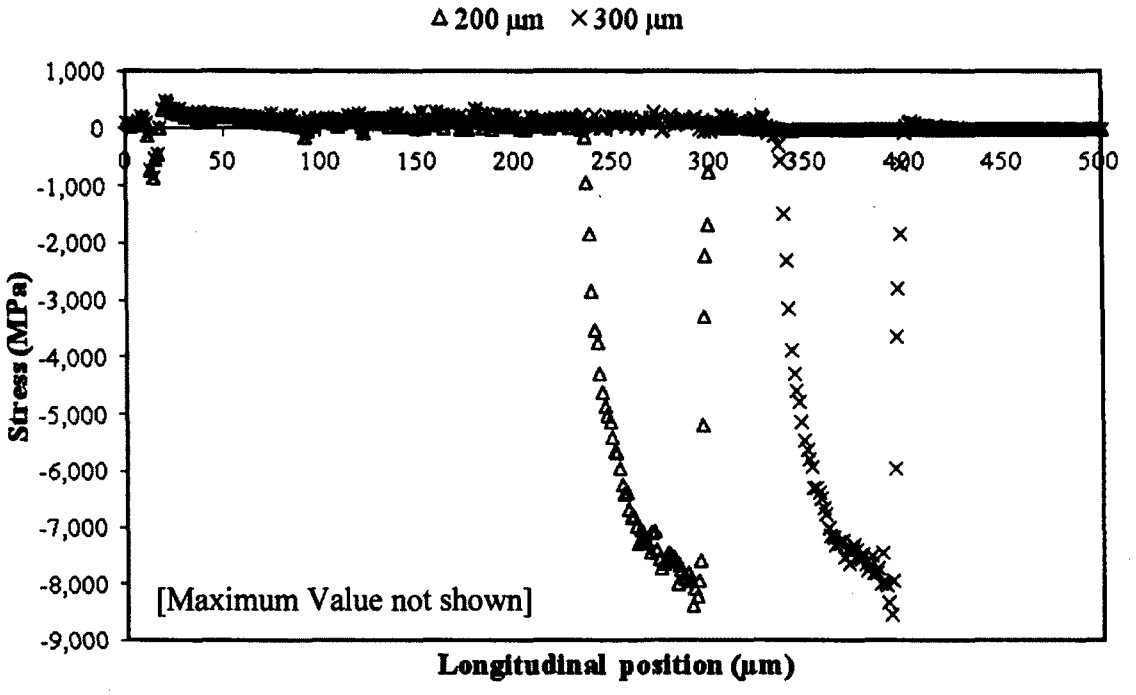

(a) coating

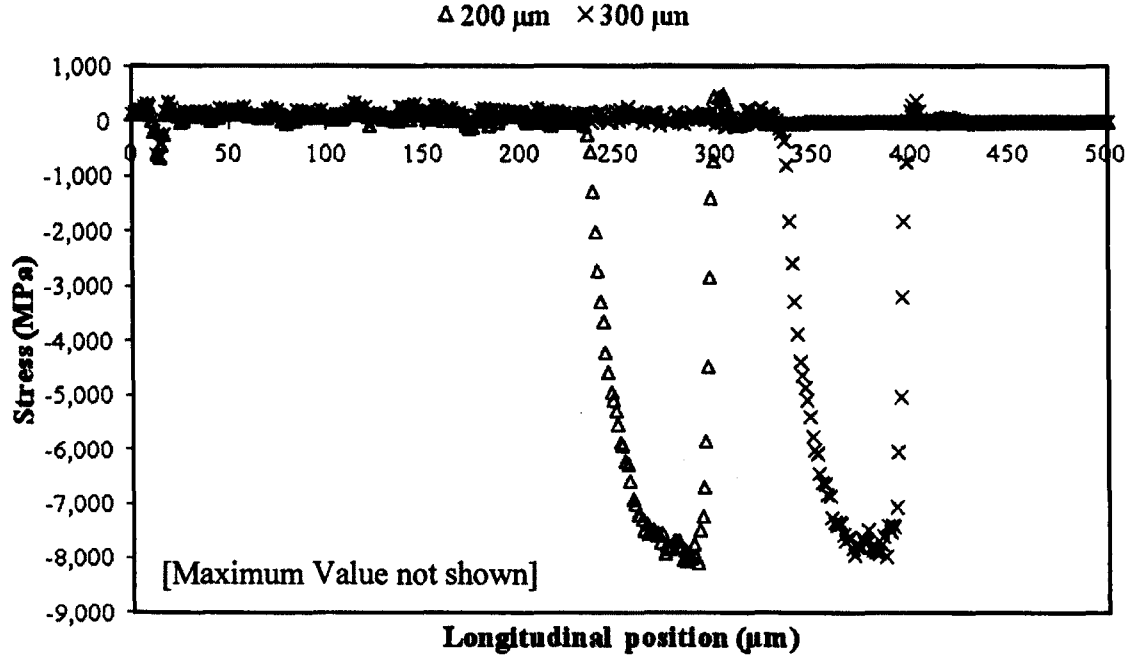

(b) substrate

Figure 5.12: Opening stress along the longitudinal node set after 200 and 300 μm of translation; (a) in coating, (b) in substrate

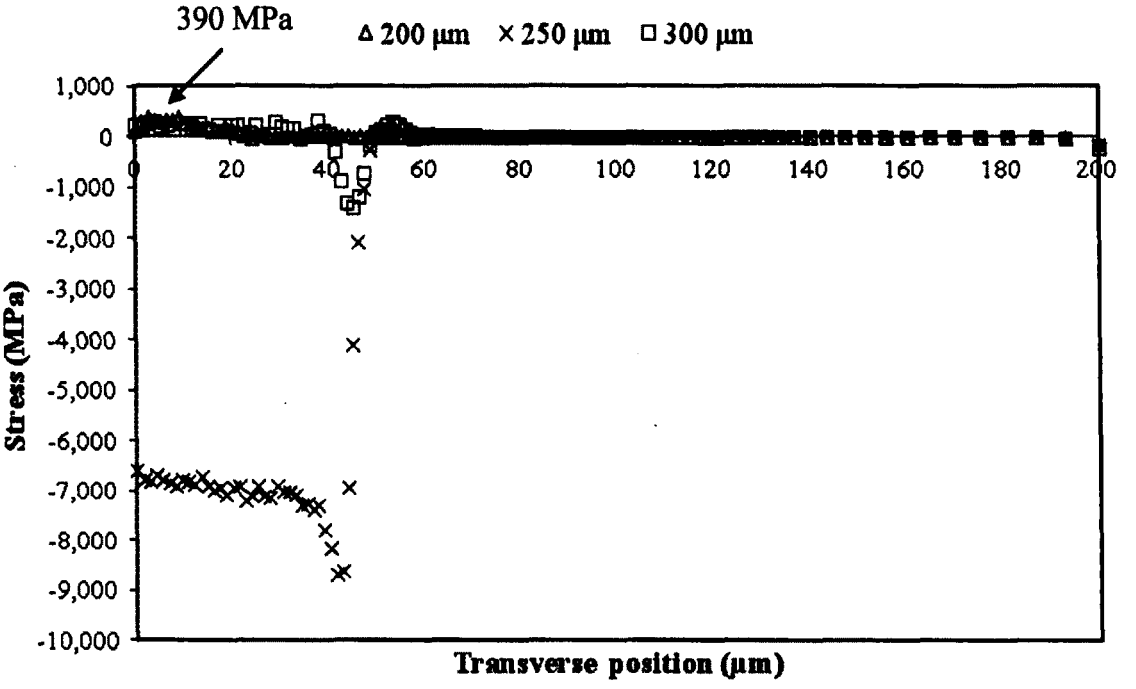

(a) coating

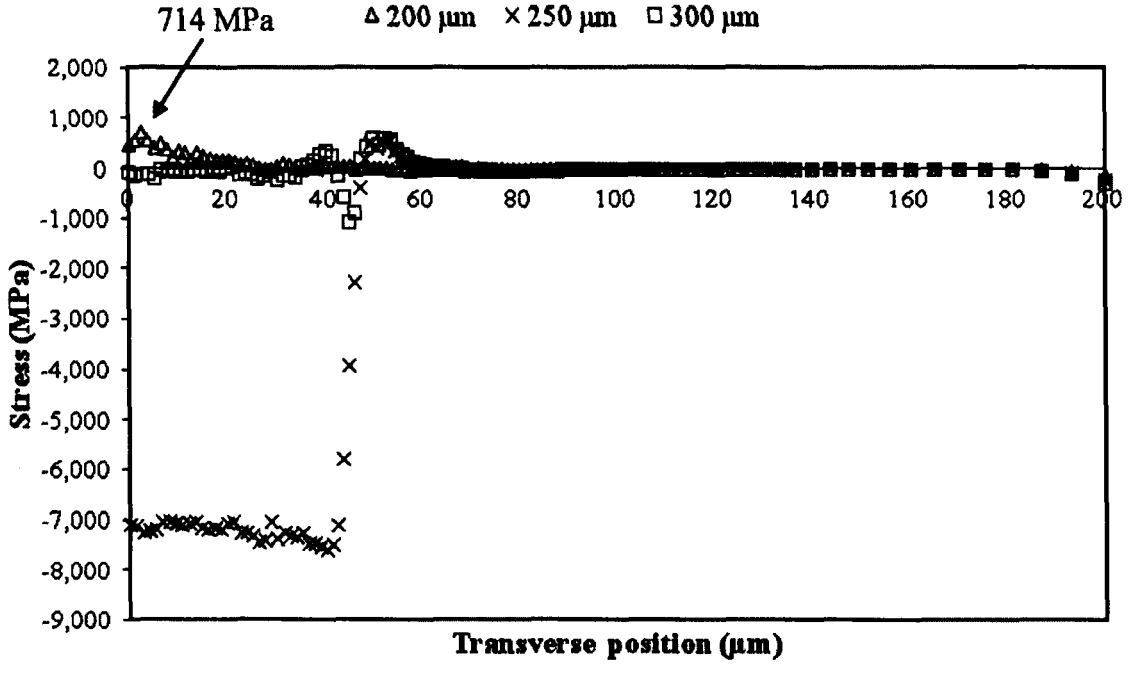

(b) substrate

Figure 5.13: Opening stress along the transverse node set after 200, 250, and 300 μm of translation; (a) in coating, (b) in substrate

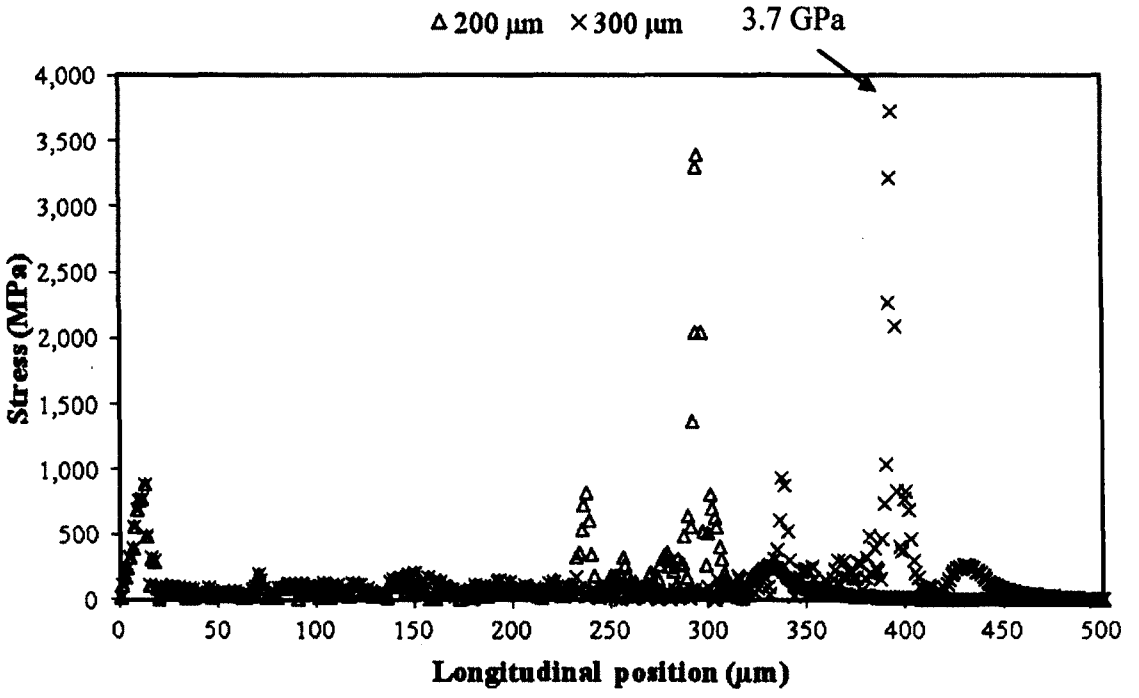

(a) coating

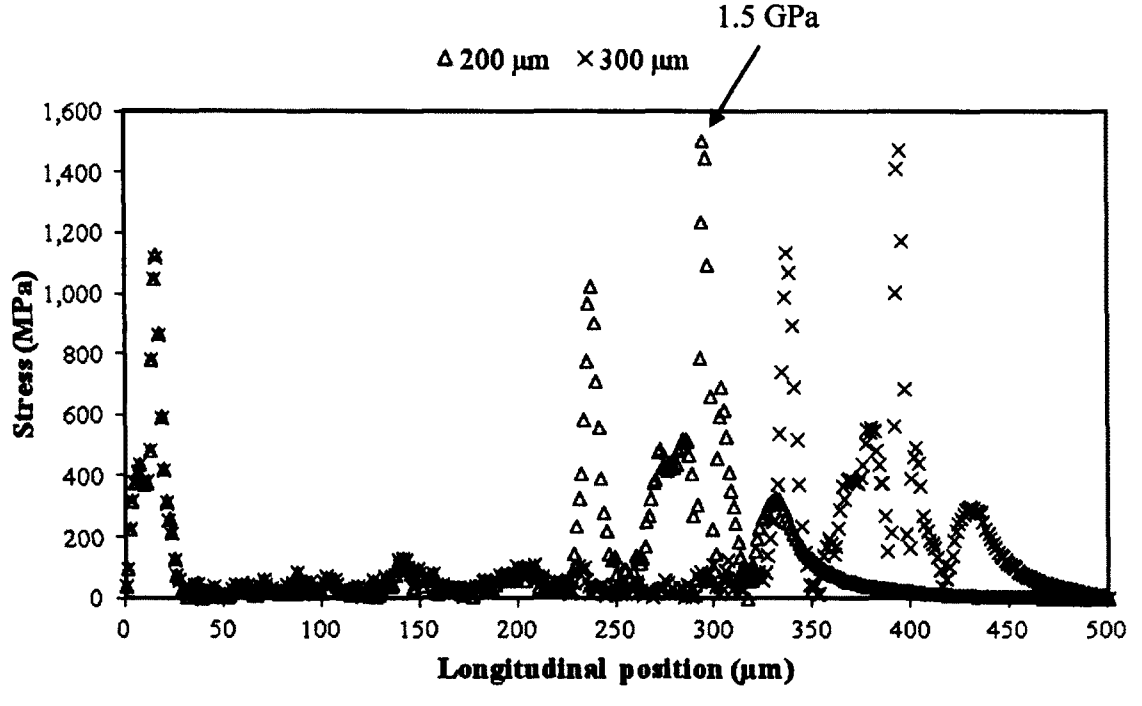

(b) subsrtate

Figure 5.14: In-plane maximum shear stress along the longitudinal node set after 200 and 300 μm of translation; (a) in coating, (b) in substrate

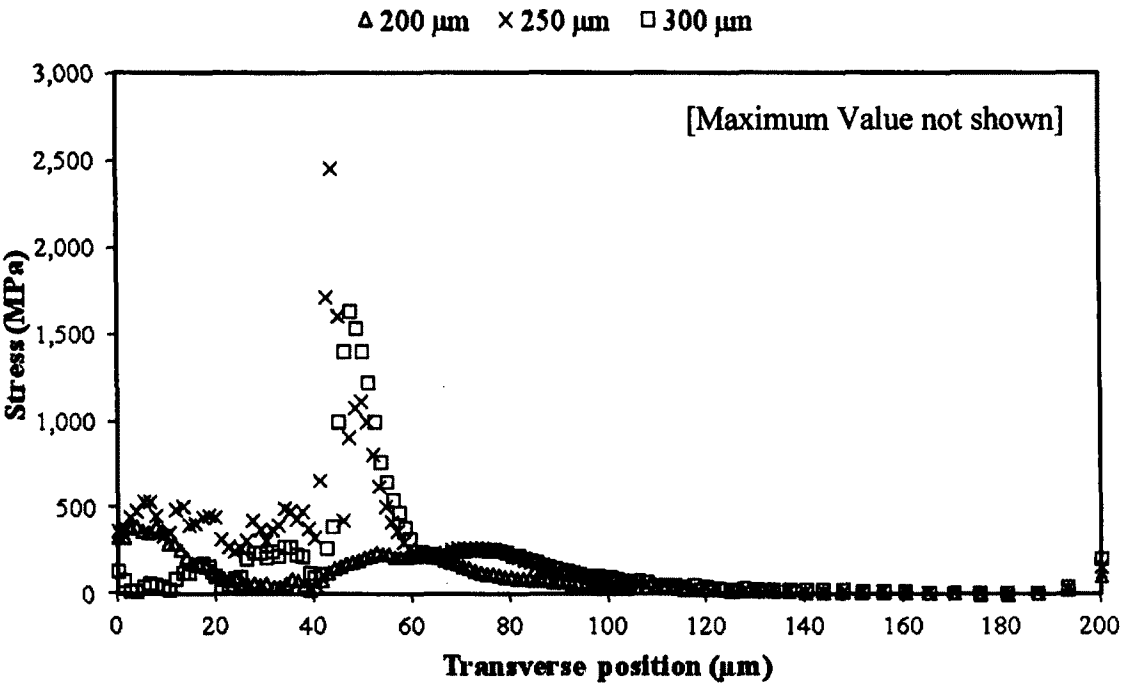

(a) coating

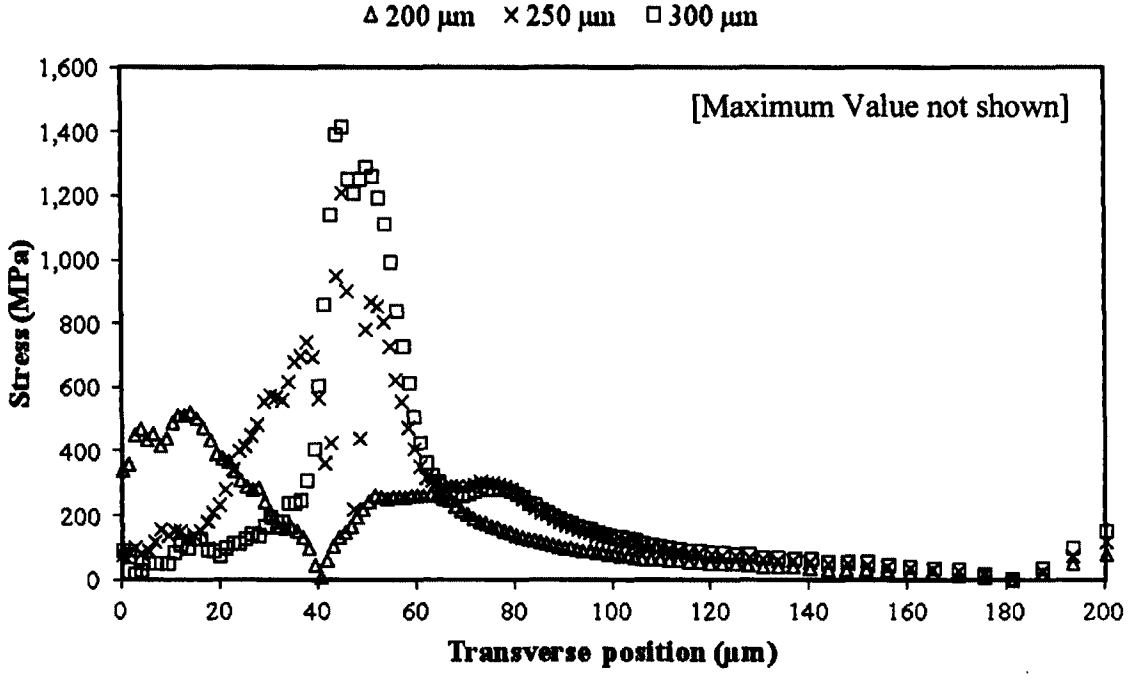

(b) subtrate

Figure 5.15: In-plane maximum shear stress along the transverse node set after 200, 250, and 300 μm of translation; (a) in coating, (b) in substrate

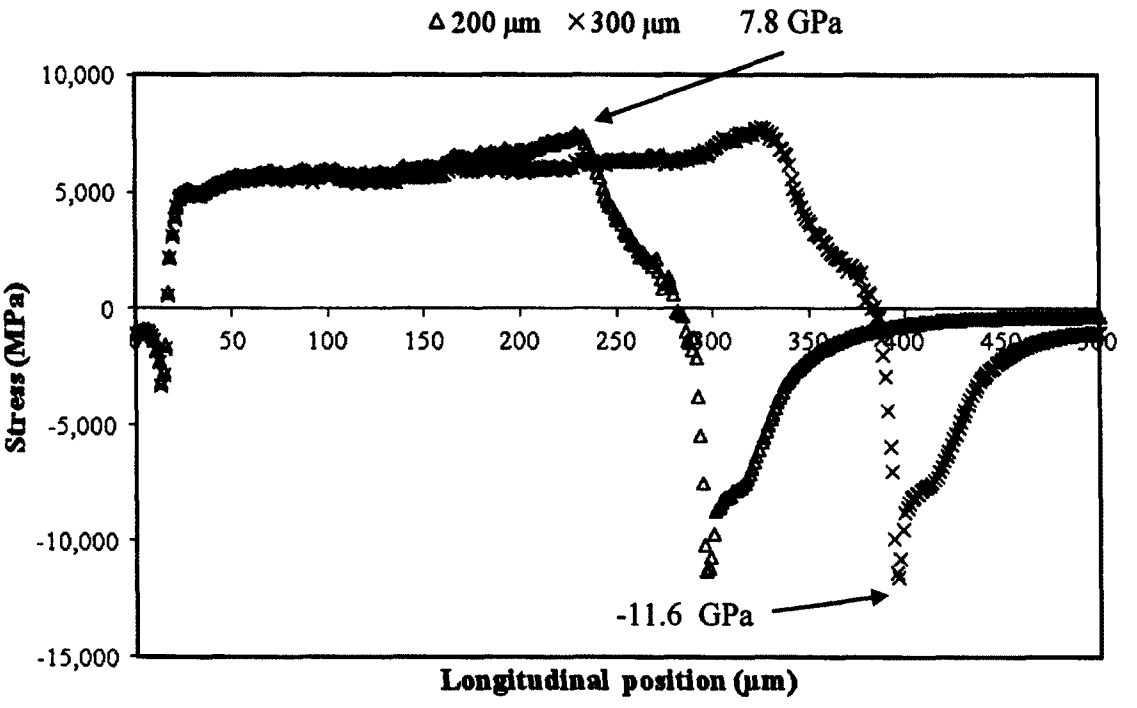

Figure 5.16: Longitudinal stress in the coating along the longitudinal node set after 200 and 300 μm of translation

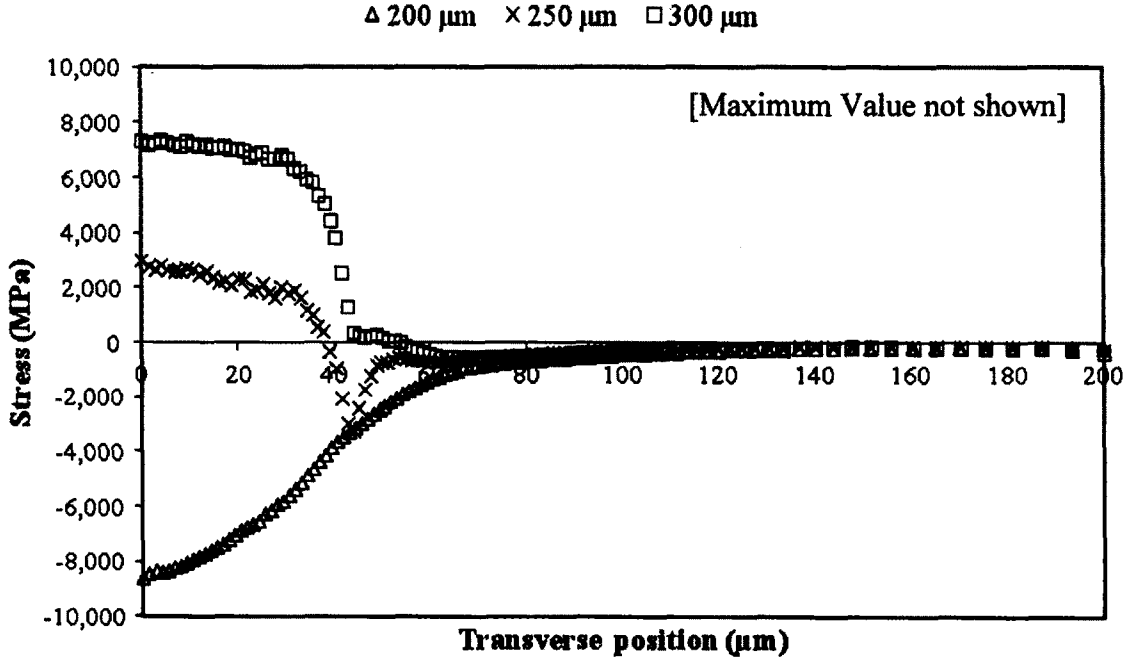

Figure 5.17: Longitudinal stress in the coating along the transverse node set after 200, 250, and 300 μm of translation

Chapter 6: Conclusions and Recommendations

In this thesis, the adhesion of the RCM's hard PVD coating to a mirror surface and to four laser frosted surfaces was examined using a combination experimental testing and finite element simulations. The following summarizes the conclusions drawn from the testing and simulation of indentation and scratch adhesion tests. Finally, potential future research directions are discussed.

6.1 Conclusions

Indentation adhesion testing was completed for the PVD coating deposited on the polished mirror surface and the laser frosted surfaces. The Rockwell-C indentation adhesion test successfully defined the adhesion of the PVD coating to each surface type semi-quantitatively except for the AlOx laser frosted surface. The stepped indentation adhesion tests successfully estimated the critical indentation load for coating failure for the PVD coating deposited on a mirror surface and the Bullion and Glass Bead laser frosted surfaces. Below the critical load, through-thickness cracking of the coating is present in the form of circumferential cracks near the crater edge and radial cracks extending away from the crater edge. Above the critical indentation load, coating delamination was found to occur at the edge of the indentation crater and extend outward.

Using the maximum indentation load survived without coating delamination, the critical stresses at the coating-substrate interface were obtained using finite element simulations of the indentation adhesion test of the PVD coating on a mirror surface and on Bullion and Glass Bead laser frosted surfaces. Maximum opening, shear and compressive stresses at the coating-substrate interface were found near the crater edge where coating delamination

occurred during experimental testing. These three maximum stress values provide a characterization of the adhesion strength.

Scratch adhesion testing was also completed for the PVD coating deposited on the mirror and laser frosted surfaces. The scratch adhesion test successfully defined the adhesion of all the samples except for the AlOx laser frosted surface. The critical scratch loads were determined for the surfaces and significant variation was found in the results. Through-thickness cracking of the coating was found to occur within the scratch path prior to coating delamination. Above the critical load, coating spallation occurred in the scratch track and chipping was observed at the track edges.

The critical scratch load found during experimental testing of the coated mirror surface was used to determine the critical stresses at the coating-substrate interface through finite element simulation of the scratch adhesion test. In the region ahead of the indenter opening stress, shear stress, and in-plane compressive stress in the coating-substrate interface are at their maximum. Compared to the indentation test, the maximum compressive stresses are very similar and the shear and opening stresses are also in reasonable agreement.

Overall, it has been demonstrated that either indentation or scratch adhesion tests can be used to characterize the adhesion of a PVD coating.

6.2 Recommendations

The large variations of the scratch adhesion testing results might be reduced by performing the scratch adhesion test using a scratch tester equipped with friction and acoustic monitoring systems. The added failure monitoring types could provide more accurate and repeatable critical load values.

The definition of the interaction between the coating and substrate used during the indentation and scratch simulations could be modified to include the possibility of delamination growth along the interface. Stress intensity factors at the edges of interface delamination could then be determined to further the understanding of the interface failure. Through thickness cracking of the coating could also be modeled to more accurately represent the stresses in the coating.

Parametric studies could be performed to isolate the effect of coating and substrate material properties and coating thickness on interface stresses. This work could lead to improved material selection and thin film system design.

Appendix A

Closed-Field Unbalanced Magnetron Sputter Ion Plating Process

The CFMSIP process is a type of PVD coating used at the RCM for increasing die life. The process can be split into three steps: preparation, vaporization and deposition.

Preparation

A thorough preparation process is very important as any contaminants can adversely affect coatings adhesion. First, the armature being used to hold the part is placed in the coating chamber and a "bake out" procedure is performed. This consists of creating a vacuum and applying heat to remove contaminants from the armature. The part, or substrate, surface must be cleaned using alcohol and a degreasing agent to remove surface contaminants. The part being coated is then attached to the armature and placed under vacuum in the coating chamber. A final substrate cleaning step, ion bombardment, is then used to further clean the substrate surface. The parts being coated are negatively charged and argon gas which is pumped into the chamber at a very small pressure becomes positively charged. The positively charged argon gas ions are attracted to the negatively charged substrate. The argon ions accelerate toward the substrate and bombard the surface removing some of the surface. Once the surface is adequately prepared, the coating process can begin. It is important to note that during cleaning of the armature and during the coating process, the armature is continuously rotating to provide even cleaning and coating coverage respectively. (Martin, 2010)

Vaporization

The material being vaporized, called the targets, are mounted on the walls of the vacuum chamber. The targets can be of the same material or varied materials, depending on the desired coating. Figure A.1 shows a four magnetron closed field arrangement. The magnetrons are placed in such a way that the polarity of the magnetrons reverses from neighbour to neighbour. This creates a closed magnetic field. The targets are placed in front of the magnetrons and are negatively charged. Electron racetracks form at the surface of the targets as shown in Figure A.2. The fast moving electrons ionize a portion of the argon gas near the target causing the ions to accelerate towards the oppositely charged target. The ionized argon ions hit the target surface with enough energy to liberate atoms from the target, vaporizing a small amount of the target by sputtering. The sputtered atoms are uncharged and are therefore unaffected by the negatively charge targets and are free to travel away from the target.

Depending on the strength of each of the magnetron pole, three configurations can be achieved as shown in Figure A.3. The conventional magnetron setup uses two poles of equal strength, the type-1 unbalanced magnetron uses a stronger inner pole, and type-2 unbalanced magnetron uses a stronger outer pole. Type-2 unbalanced magnetrons are used in the CFMSIP process and plasma can be present at the surface of the substrate, which increases coating deposition rate (Kelly, et al., 2000).

Deposition

Now that some of the target material is vaporized, it is free to deposit onto the part being coated. The sputtered atoms travel from the target surface to the substrate surface where they

react with ionized nitrogen gas and deposit to form a thin film. Plasma at the substrate surface provides energy to increase the deposition rate. By varying what elements are vaporized during different periods of the coating process, graded or multilayered coatings can be created. The CrTiN coating used at the RCM is formed by first create a chromium bond layer followed by a CrN to CrTiN graded layer and finally alternating nano-layers are applied. The coating structure can be seen in Figure A.4. Once the desired coating thickness is achieved, the die is removed from the chamber and the coated surface is buffed to remove any surface undesired roughness.

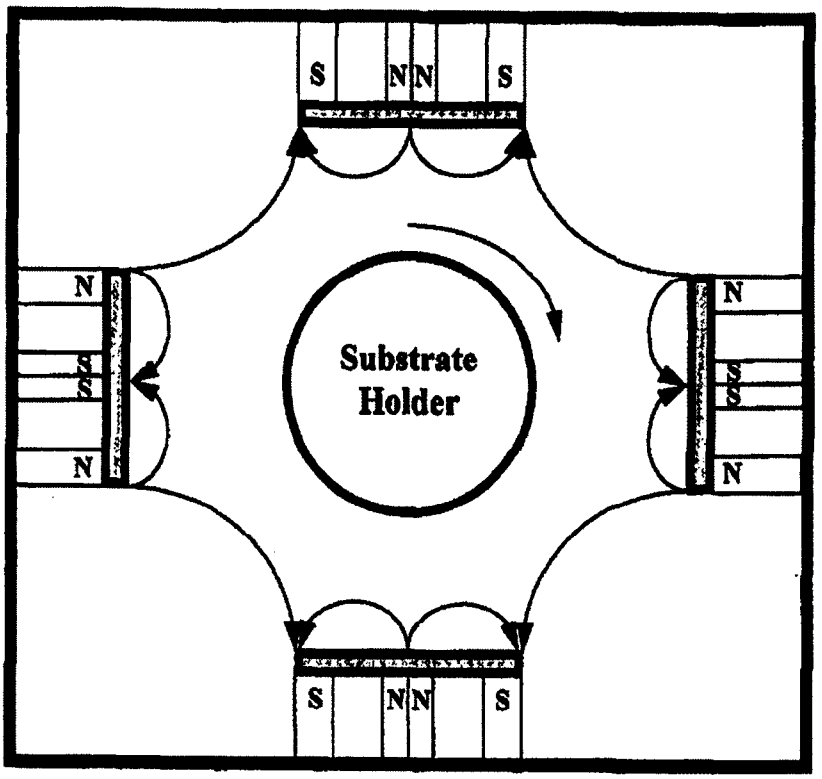

Figure A.1: Four magnetron closed field arrangement (Sproul, 1996)

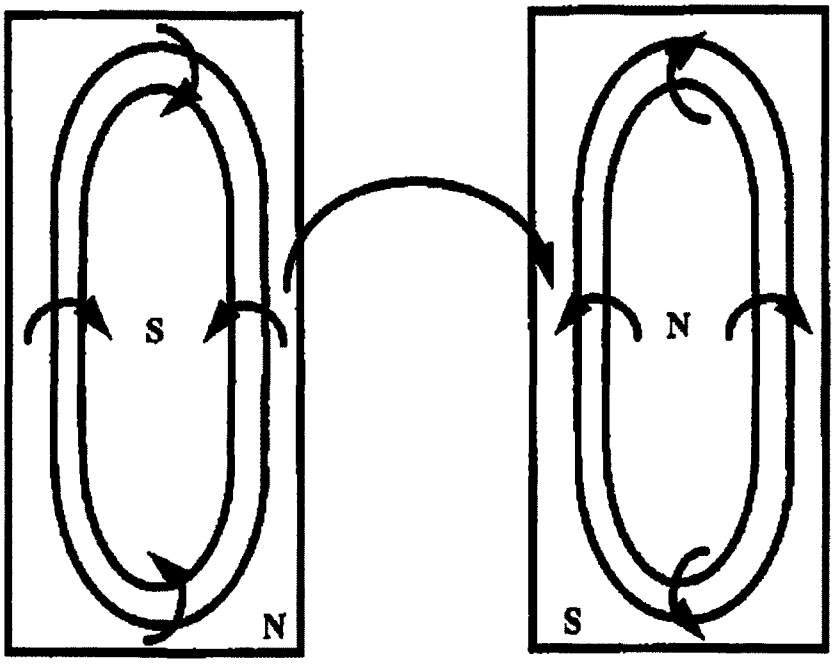

Figure A.2: Magnetron pair (Sproul, 1996)

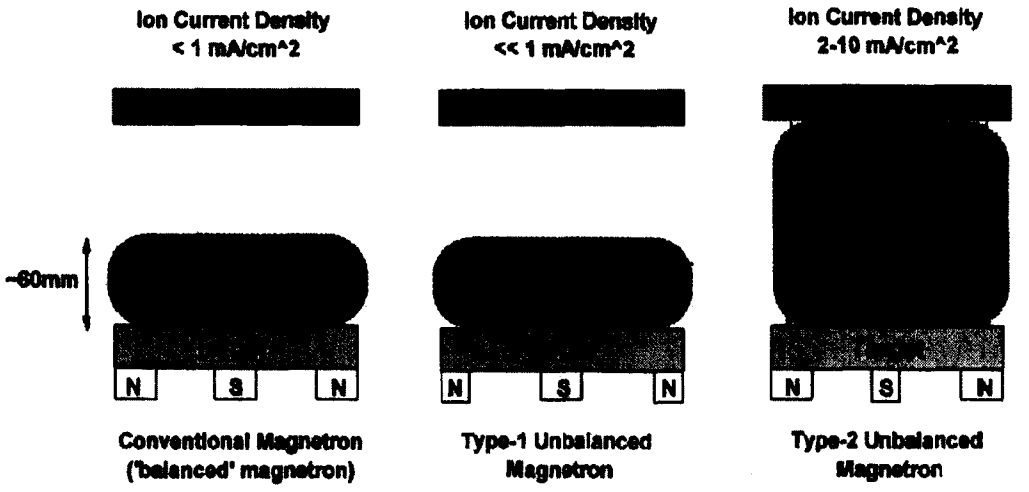

Figure A.3: Distribution of plasma for various magnetron configurations (Kelly, et al., 2000)

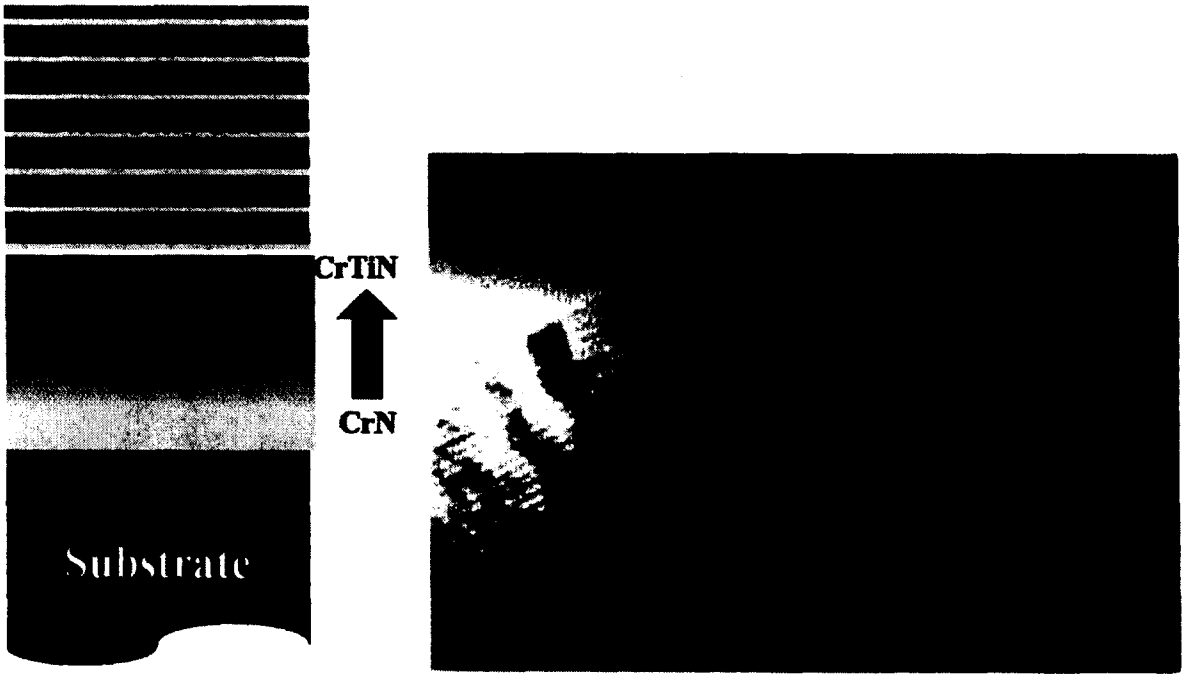

(a) (b)

Figure A.4: Coating structure, (a) schematic cross-section, (b) Microstructure cross-section (Teer, et al., 2008)

Appendix B

Other Adhesion Testing Methods

The following sections summarize the other prominent adhesion test methods used today. The adhesion testing methods covered are the peel test, the tape test, the blister test, the self loading test, the beam bending test, the pull test, and the laser spallation test.

Peel test

In a peel test, a coating on a substrate is peeled off and the force required to peel the coating off is measured. Figure B.1 shows a 90° peel test (other angles can also be used). The adhesion strength is quantified by measuring the force required to peel the coating, and stating the angle at which it was peeled. The major limitation of this type of adhesion test is that the coating must be flexible to avoid coating cracking.

Tape test

The tape test is very similar to the peel test, but instead of directly peeling off the coating, a tape is applied to the coated surface and is then removed in a controlled manner. The coated surface is then examined to determine if any coating was removed. The tape used in these tests are manufactured and applied according to specification to help semi quantify the adhesion strength of the coating to the substrate. The advantage of the tape test over the peel test is that the coating does not need to be flexible. The test is best used as a quality control test, since the adhesion of the tape to the coating cannot always be manufactured to provide a high enough minimum adhesion strength reference point.

Blister test

In a blister test a hole is etched through the substrate up until the coating, see Figure B.2. Pressure is then applied to the opposite side of the coating and the delamination growth of the coating is observed. Using this test, the pressure at which the coating delaminates can be determined. This test method is only applicable to flexible coatings.

Self loading test

A self loading test consists of first intentionally creating a surface defect, followed by changing the part temperature to induce thermal expansion or contraction. For this test, the coefficient of thermal expansion of both the coating and the substrate must be known to adequately estimate the shear loading induced for a given temperature change. Figure B.3 shows a circle cut self loading test. A hole of reduce "R" is cut through the coating, a temperature change is then applied and the crack growth, "a", is monitored. The disadvantages of this test are that it can only to test coatings with weak adhesion due to the limited loads which can be created by temperature variation and that the loading condition cannot be directly measured.

Beam-bending test

The beam-bending tests use specified beam geometries and loading arrangements to determine at what loading crack growth occurs. The beam geometry must be manufactured and the coating must then be applied. Next, a crack is intentionally formed at a region where the loading parameters are well understood. Figure B.4 shows a three point beam bending test geometry and loading arrangement. A force, "F", is applied on the opposite surface of a preset cut and the bar is supported at both ends. The primary benefit of the beam bending

test, is that a well understood loading condition can be achieved by using specific beam geometries and loading conditions. Unfortunately, the controlled parameters of this test, which help calculate the loading at the crack tip, also lead to added fabrication cost of test specimens.

Pull test

The pull test is performed by first, adhering a test stud to the coating (see Figure B.5). The assembly is then placed in a tensile test apparatus and tensile load is applied until failure or a proof loading is achieved. The adhesion strength is defined as the maximum stress applied. The advantages of this test method are that different coating adhesions can be quantitatively compared and that a large area can be tested, which helps identify localized coating defects that could be overlooked. The disadvantages of this test are that significant sample preparation is required and that the failure can occur through the adhesive connecting the test stud to the coating. For this reason, this test method is not used on coating with very good adhesion.

Laser spallation test

A schematic of a laser spallation test is shown in Figure B.6. A backing layer must be applied opposite to coated surface to ensure the laser pulses are adequately absorbed. A laser is directed at the backing layer, which causes it to heat and expand. The expansion of the backing layer causes a compressive shock wave which travel towards the coated surface. The compressive shock wave can, if strong enough, cause delamination of the coating. A major benefit of this test method is that repeated loading can be simulated by cycling the

laser on and off. The disadvantages of this test method are that a backing layer must be applied and the test requires advanced test equipment.

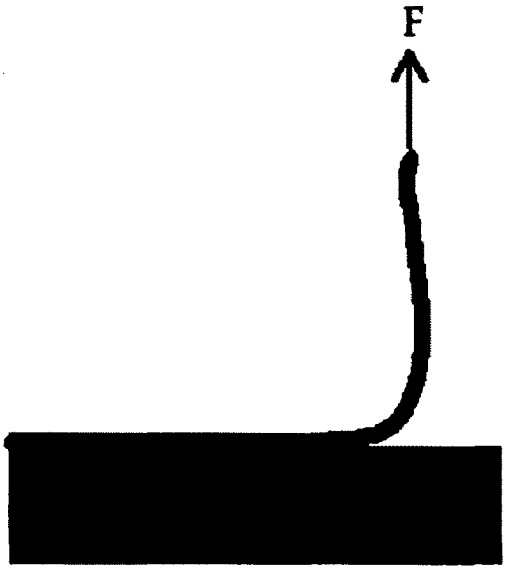

Figure B.1: 90° peel test (Lacombe, 2006)

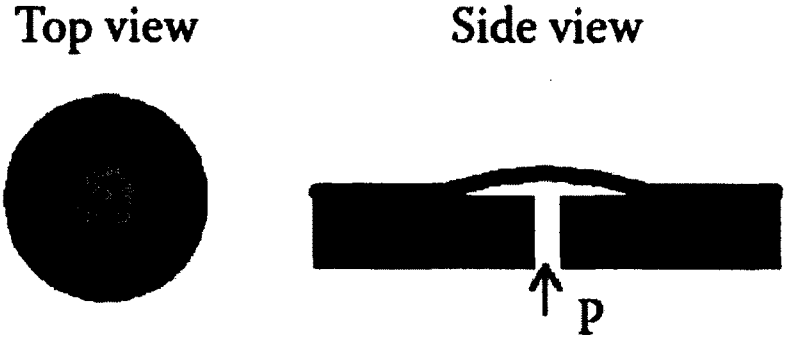

Figure B.2: Blister test (Lacombe, 2006)

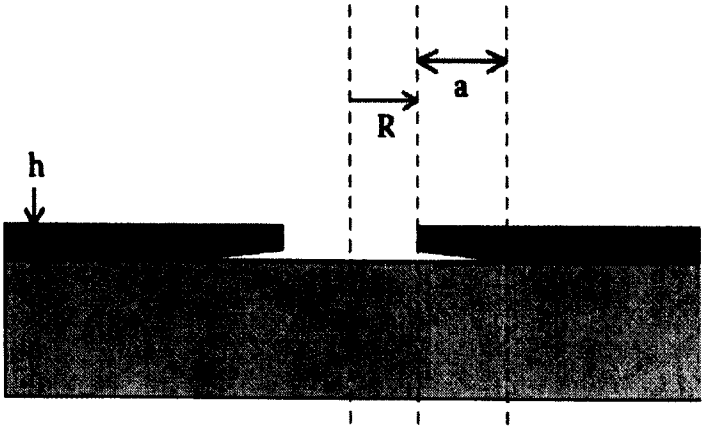

Figure B.3: Cross section view of a circle cut self loading test (Lacombe, 2006)

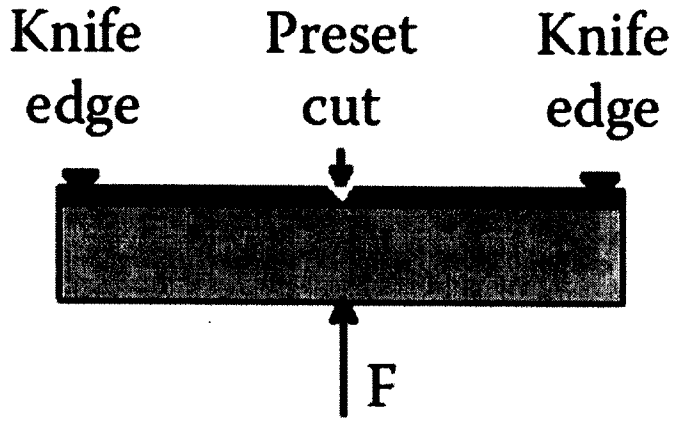

Figure B.4: Three point beam bending test (Lacombe, 2006)

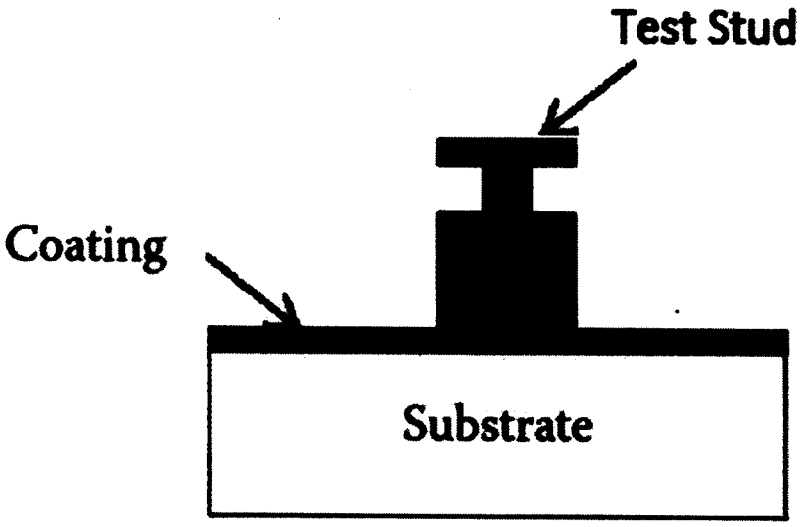

Figure B.5: Pull test schematic (Lacombe, 2006)

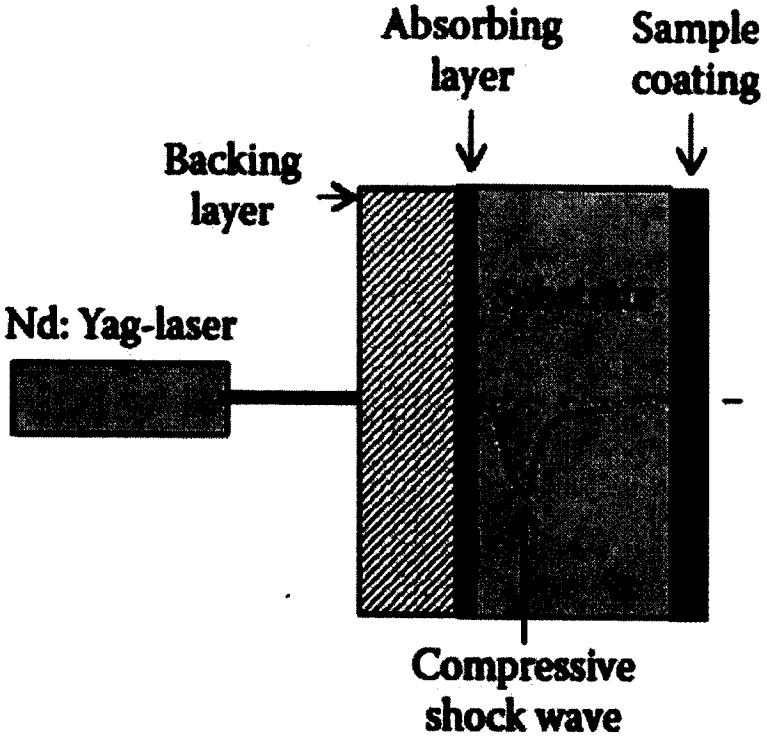

Figure B.6: Laser spallation test (Lacombe, 2006)

References

ABAQUS (2008). ABAQUS Analysis User's Manual. ABAQUS *Online Documentation, Dassault Systèmes*, Version 6.8.

ASTM C1624-05 (2010). Standard Test Method for adhesion Strength and Mechanical Failure Modes of Ceramic Coatings by Quantitative Single Point Scratch Testing. *ASTM International.*

ASTM E10-10 (2010). Standard Test Method for Brinell Hardness of Metallic Materials. *ASTM International.*

ASTM E18-8b (2008). Standard Test Methods for Rockwell Hardness of Metallic Materials. *ASTM International.*

ASTM E384-11 (2011). Standard Test Method for Knoop and Viquers Hardness of Metallic Materials. *ASTM International.*

Benham, P. P., Crawford, R. J., Armstrong, C. G. (1996). Mechanics of Engineering Materials, Prentice Hall, 2nd Ed., pp. 292-521.

Bodor, S., (2010). Personal interview at Royal Canadian Mint, Sept. 28 2010.

Bohler Uddeholm (Novembe 15, 2010). Plastic Mold Steel. Retrieved November 15, 2010, from Bohler Uddeholm Web site: http://www.bucorp.com/plastics.htm

EN 1071-3 (2005). Advanced technical ceramics – Methods of test for ceramic coatings – Part 3: Determination of adhesion by scratch test, *European Standards.*

Feild, J. E., and Pickles, C. S. J. (1996). Strength, fracture and friction properties of diamond. *Diamond and Rekated Material*,Vol. 5, pp. 625-634.

György, E., Mihailescu, I. N., Serra, P., Pérez del Pino, A., Morenza, J. L. (2002). Single pulse Nd:YAG laser irradiation of titanium: influence of laser intensity on surface morphology. *Surface and Coating Technology*, Vol. 154, pp. 63-67.

Heinke, W., Leyland, A., Matthews, A., Berg, G., Friedrich, C., Broszeit, E. (1995). Evaluation of PVD nitride coatings, using impact, scratch and Rockwell-C adhesion tests. *Thin Solid Film*, Vol. 270,pp. 431-438.

ISO 20502:2005(E) (2005). Fine Ceramics (advanced seramics, advanced technical ceramics) – Determination of adhesion of ceramic coatings by scratch testing. *International Standards Organization.*

Jiang, X., Lauke, B., Beckert, W., Schüller, T. (2001). Numerical simulation of micro-scratch tests for coating/substrate composites. *Composite Interfaces*, Vol. 8, No. 1, pp. 19-40.

Kelly, P. J., Arnell, R. D. (2000). Magnetron Sputtering: A review of recent developments and applications. *Vacuum*, Vol. 56, pp. 159-172.

Lacombe, R. (2006). Adhesion measurement methods: Theory and Practice. *CRC Press*, pp. 7-73.

Lee, L. H. (ed.). (1991). Fundamentals of Adhesion. *Plenum Publishing Corporation*, pp. 363-381.

Li, J., Beres, W. (2005). Three-dimensional finite element modeling of the scratch test for a TiN coated titanium alloy substrate. *Wear*, Vol. 260, pp. 1232-1242.

Li, H., Costil, S., Barnier, V., Oltra, R., Heintz, O., Coddet, C. (2006). Surface modification induced by nanosecond pulsed Nd:YAG laser irradiation of metallic substrates. *Surface and Coating Technology*, Vol 201, pp. 1383-1392.

Nygards, C. M., White, K. W., Ravi-Chander, K. (1998). strength of HVOF coating-substrate interfaces. *Thin Solids Films*, Vol. 332, pp. 185-188.

McLean, D. A. (2010). The characterisation and performance of magnetron sputter coatings on minting dies. Department of Mechanical and Aerospace Engineering, Carleton University.

Martin, P. M. (Ed.). (2010). Handbook of deposition technologies for thin films and coatings – Science, Applications and Technology. *William Andrew Publishing*, 3rd edition, pp. 3-23.

Meneve, J., Ronkainen, H., Anderson, P., Vercammen, K., Camino, D., Teer, D. G., Von Stebut, J., Gee, M. G., Jennett, N. M., Banks, J., Bellaton, B., Matthaei-Shulz, E., Vetters, H. (2002). Scratch adhesion testing of coated surfaces – Challenges and new directions. *Adhesion Measurement of Films and Coatings*, Vol. 2, pp. 79-106.

Pachler, T., Souza, R. M., Tschiptschin, A. P. (2007). Finite element analysis of peak stresses developed during indentation of ceramic coated steel. *Surface and Coating Technology*, Vol. 202, pp. 1098-1102.

Piana, L. A., Pérez, R. E., Souza, R. M., Kunrath, A. O., Strohaecker, T. R. (2005). Numerical and experimental analyses on the indentation of coated systems with different mechanical properties. *Thin Solid Films*, Vol. 491, pp. 197-203.

Ramalingam, S., Zheng, L. (1995). Film-substrate interface stresses and their roles in the tribological performance of surface coatings. Tribology International, Vol. 28, No. 3, pp. 145-161.

Ramberg, W., Osgood, W. R. (1943). Description of stress-strain curves by three parameters. *National Advisory Committee For Aeronautics,* pp. 1-27.

Ribeiro, A. F. (2003). Duplex Coatings on AISI H13 and AISI D2 tool steels by using plasma nitriding and TiN-PVD. *Sao Paulo University.*

Sproul, W. D. (1996). Physical vapor deposition tool coatings. *Surface and Coatings Technology*, Vol. 81, pp. 1-7.

Sun, X., Liu, W. N., Stephens, E., Khaleel, M. A. (2008). Determination of interfacial adhesion strength between oxide scale and substrate for metallic SOFC interconnects. *Journal of Power Sources*, Vol. 176, pp. 167-174.

Teer, D. G., Li, L. (2008). Sputter coatings for proof coining dies.

VDI Guideline 3198 (1991). Verein Deutscher Ingenieur Normen, *VDI-Verlag.*

Xu, M., Li, L., Liu, Y., Cai, X., Chen, Q., Chu, P. K. (2007). Experimental tests and numerical simulation studies on nano-indenation of TiN film deposited on N+-implanted aluminum. *Surface and Coatings Technology*, Vol. 201, pp. 6707-6711.

Yan, J., Karlsson, A. M., Chen, X. (2007). Determining plastic properties of a material with residual stress by using conical indentation. International Journal of Solids and Structures, Vol. 44, Issue 11-12, pp. 3720-3737.